University of Szeged
Faculty of Pharmacy
Institute of Pharmaceutical Technology and Regulatory Affairs
Head: Prof. Dr. Ildikó Csóka, Ph.D.

Ph.D. Thesis

INHALABLE KETOPROFEN NANOCRYSTAL-BASED DRY POWDERS FOR LOCAL AND SYSTEMIC PULMONARY DELIVERY: A PATIENT-CENTRIC APPROACH

By
Heba Banat
Pharmacist

Supervisor:
Prof. Dr. Ildikó Csóka
and
Prof. Dr. Rita Ambrus

SZEGED
2025

PUBLICATIONS RELATED TO THE SUBJECT OF THE THESIS

I. **Heba Banat**, Rita Ambrus, Ildikó Csóka, “Drug combinations for inhalation: Current products and future development addressing disease control and patient compliance”. International Journal of Pharmaceutics. 2023; 643:123070. https://doi.org/10.1016/j.ijpharm.2023.123070

(**D1, IF: 5.3**)

II. **Heba Banat**, Ildikó Csóka, Dóra Paróczai, Katalin Burian, Árpád Farkas, Rita Ambrus. “A Novel Combined Dry Powder Inhaler Comprising Nanosized Ketoprofen-Embedded Mannitol-Coated Microparticles for Pulmonary Inflammations: Development, In Vitro–In Silico Characterization, and Cell Line Evaluation”. Pharmaceuticals. 2024; 17(1):75. https://doi.org/10.3390/ph17010075

(**Q1, IF: 4.3**)

III. **Heba Banat,** Ilona Gróf, Mária A. Deli, Rita Ambrus, Ildikó Csóka. “Evaluation of Permeability, Safety, and Stability of Nanosized Ketoprofen Co-Spray-Dried with Mannitol for Carrier-Free Pulmonary Systems”. Applied Sciences. 2025; 15(3):1547. https://doi.org/10.3390/app15031547

(**Q2, IF: 2.5**)

IV. **Heba Banat**, Attila Nagy, Árpád Farkas, Rita Ambrus, Ildikó Csóka. “Comprehensive Aerodynamic and Physicochemical Stability Evaluations of Nanocrystal-Based Dry Powder Inhalers: The Role of Mannitol and Leucine in Enhancing Performance”. Pharmaceutics. 2025; 17(4), 436. https://doi.org/10.3390/pharmaceutics17040436

(**D1, IF: 4.9**)

V. **Heba Banat**, Ildikó Csóka, Fruzsina Kun-Szabó, Gergely H. Fodor, Petra Somogyi, Ferenc Peták, Petra Party, Anita Sztojkov-Ivanov, Eszter Ducza, Róbert Berkecz, Ilona Gróf, Mária A. Deli, Rita Ambrus. “Mannitol-leucine synergy in nanocrystal agglomerates for enhanced systemic delivery of inhaled ketoprofen: Pharmacokinetics and safety in ovalbumin-sensitized rats”. International Journal of Pharmaceutics. 2025; 676:125610. https://doi.org/10.1016/j.ijpharm.2025.125610

(**Q1, IF: 5.3**)

Total IF: **22.3**, Total citation: **30**

PRESENTATIONS RELATED TO THE SUBJECT OF THE THESIS

I. **Heba Banat**, Ildikó Csóka, Rita Ambrus, "Formulation of a combined dry powder inhalation therapy for cystic fibrosis". IV. Symposium of Young Researchers on Pharmaceutical Technology, Biotechnology and Regulatory Science. January 19-21, 2022. Szeged, Hungary. Flash Presentation.

II. **Heba Banat**, Ildikó Csóka, Rita Ambrus, "Development of a combined nanosystem as a dry powder inhaler for the treatment of pulmonary inflammations". V. Symposium of Young Researchers on Pharmaceutical Technology, Biotechnology and Regulatory Science. January 18-20, 2023. Szeged, Hungary. Oral Presentation.

III. **Heba Banat**, Ildikó Csóka, Rita Ambrus, "Design, formulation and evaluation of a dry powder inhaler comprising a combination therapy to target chronic respiratory diseases". EUFEPS Annual Meeting 2023. May 31 – June 2, 2023, Lisbon, Portugal. Poster presentation.

IV. **Heba Banat**, Ildikó Csóka, Rita Ambrus, "Optimizing Aerodynamic Performance of an Anti-Inflammatory-Containing Dry Powder Inhaler via Nano-Spray Drying". VI. Symposium of Young Researchers on Pharmaceutical Technology, Biotechnology and Regulatory Science. January 24-26, 2024. Szeged, Hungary. Oral Presentation.

V. **Heba Banat**, Ildikó Csóka, Dóra Paróczai, Katalin Burian, Árpád Farkas, Rita Ambrus, "Development and formulation of a single dry powder inhaler combining ketoprofen nanoparticles-embedded mannitol microparticles for pulmonary inflammations: in vitro and in silico analysis, and cell line assessment". XVI. Hungarian Aerosol Conference. 2024. April 25-27, 2024 - Szarvas, Hungary. Oral Presentation.

VI. **Heba Banat**, Ildikó Csóka, Rita Ambrus, "Enhancing Pulmonary Delivery of Ketoprofen: Comparative Study of Spray Drying Approaches". Exploring the Future of Inhalation Drug Delivery. September 11-13, 2024. Parma, Italy. Oral Presentation.

VII. **Heba Banat**, Ildikó Csóka, Rita Ambrus, "Carrier-Free Dry Powder Inhaler Formulation for Pulmonary Delivery: Insights into Stability, Safety, and Aerodynamic Performance". VII. Symposium of Young Researchers on

Pharmaceutical Technology, Biotechnology and Regulatory Science. January 29-31, 2025. Szeged, Hungary. Oral Presentation.

VIII. **Heba Banat**, Rita Ambrus, Ildikó Csóka, "Enhancing Bioavailability of a Non-Steroidal Anti-Inflammatory Drug Through Pulmonary Delivery". Drug Delivery Through Physiological Barriers. International Symposium April 24-26, 2025. Budapest, Hungary. Oral Presentation.

ABBREVIATIONS

A549	Adenocarcinomic human alveolar basal epithelial cells
Ac	Acinar region
ACI	Andersen cascade impactor
A	Surface area of the membrane
ANOVA	Analysis of Variance
API	Active pharmaceutical ingredient
APS	Aerodynamic Particle Sizer
AUC	Area under the curve
BBD	Box-Behnken factorial design
BCS	Biopharmaceutical Classification System
BH	Breath-hold
Br	Bronchial region
C	Control
C_A	Concentration of the acceptor phase
C_D	Concentration of the donor phase
CF	Cystic fibrosis
CFBE	Cystic fibrosis bronchial epithelial cells
CFTR	Cystic fibrosis transmembrane conductance regulator
CMAs	Critical Material Attributes
C_{max}	Maximum concentration
CPPs	Critical Process Parameters
CQAs	Critical Quality Attributes
COPD	Chronic obstructive pulmonary disease
COX-1	Cyclooxygenase-1 enzyme
COX-2	Cyclooxygenase-2 enzyme
D[0.1]	10% of the volume distribution is below this value
D[0.5]	50% of the volume distribution is below this value
D[0.9]	90% of the volume distribution is below this value
DL	Drug loading
DLS	Dynamic light scattering
DMSO	Dimethyl sulfoxide
DNA	Deoxyribonucleic acid

DPI	Dry powder inhaler
DSC	Differential scanning calorimetry
EE	Encapulation efficiency
EELV	End-expiratory lung volume
EF	Emitted fraction
EMA	European Medicines Agency
ET	Extra-thoracic
EXH	Exhaled
F	Relative bioavailability
FBS	Fetal bovine serum
FDA	U. S. Food and Drug Administration
FPF	Fine particle fraction
f_t	Tissue availability
FT-IR	Fourier-Transform Infrared Spectroscopy
G	Tissue damping
GSD	Geometric standard deviation
H	Tissue elastance
HEPES	4-(2-hydroxyethyl)-1-piperazineethanesulfonic acid
HPMC	Hydroxypropyl methylcellulose
ICH	The International Council for Harmonization of Technical Requirements for Pharmaceuticals for Human Use
IVIVC	*In vitro-in vivo* correlation
IL-6	Interleukin 6
IUPAC	International Union of Pure and Applied Chemistry
k_e	Elimination rate constant
KTP	Ketoprofen
LPS	Lipopolysaccharide
MCh	Methacholine
MEM	Minimum Essential Medium
MMAD	Mass median aerodynamic diameter
MRT	Mean residence time
M_w	Molecular weight
NCA	Nanocrystal agglomerate
NS	Nanosuspension

NSAID	Non-steroidal anti-inflammatory drug
NTA	Nanoparticle Tracking Analysis
OVA	Ovalbumin
P_{app}	Apparent permeability coefficient
PDI	Polydispersity index
PEEP	Positive end-expiratory pressure
PK	Pharmacokinetics
PM	Physical mixture
PS	Particle size
PVA	Polyvinyl alcohol
QbD	Quality by Design
qPCR	Quantitative polymerase chain reaction
QTPP	Quality Target Product Profile
R_{aw}	Airway resistance
RI	Refractive index
RNA	Ribonucleic acid
RPMI	Roswell Park Memorial Institute medium
S.D.	Standard deviation
SDS	Sodium dodecyl sulphate
SEM	Scanning electron microscopy
SSA	Specific surface area
t	Time
TEER	Transepithelial electrical resistance
U937	Promonocyte cells
X_c	Crystallinity index
XRPD	X-ray powder diffraction
ZP	Zeta potential
ZrO_2	Zirconium-dioxide
ρ_b	Bulk density
ρ_t	Tapped density

TABLE OF CONTENTS

1. Introduction

Pulmonary drug delivery offers a non-invasive route for both local and systemic therapy, leveraging the lungs' large surface area, rich vascularization, and avoidance of first-pass metabolism to enhance bioavailability. Dry powder inhalers (DPIs) are particularly advantageous due to their stability, propellant-free design, and ease of use [1,2]. While inhaled non-steroidal anti-inflammatory drugs (NSAIDs) have shown promise for treating local lung inflammation, their systemic applications remain underexplored, despite the potential for lower therapeutic doses and reduced systemic side effects compared to oral administration [3].

NSAIDs are widely used to treat inflammatory conditions, including cystic fibrosis (CF) and acute pain; however, oral administration is limited by gastrointestinal toxicity, poor solubility, and variable bioavailability. Pulmonary delivery could overcome these challenges, yet no inhaled NSAID has been translated into a marketed product [4–6]. Nanocrystals, as a carrier-free platform (typically 1–1000 nm), offer distinct advantages for pulmonary delivery, including enhanced dissolution, improved mucus penetration, and high drug loading [7]. However, their small size necessitates precise particle engineering to ensure aerodynamic diameters within the optimal range (1–5 μm) for lung deposition.

This work introduces two patient-centric ketoprofen (KTP)-based DPI formulations derived from a unified nanocrystal platform. The first combines KTP with the mucolytic agent mannitol for localized pulmonary therapy, targeting both inflammation and mucus clearance in diseases such as CF. The second leverages nanocrystal engineering for systemic NSAID delivery, aiming to improve bioavailability while minimizing gastrointestinal irritation. Both formulations are designed to simplify treatment regimens and enhance tolerability.

By integrating Quality by Design (QbD) principles with nanocrystal technology, this study advances the development of inhaled NSAIDs through tailored strategies for local and systemic indications. The approach not only addresses current therapeutic gaps but also establishes a framework for repurposing poorly soluble drugs via pulmonary delivery—aligning with regulatory priorities for patient-centric, innovative drug products.

2. Aim of the work

This study proposes a patient-centric strategy for pulmonary drug delivery through the development of two distinct DPI systems derived from a unified KTP nanocrystal platform. One formulation targets local lung inflammation and mucus obstruction in CF, while the other is designed for systemic delivery to enhance bioavailability via the pulmonary route. The overarching aim is to tailor drug formulation to meet different therapeutic needs while aligning with patient expectations for rapid relief, reduced dosing burden, and improved tolerability. The specific objectives are as follows:

A. Nanocrystal dispersion development

I. Formulate and optimize a stable KTP nanosuspension as a versatile intermediate for both local and systemic DPI products, ensuring suitability for downstream powder engineering.

B. Local pulmonary delivery (Anti-inflammatory and mucolytic combination):

II. Establish a rational inhalable combination of KTP and mannitol guided by a QbD approach.

III. Develop the combined dry powder formulation using mini spray-drying with varying mannitol ratios to optimize the combination while maintaining KTP integrity.

IV. Assess the dual functionality of the formulation through evaluation of local efficacy, biocompatibility, and epithelial permeability.

C. Systemic pulmonary delivery (Nanocrystal-engineered DPI):

V. Optimize the nano spray-drying process parameters, with a factorial design, to produce nanocrystal-engineered powders suitable for deep lung deposition and systemic absorption.

VI. Investigate the influence of excipients (mannitol and leucine) on aerosol performance, biocompatibility, and cellular diffusion.

VII. Assess the pharmacokinetic profile of the inhaled nanocrystal formulation compared to the oral route, alongside tolerability and safety in ovalbumin-sensitized rats.

D. Stability evaluation:

VIII. Determine the physicochemical stability of both DPI systems under accelerated storage conditions, ensuring maintenance of performance-critical attributes.

3. Literature background

3.1. Pulmonary drug delivery: Local and systemic applications

The lungs provide a highly accessible and efficient route for drug administration due to their extensive surface area (~100 m²) and rich vascular network. The efficiency of drug delivery largely depends on where particles deposit within the respiratory tract. Particles with an aerodynamic diameter of <5 µm are optimal for reaching the lungs, with smaller particles penetrating deeper to the alveolar region, thereby enhancing systemic uptake [8–11]. As illustrated in Figure 1, deposition occurs through three principal mechanisms: inertial impaction (>5 µm) in the upper airways, gravitational sedimentation (1–5 µm) in smaller bronchioles, and Brownian diffusion (<1 µm) in the alveoli [12]. While submicron particles can reach the deepest regions, they are also more likely to be exhaled [13,14]. In addition, particle morphology (e.g., corrugated or porous structures) and low particle density (<1 g/cm³) are critical for improving dispersibility and achieving deep lung deposition [15–18].

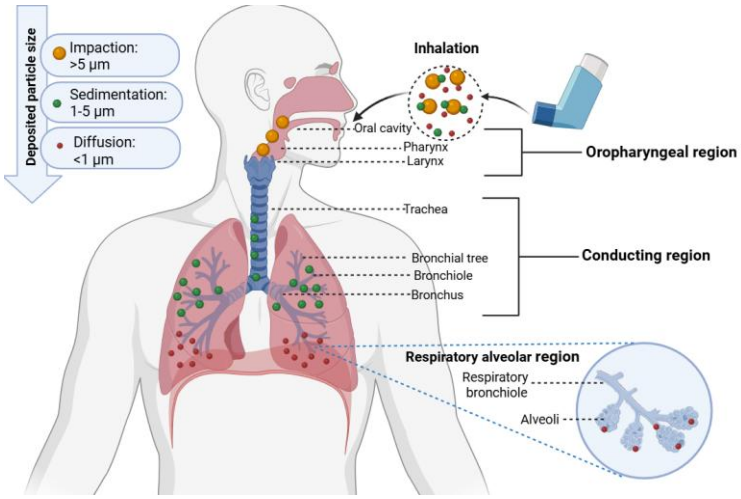

Figure 1: An overview of the parts of the respiratory system and how particles deposit in the lungs based on the size. Adapted from [1], with slight modifications.

Pulmonary drug delivery can be classified into two main strategies: (i) local delivery for respiratory conditions, and (ii) systemic delivery of various drugs [19]. Although bronchodilators and corticosteroids remain the most common inhaled therapies for local lung targeting, other drug classes—such as antibiotics, anti-tuberculosis agents, anticancer drugs, and mucolytics—are gaining attention. For instance, inhaled antibiotics can achieve high local concentrations in the lungs, improving efficacy and minimizing systemic side effects, while potentially limiting resistance development by sparing non-target microbiota [20]. Table 1 summarizes recent developments in inhaled formulations for local pulmonary therapy.

Table 1: Inhaled products, marketed or in-developing, intended for local delivery [21–27].

Product	Indication	API	Advancement	Manufacturer	Status
Tobi® Podhaler	CF	Tobramycin	PulmoSphere®	Viatris	Marketed-2013
Trixeo Aerosphere	COPD	Budesonide, Glycopyronium, Formetrol fumerate	Aerosphere™	AstraZeneca	Marketed-2020
Ohtuvayre®	COPD	Ensifentrine	Unique MoC (Dual PDE3/4 inhibitor)	Verona Pharma	Marketed-2024
RT234-PAH	PAH	Vardenafil	AOS™ DPI	Respira Therapeutics	Phase II-2024
AP01	IPF	Pirfenidone	Novel inhaled product (details undisclosed)	Avalyn Pharma	Phase II-2025
AP02	IPF	Nintedanib	Novel inhaled product (details undisclosed)	Avalyn Pharma	Phase I-2024

CF: cystic fibrosis, COPD: chronic obstructive pulmonary disease, PDE: phosphodiesterase, PAH: pulmonary arterial hypertension, IPF: idiopathic pulmonary fibrosis, MoC: mechanism of action.

Although pulmonary delivery is well established for local treatment, achieving efficient systemic absorption remains challenging. Success relies on deep lung deposition, where high surface area and vascularization enable optimal uptake, unlike the upper airways with limited absorption and rapid clearance [28]. Nonetheless, progress has been made, with several inhaled products reaching clinical development or market approval. Table 2 highlights key examples, demonstrating the growing interest in this non-invasive route.

Table 2: Inhaled products, marketed or in-developing, intended for systemic delivery [1,29–31].

Product	Indication	API	Manufacturer	Status
Exubera®	Diabetes	Insulin	Pfizer, Nektar Therapeutics	Withdrawn-2007
Afrezza®	Diabetes	Insulin	MannKind Corporation	Marketed-2014
AIR® insulin	Diabetes	Insulin	Lilly	Withdrawn-2007
Inbrija®	Parkinson’s disease	Levodopa	Merz Therapeutics	Marketed-2018
Adasuve®	Schizophrenia	Loxapine	Alexza Pharmaceuticals	Marketed-2012
Levadex®	Migraine	Dihydroergotamine	MAP Pharmaceuticals	Phase III-2014 (declined)
CVT427	Migraine	Zolmitriptan	Acorda Therapeutics	Phase I-2016

Several pulmonary barriers—such as mucociliary clearance, alveolar macrophages, and enzymatic degradation—limit drug delivery and reduce bioavailability [32,33]. Addressing these challenges is critical in the design of effective inhalable formulations. Despite such limitations, the substantial advantages of pulmonary drug delivery—such as rapid onset, reduced systemic side effects, and lower dosing—support the continued development of inhalable therapies for both local and systemic applications. These benefits are summarised in Figure 2.

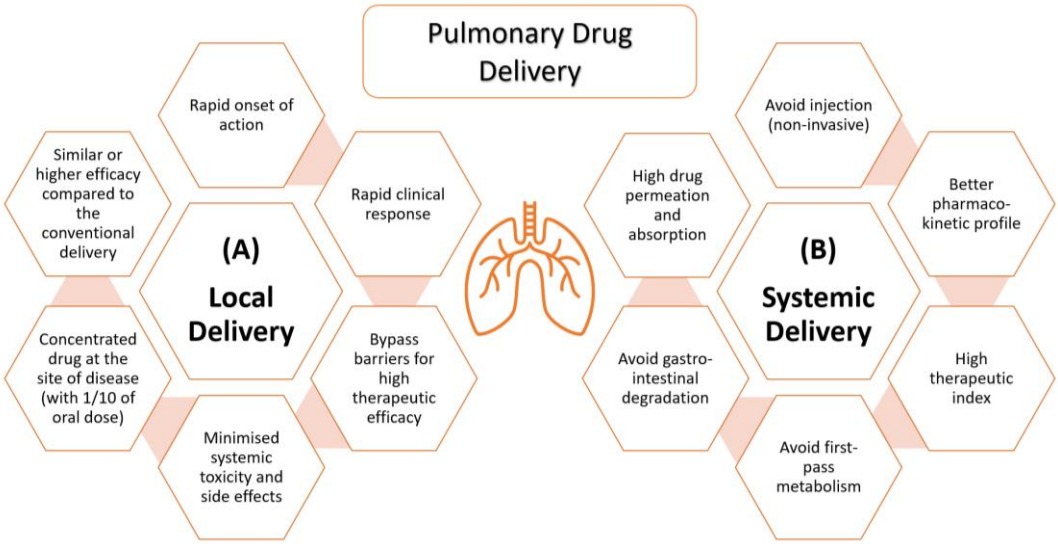

Figure 2: Advantages of local and systemic pulmonary drug delivery [1].

3.2. Inhaled non-steroidal anti-inflammatory drugs

NSAIDs are increasingly recognized for their role in managing chronic respiratory conditions such as CF, where persistent neutrophilic inflammation drives lung damage. High-dose oral ibuprofen has shown efficacy in slowing lung function decline in CF and is included in treatment guidelines [34–38]. However, long-term systemic use is limited by significant side effects. Despite their therapeutic value, no inhaled NSAID formulations are currently approved for CF or other pulmonary conditions, highlighting a gap for targeted pulmonary delivery to enhance efficacy and reduce systemic risks.

Beyond respiratory diseases, NSAIDs remain among the most widely used drugs globally, indicated for pain, fever, and inflammation in conditions like arthritis and migraines [39–44]. Their mechanism—primarily inhibition of cyclooxygenase (COX) enzymes—offers broad therapeutic benefits but is offset by gastrointestinal, cardiovascular, and renal adverse effects [45–48]. Additionally, poor water solubility hinders formulation and bioavailability [49].

Inhaled NSAIDs, such as ibuprofen and meloxicam, have been explored for local pulmonary action [4–6], but their systemic potential remains underutilized. Preclinical data suggest that pulmonary administration of NSAIDs can achieve therapeutic effects at lower doses than oral routes [50], offering a promising alternative with fewer side effects. Given regulatory recommendations to minimize NSAID exposure, alternative delivery strategies like inhalation are urgently needed.

3.3. Ketoprofen as a candidate for inhaled delivery

KTP is a potent NSAID with antipyretic, analgesic, and anti-inflammatory properties. Compared to other NSAIDs, it offers superior analgesic efficacy—particularly in inflammatory and postoperative pain—with a favorable safety profile. Clinical and preclinical studies support its dual anti-inflammatory and antinociceptive effects, including inhibition of edema, IL-8 suppression, and enhanced antioxidant activity [51,52].

Meta-analyses further show KTP outperforms ibuprofen in managing rheumatoid arthritis and provides better outcomes in moderate-to-severe pain while maintaining tolerability [53–55]. Topical formulations, such as KTP plasters, have shown comparable efficacy to diclofenac with good safety in osteoarthritis [56]. Despite its therapeutic potential, KTP remains underexplored for pulmonary delivery, with only limited investigations [57], indicating a promising area for further development.

3.4. Dry powder inhalers: Formulation, advantages and challenges

A critical determinant of therapeutic efficacy in pulmonary drug delivery is the inhalation device, which ensures that the drug is effectively deposited within the bronchial tree, with potential for deep lung penetration [58,59]. Among the various pulmonary delivery devices shown in Figure 3, DPIs have gained increasing preference in pulmonary delivery due to their solid-state stability, absence of harmful propellants, user-friendly design, and breath-actuated mechanism, which removes the need for patient coordination during inhalation [29].

Unlike nebulizers and pressurized metered dose inhalers (pMDIs), which rely on external power sources or propellants, DPIs are portable and environmentally friendly. Their compatibility with engineered particles, makes them particularly suitable for modern inhalation therapies targeting both local and systemic effects.

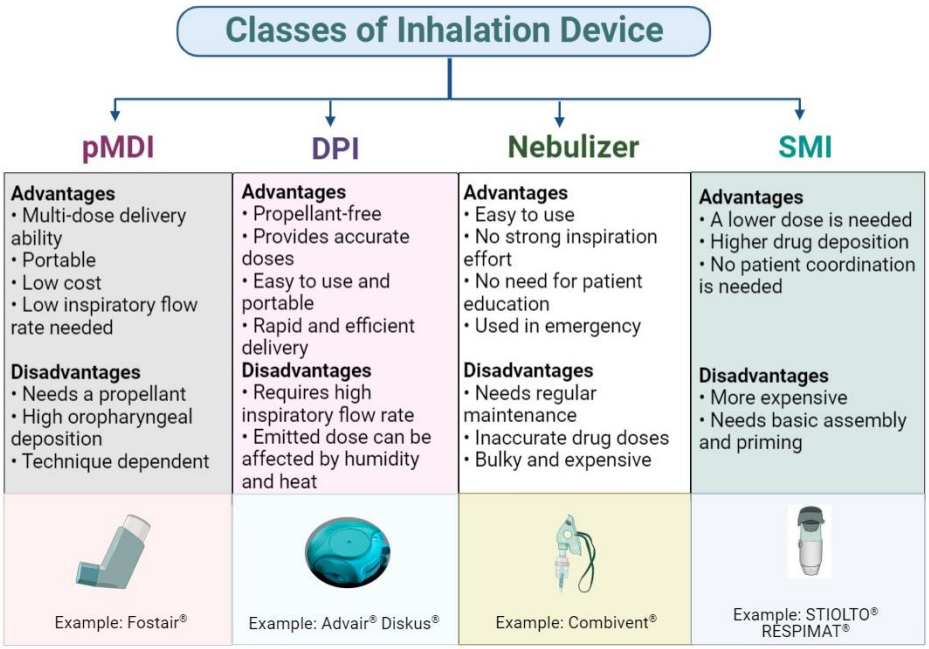

Figure 3: Illustration of devices used for inhaled products, alongside examples of selected marketed brands. Abbreviation: pMDI: pressurized metered dose inhaler, DPI: dry powder inhaler, SMI: soft mist inhaler [1].

DPIs are generally formulated using one of two strategies: (i) carrier-based systems, where the drug is blended with larger excipient particles, and (ii) carrier-free systems, which contain only the drug particles, often engineered using advanced techniques and excipients to enhance aerodynamic properties. In carrier-based DPIs, the active pharmaceutical ingredient (API) adheres to coarse carrier particles—typically lactose, mannitol, or glucose—ranging from 50 to 100 µm in size [60]. However, during inhalation, drug detachment from the carrier is often incomplete, resulting in reduced deposition of the drug in the lower lungs and accumulation in the upper airways. This inefficiency underscores the importance of optimizing aerosolization and dispersion performance. In light of these limitations, carrier-free DPIs have emerged as a promising alternative, offering greater potential for efficient lung delivery and improved therapeutic outcomes.

Carrier-free DPI formulations aim to reduce interparticle cohesion, enhancing dispersion and improving drug release efficiency from the inhaler. These systems typically involve engineering complex powders by combining the API with functional excipients to optimize aerodynamic properties and lung deposition [61–63]. Additives such as hydrophobic agents, lipids, amino acids, and biodegradable polymers have been explored to enhance aerosolization and stability [64,65]. However, pulmonary delivery imposes stricter safety requirements, and only a limited number of excipients are approved for inhalation due to

potential risks of accumulation and irritation in lung tissue [29,64,66,67]. This restricts formulation options and complicates the development process.

Building on these advances, nanoscale drug delivery systems—such as nanoparticles and nanocrystals—offer new opportunities to further improve pulmonary drug delivery by enhancing deposition, dissolution, and systemic absorption. These technologies are discussed in the following sections.

3.5. Impact of nanotechnology on pulmonary drug delivery

Nanotechnology has revolutionized drug delivery, including inhalation therapies. In pulmonary administration, nanoparticles improve the solubility and bioavailability of poorly soluble drugs, enabling enhanced therapeutic efficacy at lower doses and potentially minimizing systemic side effects [68,69]. They also help overcome biological barriers within the lungs. Notably, particles smaller than 200 nm can evade clearance by alveolar macrophages, promoting deeper lung deposition and prolonged retention [70,71]. Additionally, nanoparticles can be tailored through surface modifications to improve critical aspects of pulmonary delivery, such as enhancing cellular uptake [72].

Nanoparticles used in inhalation therapy are typically classified as carrier-based or carrier-free, depending on their composition. Among carrier-based systems, lipid-based nanoparticles—including liposomes, solid lipid nanoparticles, and nanoemulsions—are widely applied for their capacity to encapsulate both hydrophilic and hydrophobic drugs [73,74]. Polymeric nanoparticles, such as those made from PLGA or chitosan, offer benefits like biodegradability, mucoadhesiveness, and extended lung retention [75–78]. Inorganic nanoparticles, such as mesoporous silica, provide high drug-loading capacity and modifiable surfaces, contributing to targeted delivery and controlled release [79]. Hybrid nanoparticles, which combine materials (e.g., lipids with polymers), are engineered to harness the advantages of multiple platforms and further optimize drug delivery [80]. Each nanoparticle class presents distinct benefits, supporting a broad range of therapeutic and diagnostic applications in pulmonary medicine.

In contrast, nanocrystals represent a carrier-free nanotechnology platform that has attracted growing interest for inhalation delivery. These are pure drug particles, typically 1–1000 nm in size, stabilized by surfactants or polymers [81,82]. Nanocrystals enhance the dissolution rate and saturation solubility of poorly water-soluble drugs while maintaining favorable biological compatibility and low toxicity. Their high surface area improves bioavailability

and facilitates better drug adhesion to lung tissues. Compared to carrier-based systems, nanocrystals offer advantages such as higher drug loading, improved mucus penetration, reduced macrophage clearance, and efficient drug release—making them especially promising for DPI formulations [7]. Table 3 summarizes selected nanoparticle platforms under investigation for pulmonary delivery.

Table 3: An overview of nanoparticle systems used in pulmonary drug delivery [1].

Nanosystem	Preparation techniques	Example	Reference
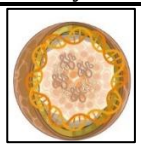 **Nanosphere**	Nanoprecipitation Ionic gelation	Combination of rifampicin/isoniazid nanosphere to target macrophage using solvent injection method.	[83]
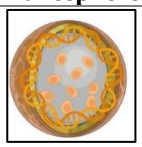 **Nanocapsule**	Solvent displacement Double emulsion Emulsion diffusion	Combination of fluticasone propionate/salmeterol nanocapsule using interfacial polycondensation based on L-lysine.	[84]
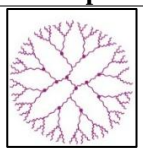 **Dendrimers**	Microfluidic process Ionic gelation Cross-linking strategy	Combination of nucleic acid and anti-cancer loaded in dendrimers carrier.	[85]
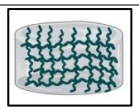 **Nanogel**	Polymerization Precipitation	Combination of graphene oxide -hybridized nanogels for combinative anticancer therapy.	[86]
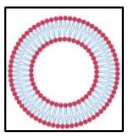 **Liposome**	Then film hydration Reverse phase evaporation Solvent injection Cross flow injection Membrane contractor Supercritical fluid Microfluidics	Synergistic combinations of levofloxacin/serratiopeptidase to improve antimicrobial and antibiofilm activity in treating *S. aureus* infection.	[87]
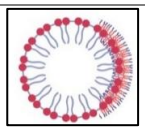 **Lipid nanoparticles**	High shear homogenisation Microemulsion Solvent emulsification	Combination of afatinib/paclitaxel loaded lipid nanoparticle in porous microsphere for the treatment of EGFR TKIs resistant NSCLC.	[88]
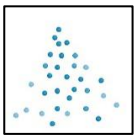 **Nanocrystals**	A. Top-down techniques Media milling High-pressure homogenisation B. Bottom-up techniques Nanoprecipitation	Combination of doxorubicin/ellagic acid nanocrystals using spray dryer to target lung cancer cells.	[89]

3.6. Nanocrystalline suspension: Preparation and stabilization

3.6.1. Production of nanosuspension by wet media milling

The top-down approach is commonly used to produce drug nanocrystals by mechanically reducing larger particles to the nanoscale. Wet media milling is a cost-effective and scalable nanosizing technique that avoids the use of organic solvents, valued for its simplicity and reproducibility. It enables the preparation of stable nanosuspensions of poorly water-soluble APIs. Key factors affecting wet media milling include milling speed, duration, bead size, and filling volume, while stabilizer type and concentration are critical for preventing uncontrolled agglomeration and achieving optimal particle size [90–92].

3.6.2. Stabilization of nanosuspension

Stabilizers are indispensable in wet media milling process to prevent particle aggregation and maintain long-term stability [93]. They function by adsorbing onto the surface of drug nanoparticles and providing steric or electrostatic repulsion [94]. Commonly used stabilizers include polymers such as polyvinylpyrrolidone (PVP), hydroxypropyl methylcellulose (HPMC), hydroxypropyl cellulose (HPC), polyethylene glycol (PEG), polyvinyl alcohol (PVA), and poloxamer 188. Surfactants also play a crucial role: ionic surfactants like sodium dodecyl sulfate (SDS), sodium lauryl sulfate (SLS), poly(ethylene imine) (PEI), and chitosan stabilize via electrostatic interactions, while nonionic surfactants such as polysorbates (Tweens) and Pluronics®, act primarily through steric hindrance [95]. The choice and concentration of stabilizer must be carefully optimized, as they significantly influence particle size, surface properties, and suspension stability. Moreover, the stabilizer must be suitable for pulmonary administration, making biocompatibility and regulatory acceptance critical considerations [96].

3.7. Nanocrystal-based dry powder inhalers

3.7.1. Particle-engineered dry powder using spray drying

Particle engineering is a versatile and essential approach in the development of DPIs, enabling control over the surface characteristics of drugs, carriers, or excipients [97]. This technique helps balance interparticle forces, enhance stability during processing and storage, and improve aerodynamic performance [98]. As previously discussed, achieving an aerodynamic diameter of 1–5 μm is critical for efficient deposition in the lower respiratory tract [99]. While nanoparticles such as nanocrystals are favorable for deep lung penetration due to their small size, they face a high risk of being exhaled before deposition can occur [100–102]. Therefore, nanocrystals often require particle engineering strategies

to increase their aerodynamic diameter into the respirable range, ensuring effective lung deposition.

Among various particle engineering techniques, spray drying stands out for producing inhalable powders with optimized characteristics. This method allows fine-tuning of critical parameters such as drying temperature, feed rate, solvent composition, and atomization settings, making it highly adaptable for tailoring particle size, morphology, flowability, and moisture content [103,104]. In a single-step process, spray drying converts liquid formulations—such as solutions, suspensions, or emulsions—into dry powders suitable for inhalation [105].

Nano spray drying, a more recent advancement, offers enhanced control over droplet formation, producing highly uniform particles with narrow size distributions. Unlike traditional spray dryers that use pressure or centrifugal atomization, nano spray dryers utilize a vibrating mesh nebulizer to create fine and consistent microdroplets. This enables efficient powder production from small-volume samples and results in higher yields [106,107]. Its ability to precisely control particle size and morphology makes it particularly suited for pulmonary applications requiring deep alveolar deposition. However, it is important to carefully choose the excipients during spray drying, as the play a critical role in engineering the size and shape of nanocrystals and achieving desirable aerosol performance.

3.7.2. Role of excipients in spray drying

The selection of excipients during spray drying significantly influences the physicochemical properties of the final powder. Common excipients, such as mannitol, trehalose, and leucine, play a critical role in stabilizing formulations during drying and ensuring product stability. Mannitol is commonly used as a cryoprotectant, bulking agent, preserving structural integrity and enhancing formulation stability [108]. However, its tendency to crystallize can impact aerosol performance and fine particle fraction (FPF) upon storage [109]. In contrast, leucine improves powder dispersibility and stability in dry powder formulations by reducing particle cohesion and enhancing aerosolization [110]. Since excipients in spray drying serve multiple roles, including thermal protection, aggregation prevention, and maintaining API bioactivity, the ideal spray-dried preparations may necessitate a combination of various excipients [111]. Moreover, their influence on

spray-dried powder should be carefully evaluated to ensure optimal characteristics and to achieve the desired powder properties.

3.8. Regulatory considerations and the QbD framework

Regulatory authorities such as the U.S. Food and Drug Administration (FDA) and the European Medicines Agency (EMA) impose strict requirements to ensure the safety, efficacy, and consistency of pulmonary drug delivery systems, especially DPIs [112]. Inhaled products require thorough characterization, including aerodynamic particle size distribution, emitted dose uniformity, and moisture sensitivity [1]. For advanced systems such as nanocrystal-based DPIs, stability remains a particular concern, as hygroscopicity, particle aggregation, and morphological changes can compromise delivery efficiency [113]. Preclinical studies are essential to assess lung toxicity and local tolerability, followed by clinical trials to establish therapeutic efficacy.

To support regulatory compliance and streamline development, the QbD framework offers a risk-based, science-driven strategy for product optimization [114]. The process begins with a pre-formulation or "Zero Phase", where unmet therapeutic needs and key characteristics of the drug–dosage form–delivery route triangle are evaluated. This phase lays the foundation for defining a suitable design space [115].

Subsequent QbD stages involve identifying the Quality Target Product Profile (QTPP), Critical Quality Attributes (CQAs), Critical Process Parameters (CPPs), and Critical Material Attributes (CMAs) [116–118]. This structured methodology ensures that development objectives, materials, and manufacturing processes align with both regulatory expectations and clinical performance. For inhaled products, QbD can guide decisions related to aerosolization efficiency, powder flowability, and formulation-device compatibility—ultimately supporting cost- and time-efficient scale-up [119].

In addition to facilitating smoother regulatory approval, integrating QbD strengthens product design by balancing patient-centric needs with industrial feasibility and regulatory standards. This is especially valuable in the context of next-generation inhalation therapies, where personalized treatment approaches are becoming increasingly important—the focus of the following section.

3.9. Patient-centric pulmonary drug delivery systems

Patient-centricity in pharmaceutical development means designing therapies to meet real-world patient needs, including efficacy, ease of use, tolerability, and convenience. Patient-

centricity is a relatively new term as applied to the relationship between quality attribute levels and the impact on safety and efficacy [120]. While not classified as such until recently, a patient-centric approach has been shaping industry development strategies for more than two decades. Inhaled drug delivery—especially for chronic respiratory diseases—requires thoughtful consideration of user preferences to ensure long-term adherence [121]. This concept now extends beyond patient interviews and clinical trials to include the formulation of drug products that integrate usability, safety, adherence, and overall patient experience. By involving both patient needs and therapeutic outcomes early in the development process, inhalation therapies can be optimized to improve treatment satisfaction and disease management [64,112]. The transition to patient-centricity is a major step toward driving patient engagement and satisfaction, bringing positive direction to drug development and medical care.

One practical patient-centric strategy is the development of combination inhalers, which deliver two or more therapeutic agents within a single device. Originally introduced in the mid-1990s, these systems were designed to enhance asthma and chronic obstructive pulmonary disease (COPD) management by simplifying treatment regimens [122–124]. Patients often favor drugs that provide fast symptom relief (e.g., bronchodilators), but long-term control requires anti-inflammatory agents like corticosteroids [125]. Administering both in a single inhaler reduces dosing complexity, minimizes training errors, and increases compliance—particularly important given that poor adherence is a leading cause of uncontrolled respiratory disease [124,126–128]. Furthermore, patients often gauge treatment effectiveness by how quickly they feel relief [129,130]. Thus, combined inhalers—designed to provide both rapid relief and long-term control—better align with patient behavior and therapeutic goals. However, this strategy has primarily been applied to asthma and COPD, highlighting a broader opportunity to extend combination inhaler approaches to other respiratory conditions.

Another key strategy in patient-centric drug delivery is enhancing the bioavailability of inhaled drugs, which can lead to faster therapeutic effects, fewer side effects, and improved patient satisfaction. The pulmonary route offers notable advantages for systemic drug delivery, including bypassing first-pass metabolism and enabling rapid absorption—particularly beneficial for compounds with poor oral bioavailability (as discussed in Section 3.1).

Regulatory authorities, such as the FDA, have shifted toward science- and risk-based frameworks that prioritize patient outcomes over rigid compliance checklists [120]. For instance, guidance like SUPAC-IR emphasizes physiologically relevant *in vitro* dissolution testing as a surrogate for *in vivo* bioavailability, especially for highly soluble drugs. This aligns with the broader adoption of Patient-Centric Quality Standards (PCQS), where clinical relevance, therapeutic performance, and real-world patient variability take precedence [131,132]. Within this framework, optimizing dissolution is not just a manufacturing requirement but a critical step in developing effective pulmonary drug products. By improving systemic bioavailability, these innovations can accelerate therapeutic action, minimize side effects, and ultimately enhance patient adherence—fulfilling the core objectives of patient-centric delivery.

Translating these frameworks to novel DPI designs—particularly for non-traditional indications—demands a departure from conventional development paradigms. Central to this evolution is the synergy between particle engineering, device design, and patient behavior, where rapid symptom relief remains a frequently neglected priority in chronic disease therapeutics. As Figure 4 demonstrates, successful patient-centric DPI development emerges from the integration of clinical needs, technical feasibility, and real-world usability— a triad that unlocks new potential for pulmonary delivery, particularly in indications extending beyond classical respiratory applications.

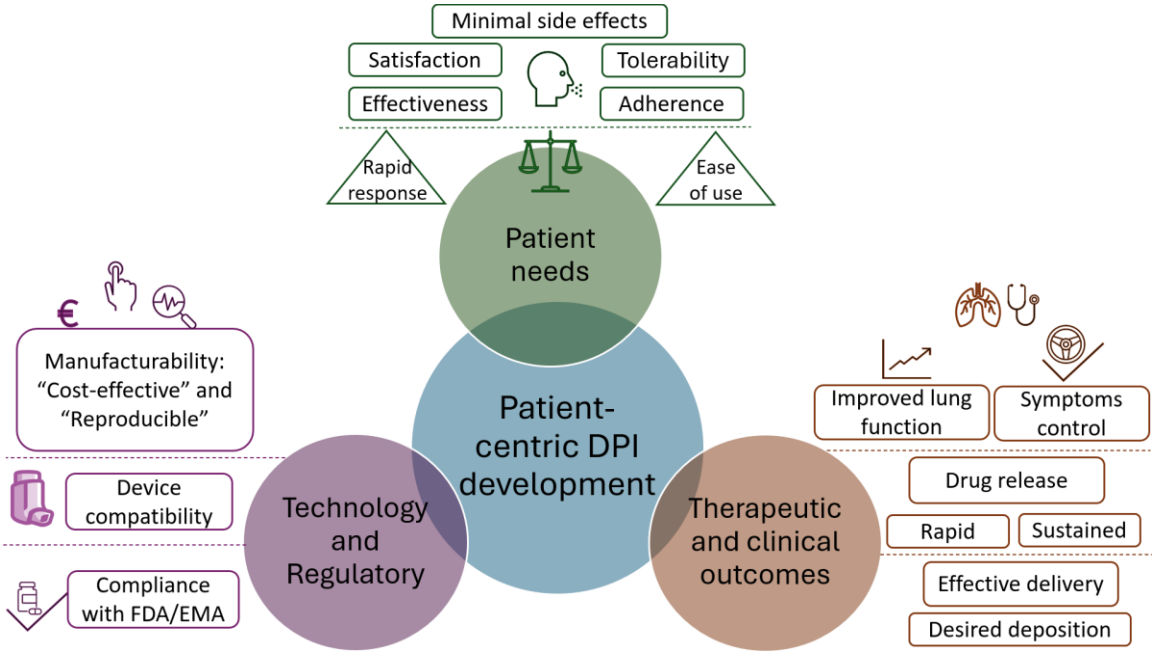

Figure 4: A conceptual framework illustrating the three core pillars of patient-centered DPI development.

4. Materials

4.1. Active pharmaceutical ingredient

KTP, with the IUPAC name *2-(3-benzoylphenyl)propanoic acid*, was used as the primary API (TCI Chemicals, Shanghai, China). Its chemical structure is shown in Figure 5. KTP is an NSAID classified under Biopharmaceutical Classification System (BCS) class II. This class indicates its poor water solubility (51 mg/L at 22 °C) and high permeability (log P = 3.12). It is a propionic acid derivative with a molecular weight (M_w) of 254.28 g/mol, a melting point of 94 °C, and a pKa of 4 [133].

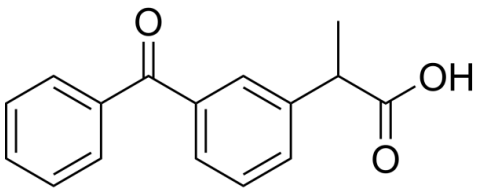

Figure 5: KTP chemical structure [133].

4.2. Excipients

PVA (Mw ~27,000 g/mol; Aldrich Chemistry, Darmstadt, Germany) was employed as a steric stabilizer during the wet media milling process. It adsorbs onto nanoparticle surfaces, providing steric hindrance to prevent uncontrolled aggregation [134,135]. SDS (Mw 288.38 g/mol; VWR Chemicals, Leuven, Belgium) was utilized as a co-stabilizer in the nanosuspension preparation. It acted as an electrostatic stabilizer by imparting surface charge, thereby inducing repulsive forces between particles and enhancing colloidal stability [136–138]. The combination of steric (PVA) and electrostatic (SDS) stabilizers helps maintain nanosuspension stability [96].

D-mannitol (Mw 182.17 g/mol; Molar Chemicals Ltd., Budapest, Hungary) was incorporated as a secondary API in the spray-dried formulation intended for local pulmonary delivery, owing to its muco-active properties. Mannitol is used as a mucolytic agent (Marketed brand name Bronchitol®), particularly as an add-on therapy for CF [139]. Additionally, its role as a formulation excipient was evaluated in the nano spray-dried formulations intended for systemic delivery. L-leucine (Mw 131.17 g/mol; AppliChem GmbH, Darmstadt, Germany) was included as a dispersibility enhancer during spray drying. Leucine is well recognized in pulmonary drug delivery for its ability to improve powder flow properties and aerosolization performance [140,141]. Chemical structures of excipients used are illustrated in Figure 6.

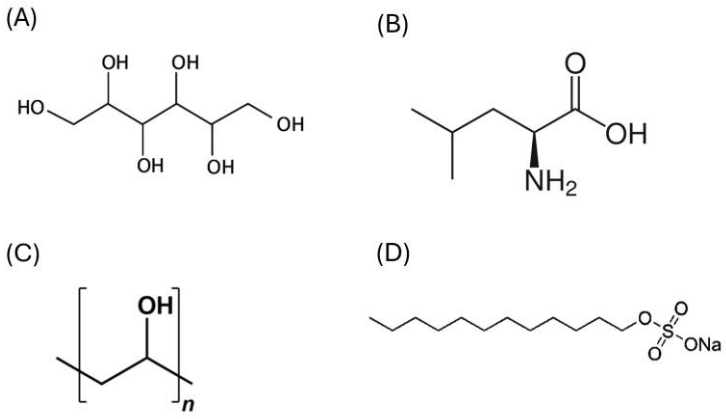

Figure 6: Chemical structures of (**A**) mannitol [142], (**B**) leucine [143], (**C**) PVA [144] and (**D**) SDS [145].

5. Methods

5.1. Production of the nanosuspension by wet media milling

A KTP-containing nanosuspension (KTP-NS) was developed using a two-step process. First, KTP particles were dispersed in an aqueous stabilizing solution and homogenized using an Ultra-Turrax homogenizer (T-25, IKA-Werke, Germany) at 17,000 rpm for 10 minutes. The resulting pre-suspension was then subjected to wet media milling using a planetary ball mill (Retsch PM 100 MA, Retsch GmbH, Haan, Germany). Milling was performed with 20.00 g of 0.3 mm zirconium dioxide (ZrO_2) beads at 400 rpm for 90 minutes in a 50 mL milling chamber. To avoid overheating, a 5-minute cooling pause was implemented every 15 minutes during the milling process. The final drug concentration in the nanosuspension was 10% (w/v), and samples were diluted as required for further analysis or processing.

5.1.1. Selection of the stabilizers

Three different stabilizers were evaluated for their ability to produce stable KTP-NS, each tested at three concentrations: i) HPMC at 0.25, 0.50, and 1.00% (w/v); ii) PVA at 1.00, 2.50, and 5.50% (w/v); iii) Poloxamer 188 at 0.20, 0.50, and 1.00% (w/v). SDS was included in all formulations at a fixed concentration of 0.10% (w/v) to enhance electrostatic stability during the milling process. The resulting nanosuspensions were characterized in terms of particle size, and the most effective stabilizer was selected for further investigations.

5.1.2. Particle size analysis of the nanosuspension

5.1.2.1. Dynamic light scattering

Particle size (PS), polydispersity index (PDI), and zeta potential (ZP) of KTP-NS were measured using a Zetasizer Nano ZS (Malvern Instruments, UK). The refractive index was

set to 1.592. Measurements were performed at 25 °C using disposable folded capillary cells (DTS1070). Each sample was analyzed in triplicate, and the average values were reported.

5.1.2.2. Nanoparticle tracking analysis

The particle size distribution of KTP-NS was determined using the NanoSight NS3000 (Malvern Instruments, UK), equipped with a 565 nm laser, sCMOS camera, and syringe pump (speed: 50). Samples were diluted and analyzed in script control mode at the refractive index for KTP set to 1.592, with three 30-second videos (1500 frames total). Particle size metrics included D[0.1], D[0.5], and D[0.9], while the size distribution span was calculated according to Equation 1.

$$\text{Span} = \frac{\text{D}[0.9] - \text{D}[0.1]}{\text{D}[0.5]} \quad (1)$$

5.1.3. Stability of the nanosuspension

To assess the stability of the KTP-NS prior to the drying process, a short-term stability study was conducted. The nanosuspension was stored at refrigeration temperature (+4 °C) and evaluated for particle size and distribution at predefined time intervals.

5.2. Inhalable ketoprofen-mannitol combination powder: Local delivery

5.2.1. Application of QbD to define the rationale for novel powder combinations

The implementation of QbD enables a rational and systematic formulation strategy to ensure high-quality inhaled therapies from early development [114]. In this study, the QbD framework was applied during the pre-formulation design (Zero Phase) to rationally select and justify the components of the novel inhalable combination [115]. Risk assessment and process parameter analysis were not within the scope of this work. The process began with structured brainstorming to identify the needs, main goals and critical steps in manufacturing. A flowchart was used to outline key challenges in CF and highlight the need for combination inhaled therapies. To further identify factors affecting product quality, an Ishikawa (fishbone) diagram was developed, helping to pinpoint variables influencing CQAs. Based on this analysis, a QTPP was defined, outlining the essential attributes for safety, efficacy, and performance, specifically tailored to inhaled combination therapies for CF.

5.2.2. Formulation of combined DPI using mini spray drying

To achieve local pulmonary targeting, combination powders were prepared using Mini Spray Dryer B-19 (Büchi, Flawil, Switzerland). Spray drying parameters were optimized based on preliminary trials and set as follows: inlet temperature, 90 °C; aspirator setting,

80%; pump rate, 2%; and air flow rate, 600 L/h. For powder preparation, the KTP-NS was diluted to 1% (w/v), and mannitol—used for its mucolytic properties—was incorporated at varying concentrations to determine the highest amount that could be included without adversely affecting the integrity of KTP. Four spray-dried formulations were prepared with mannitol-to-KTP mass ratios of 0, 0.5:1, 1:1, and 2:1, and were named F0, F0.5, F1, and F2 according to their mannitol content. Additionally, a dispersity enhancer (leucine) was included in all formulations at a fixed mass ratio of 1:1 (leucine:KTP) [146].

5.3. Inhalable ketoprofen nanocrystal-based dry powder: Systemic delivery

5.3.1. Optimization of nano spray-drying parameters

Nano Spray Dryer B-90 HP (Büchi, Flawil, Switzerland) equipped with a medium nebulizer was used to engineer KTP-containing nanocrystal agglomerates (NCAs) for targeting systemic effect. The Box-Behnken factorial design (BBD) was employed to optimize the drying parameters, assisted by TIBCO Statistica® 13.4 (Statsoft Hungary, Budapest, Hungary) for experimental design generation. Three independent factors were chosen: pump rate (%) (X_1), inlet temperature (°C) (X_2), and feed concentration (% w/v) (X_3). The effect of these factors on the dependent variables (D[0.5], span, and yield percentage) was investigated at three levels. Temperature was studied at 90, 100, and 110 °C, feed concentration was evaluated at 10% 5% and 2.5% (w/v), while pump percentage was assessed at 10%, 30%, and 50% [147].

5.3.2. Incorporation of mannitol and/or leucine as excipients

Using optimized nano spray dryer parameters, we evaluated the impact of excipients—mannitol (K1M), leucine (K1L), their combination (K1ML), and the absence of excipients (K1)—on the properties of NCAs for pulmonary delivery. The formulations were prepared as detailed in Table 4, mannitol and/or leucine were added accordingly while ensuring a constant total concentration [3,147].

Table 4: Samples annotation, composition and concentration*.

Sample	KTP (% w/v)	Mannitol (% w/v)	Leucine (% w/v)
K1	5.00	0	0
K1M	2.50	2.50	0
K1L	2.50	0	2.50
K1ML	2.50	1.25	1.25

*The concentrations of the samples were maintained to meet the optimized feed concentration of 5% w/v, as determined by the factorial design study.

5.4. Powder characterization

5.4.1. Particle size

5.4.1.1. Dynamic light scattering

Spray-dried powders were re-dispersed in deionized water and analyzed for PS, PDI, and ZP using a Zetasizer Nano ZS (Malvern Instruments, UK), as described in Section 5.1.2.1.

5.4.1.2. Laser diffraction

Laser diffraction was used to assess the particle size and distribution of the spray-dried samples with a Mastersizer Scirocco 2000 device (Malvern Instruments Ltd., UK). A dry dispersion unit was employed with 0.5–1.0 g of powder placed in the feeding tray. The air pressure was adjusted to 3.0 bar with a vibration feed of 75%. Triplicate measurements were performed for each sample. Parameters including D[0.5], and specific surface area (SSA) were evaluated, and the span was calculated as previously defined (Equation 1).

5.4.2. Density measurements

Spray-dried samples were evaluated for tapped and bulk densities using an Engelsmann Stampfvolumeter (Ludwigshafen, Germany). The bulk density (ρb) was determined by accurately weighing the samples and filling them into a 10 cm^3 graduated cylinder, then calculating the mass-to-untapped volume ratio (m/v0). The tapped density (ρt) was measured after 1250 taps and calculated by dividing the mass by the tapped volume (m/vf).

5.4.3. Drug loading, encapsulation efficiency and yield

To calculate drug loading (DL) and encapsulation efficiency (EE), a measured amount of the spray-dried samples was dissolved in 50% (v/v) methanol and analyzed by UV/VIS Spectrophotometer (ATI-Unicam, Cambridge, UK) at 258 nm (Equations 2 and 3). Moreover, percentage yields of dry powder collected after spray drying was calculated (Equation 4).

$$\text{DL}\ (\%) = \frac{\text{Weight of the drug}_{(\text{measured})}}{\text{Total weight of the dry powder}_{(\text{drug + excipients})}} \times 100\% \quad (2)$$

$$\text{EE}\ (\%) = \frac{\text{Weight of the drug}_{(\text{measured})}}{\text{Initial weight of the drug added}} \times 100\% \quad (3)$$

$$\text{Yield}\ (\%) = \frac{\text{Weight of dry powder collected}_{(\text{after spray drying})}}{\text{Weight of the initial solid composition}_{(\text{before spray drying})}} \times 100\% \quad (4)$$

5.4.4. Morphology

The morphology was analysed using a scanning electron microscope (SEM) (Hitachi Scientific Ltd. in Tokyo, Japan). Operating at 10 kV, a sputter coater from Bio-Rad coated

the samples with a gold-palladium layer using 2.0 kV electric potential, 10 mA current, and a 10-minute duration. Air pressure was maintained between 1.3 and 13.0 mPa. Also, the particle size was calculated using ImageJ 1.53e software, with measurements taken from 50 to 100 particles per sample.

5.4.5. Solid-state analysis

Differential Scanning Calorimetry (DSC) and Thermogravimetric Analysis (TGA) were performed using Mettler Toledo DSC 821e and TGA/DSC1 systems, respectively, equipped with STARe software v9.3 (Mettler Inc., Schwerzenbach, Switzerland). Analyses were conducted from 25 °C to 300 °C at 10 °C/min under an argon flow (10 L/h). TGA was coupled to a Thermostar™ GSD 320 quadrupole mass spectrometer (Pfeiffer Vacuum) for residual water analysis.

X-ray Powder Diffraction (XRPD) was carried out using a BRUKER D8 Advance diffractometer (Bruker AXS GmbH, Germany) with Cu Kα1 radiation (λ=1.5406 Å), operated at 40 kV and 40 mA. Scans were recorded over a 3°–40° 2θ range with a step size of 0.01° and step time of 0.1 s. Crystallinity index (Xc) was calculated using OriginPro v9.6.5.1, referencing pure KTP as 100% crystalline (Equation 5).

$$\text{Xc}\ (\%) = \frac{\text{A crystalline}}{\text{A crystalline} + \text{A amorphous}} \times 100\% \quad (5)$$

Fourier-Transform Infrared Spectroscopy (FT-IR) was performed using an AVATAR 330 FT-IR spectrometer (Thermo Fisher Scientific, USA). Samples were blended with dry potassium bromide (KBr) and pressed into pastilles with a Specac® hydraulic press (10-ton force). Spectra were recorded from 4000 to 400 cm^{-1} at 4 cm^{-1} resolution.

Physical mixtures (PMs) corresponding to each sample, alongside individual excipients were also analysed for their solid-state.

5.5. *In vitro* release study

A modified paddle method (Hanson SR8 Plus) using 100 mL vessels and mini paddles assessed KTP release in 50 mL simulated lung fluid (pH 7.4, 37 °C). Spray-dried samples and a PM (represents KTP and stabilizers) were dispersed in SLF, stirred at 50 rpm for 120 min. Aliquots (5 mL) were collected at set intervals, filtered (0.45 µm), and analyzed spectrophotometrically at 258 nm. All tests were run in triplicate. Full method is detailed in our papers [3,146].

5.6. Aerosol performance

5.6.1. Andersen cascade impactor

The aerosolization performance was evaluated using an Andersen Cascade Impactor (ACI, Copley Scientific Ltd., UK) at 60 L/min airflow, generated by a high-capacity pump and verified by a mass flow meter (DFM 2000, Copley Scientific Ltd.). Samples were filled in HPMC capsules and administered via a Breezhaler® device (Novartis AG, Switzerland) with a 4-second inhalation. Post-inhalation, KTP was recovered by 50% methanol and quantified spectrophotometrically at 258 nm. Key aerodynamic parameters were calculated including: MMAD (Mass Median Aerodynamic Diameter), FPF (Fine Particle Fraction), GSD (Geometric Standard Deviation), and EF (Emitted Fraction).

5.6.2. Aerodynamic particle sizer

Aerodynamic characterization was further evaluated by Aerodynamic Particle Sizer (APS 3321; TSI Inc., Shoreview, MN, USA). The setup included an induction port, a high-capacity vacuum pump (HCP5), and a critical flow controller (TPK 2000) (all from Copley Scientific Ltd., UK). Inhalation was simulated using a rectangular breathing waveform (4 s, 60 L/min). Three size-based parameters were analyzed: number particle size, surface particle size, and volume particle size. Detailed method was reported in our paper [147].

5.6.3. *In silico* modeling

The latest Stochastic Lung Model (SLM) was used to estimate regional drug deposition in the respiratory tract via Monte Carlo simulation (~10^5 particles) [148]. Inputs included particle properties and inhalation parameters: 69.5 L/min peak flow, 1.7 L volume, and 2.04 s inhalation time. Deposition fractions were expressed as lung deposition (bronchial + acinar), extra-thoracis, and exhaled percentage. Simulations also evaluated breath-hold (BH) effects at 5 and 10 s [147].

5.7. Viscosity measurement

Viscosity was assessed to evaluate potential effects on respiratory mucus properties, relevant to the management of pulmonary diseases. Type II mucin from porcine stomach (Sigma-Aldrich) — the primary glycoprotein in respiratory mucus involved in airway defense and drug transport [149] — was prepared at various concentrations, mixed with spray-dried samples, and stirred for 30 min. Viscosity was measured at 37 °C using a Rotavisk viscometer (IKA-Werke GmbH & Co. KG, Germany) equipped with spindle SP-11 at 120 rpm for 30 s. Sample tested in triplicate, and results reported as mean ± SD.

5.8. Anti-inflammatory effect

Anti-inflammatory activity was assessed using A549 (alveolar epithelial) and U937 (human pro-monocyte) cells (ATCC, Manassas, VA, USA). A549 cells were cultured in MEM and U937 cells in RPMI, both supplemented with 10% FBS, gentamicin, glucose, L-glutamine, and HEPES. Cells (1×10^6/well) were seeded into 6-well plates (n=3/group), treated with Lipopolysaccharides (LPS) and either raw KTP or spray-dried samples, and incubated for 48 h at 37 °C with 5% CO_2. LPS-only and untreated cells served as positive and negative controls, respectively. mRNA extraction, cDNA synthesis, and qPCR analysis of IL-6 expression were performed as detailed in our published paper [146].

5.9. Cell line measurements

5.9.1. Cell culture

Two cell lines were used, alveolar (A549) and bronchial (CFBE), and were cultured at 37 °C with 5% CO_2 in their respective supplemented media. For co-culture, endothelial cells were seeded at 8×10^4 cells/cm² on the underside of 3 µm PET membrane inserts pre-coated with collagen, followed by A549 or CFBE cells on the upper surface. For assays, raw KTP and spray-dried samples were dispersed in culture medium or Ringer-HEPES buffer (pH 7.4) containing 1% FBS, sonicated, and adjusted to 0.5 mg/mL before dilution. Full methods are detailed in our published papers [3,90].

5.9.2. Cell viability

The response of alveolar and bronchial epithelial cells to raw KTP and spray-dried samples was assessed via real-time impedance measurements at 10 kHz using the RTCA-SP system (ACEA Biosciences, San Diego, CA). For baseline readings, 50 µL of culture medium was added to collagen-coated E-plate 96 wells with integrated gold electrodes, followed by seeding 5×10^3 cells/well. At confluence, cells were exposed to raw KTP or spray-dried samples at 50, 300, and 500 µg/mL for 48 h. Triton X-100 ((TX), 10 mg/mL) served as a cytotoxic control. Full method is detailed in our papers [3,90].

5.9.3. Permeability measurement

Permeability was assessed using 12-well plate inserts with Ringer-HEPES buffer in the donor (0.5 mL) and acceptor (1.5 mL) compartments. Raw KTP or spray-dried samples were added to the donor side, and inserts were shaken at 120 rpm for 60 minutes. KTP concentrations were quantified spectrophotometrically at 258 nm, and apparent permeability coefficients (P_{app}) were calculated according to Equation 6.

$$P_{app}\ (cm/s) = \frac{\Delta[C]_A \times V_A}{A \times [C]_D \times \Delta t} \quad (6)$$

Transepithelial electrical resistance (TEER), marker molecule permeability assays, and immunocytochemistry were conducted to assess the integrity of intercellular junctions and confirm that barrier function remained intact post-permeability testing. Detailed methods are provided in our published papers [3,90].

5.10. *In vivo* pharmacokinetics

5.10.1. Animal model

Healthy 7-week-old male Sprague-Dawley rats (226 ± 18 g) were used. Animals were housed under standard laboratory conditions with food and water ad libitum. All procedures were approved by the *Hungarian Ethical Committee for Animal Research (IV./2706/2024)* and complied with FELASA recommendations.

5.10.2. Administration and sampling protocol

Rats (n = 48) were divided into oral (n = 4/group) and inhalation (n = 20/group) groups. Oral groups received either raw KTP unprocessed suspension (KTP-RAW) or nanosuspension (KTP-NS) by gavage. Inhalation groups received dry powders (K1 or K1ML) via intratracheal insufflation under sevoflurane anesthesia using a Penn-Century DP-4 insufflator. All animals received 3 mg/kg KTP. Blood and lung samples were collected at 15, 30, 60, 120, and 360 min post-dose.

5.10.3. UHPLC-MS/HRMS analysis for quantification

KTP concentrations in lung and plasma were quantified by UHPLC-MS/HRMS (Waters Acquity I-Class UPLC–Thermo Orbitrap Exploris 240) in PRM mode. Full method is detailed in our paper [3].

5.10.4. Pharmacokinetic analysis

Non-compartmental analysis was performed using Phoenix WinNonlin 8.5.2.4, applying the sparse sampling method. Key pharmacokinetic (PK) parameters (C_{max}, t_{max}, $AUC_{0–6}$, $AUC_{0–\infty}$, k_e, $t_{½}$) were determined from the concentration-time profiles. Relative bioavailability (F) and tissue availability (f_t) were also determined as follows:

$$F\ (\%) = \frac{AUC_{0-\infty\ (\text{intratracheal})}}{AUC_{0-\infty\ (\text{Oral})}} \times \frac{Dose_{(\text{oral})}}{Dose_{(\text{intratracheal})}} \tag{7}$$

$$f_t = \frac{AUC_{0-6\ (\text{lung})}}{AUC_{0-6\ (\text{plasma})}} \tag{8}$$

5.11. Safety and tolerance in sensitized rats

5.11.1. Animal model

Six-week-old male (n=24) and female (n=24) Wistar rats were housed under standard conditions with ad libitum access to food and water. All procedures complied with EU Directive 2010/63/EU and national regulations and were approved by the *Hungarian authorities (No. XXXII./1576/2024)*. The study followed ARRIVE guidelines.

5.11.2. Allergen-sensitized animal model

Allergen sensitization was employed based on a previously published method [150]. In brief, rats received an intraperitoneal injection of ovalbumin (OVA, 1 mg) with aluminum hydroxide (50 mg) on day 0, followed by daily inhalation of aerosolized OVA (25 mg/mL, 15 min) from days 14 to 21.

5.11.3. Treatment protocol and animal grouping

Rats were divided into five groups: three OVA-sensitized and treated with K1, K1ML, or placebo (spray-dried stabilizer), one positive control (OVA-sensitized, untreated), and one negative control (non-sensitized, untreated). Intratracheal treatments were administered every third day (days 0–14) and every other day (days 14–21).

5.11.4. Measurement of respiratory mechanics and lung responsiveness

End-expiratory lung volume (EELV) was measured using whole-body plethysmography, with box and tracheal pressures recorded during 15 s end-expiratory occlusion at positive end-expiratory pressure (PEEP) levels of 0, 3, and 6 cmH_2O, based on the Boyle-Mariotte law [151]. Respiratory impedance was assessed using the forced oscillation technique, quantifying airway resistance (Raw), tissue damping (G), and elastance (H) [152–154]. Airway hyperresponsiveness was evaluated via bronchoprovocation with methacholine (MCh) and ovalbumin (OVA), as described in our previous study [3].

5.12. Stability study

Stability testing was conducted in a Binder KBF 240 chamber at 40 ± 2 °C/75 ± 5% relative humidity (RH) per ICH guidelines. Formulations placed in HPMC capsules were assessed over 3 months, with samples taken at 0, 1, and 3 months, as detailed in [90,147].

5.13. Statistical Analysis

GraphPad Prism 8.0.1 (CA, USA) was employed using a two-way ANOVA test, with significant values at $p \leq 0.05$. All data was expressed as mean ± SD.

6. Results and discussion

6.1. Nanosuspension characterization

6.1.1. Stabilizer selection

Stabilizer effects were assessed via dynamic light scattering (DLS) (Table 5). HPMC led to the largest PSs (~450–2570 nm) and highest PDIs, indicating poor stabilization. Compared to PVA, poloxamer 188 showed good zeta potential but larger particles. PVA provided the smallest PS and lowest PDI, especially at 1% (w/v), therefore; it was selected for this study. Combining PVA and SDS optimized stability, leveraging PVA's wettability enhancement and SDS's electrostatic repulsion [155].

Table 5: A preliminary study of KTP-NS using different stabilizers and concentrations. All stabilizers were combined with 0.1% SDS [146].

Stabilizer	Conc (w/v)	PDI	PS (nm)	ZP (mV)
HPMC	0.25	0.454 ± 0.11	2570.0 ± 42.6	−5.50 ± 1.34
	0.5	0.739 ± 0.02	764.3 ± 2.79	−8.10 ± 4.24
	1	0.319 ± 0.03	453.0 ± 4.15	−6.20 ± 2.87
PVA	1	0.082 ± 0.01	238.3 ± 1.37	−9.97 ± 5.31
	2.5	0.227 ± 0.04	316.4 ± 1.91	−11.60 ± 2.75
	5	0.205 ± 0.02	431.4 ± 3.16	−4.22 ± 0.23
Poloxamer 188	0.2	0.428 ± 0.14	583.2 ± 12.6	−13.10 ± 1.18
	0.5	0.213 ± 0.05	3112.1 ± 36.4	−25.20 ± 3.17
	1	0.321 ± 0.16	415.7 ± 13.1	−17.50 ± 2.94

6.1.2. Nanosuspension stability

Although DLS is commonly used for particle sizing, it tends to overrepresent larger particles [156]. To overcome this, nanoparticle tracking analysis (NTA) was used, providing more accurate size distribution by tracking individual particle motion [157]. NTA results were as follows: D[0.1]: 119.60 ± 3.30 nm, D[0.5]: 168.70 ± 4.00 nm, D[0.9]: 230.80 ± 11.70 nm, with a span of 0.659 ± 0.024. Short-term stability over 45 days at +4 °C showed a slight D[0.5] increase (+29 nm, $P \leq 0.001$) but stable span, indicating minimal aggregation [94]. Thus, the nanosuspension was deemed suitable for dry powder production [146,147].

6.2. Powder combinations for local pulmonary delivery assessments

6.2.1. QbD approach for combined DPI development

A flowchart was employed to highlight challenges in CF treatment and the rationale for developing multi-drug inhaled therapies (Figure 7). Current single-agent treatments, such as TOBI® (tobramycin) for infection and Bronchitol® (mannitol) for mucus clearance, address limited aspects of CF pathology. NSAIDs (e.g., KTP) offer anti-inflammatory benefits and may slow disease progression [158]. While some combinations of antibiotics and mucolytics have been explored [159–161], NSAID-mucolytic combinations remain unexplored.

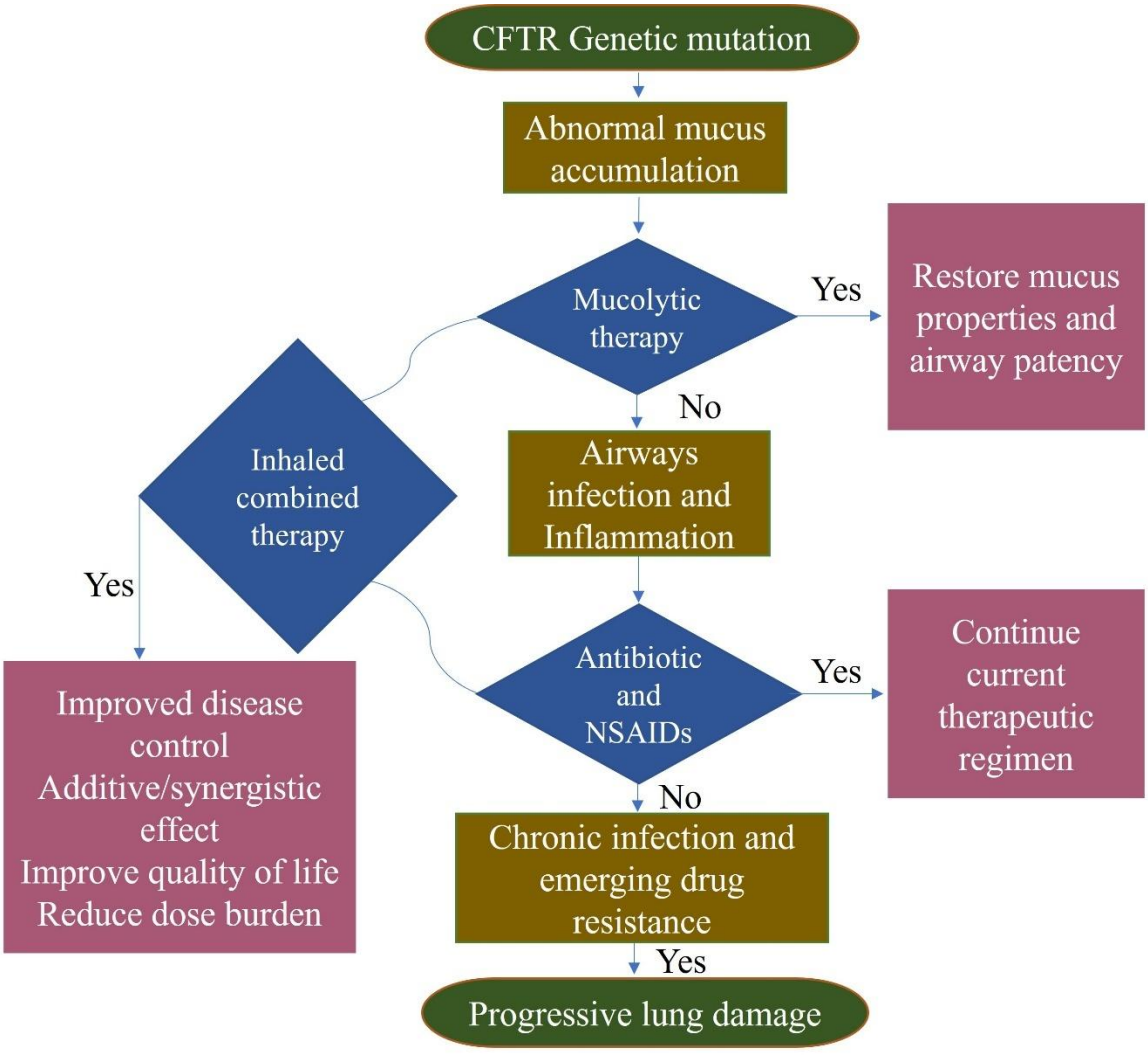

Figure 7: Flowchart illustrating the pathophysiological cascade of CF and current treatment strategies, highlighting the potential role of novel inhaled combination therapies (e.g., mucolytics, antibiotics, and NSAIDs) in enhancing airway clearance, controlling infection, improving clinical outcomes and reducing dose burden. CFTR: Cystic fibrosis transmembrane conductance regulator. Adapted from [1], with slight modifications.

Furthermore, an Ishikawa (fishbone) diagram—a tool used to identify key factors influencing product quality—was employed to support the development process (Figure 8). This diagram mapped critical elements affecting inhaled combination therapies, based on extensive literature and prior studies of pulmonary drug combinations [162–164]. Its design incorporated established scientific knowledge, considering therapeutic goals, API selection, development stages, and final product profiles.

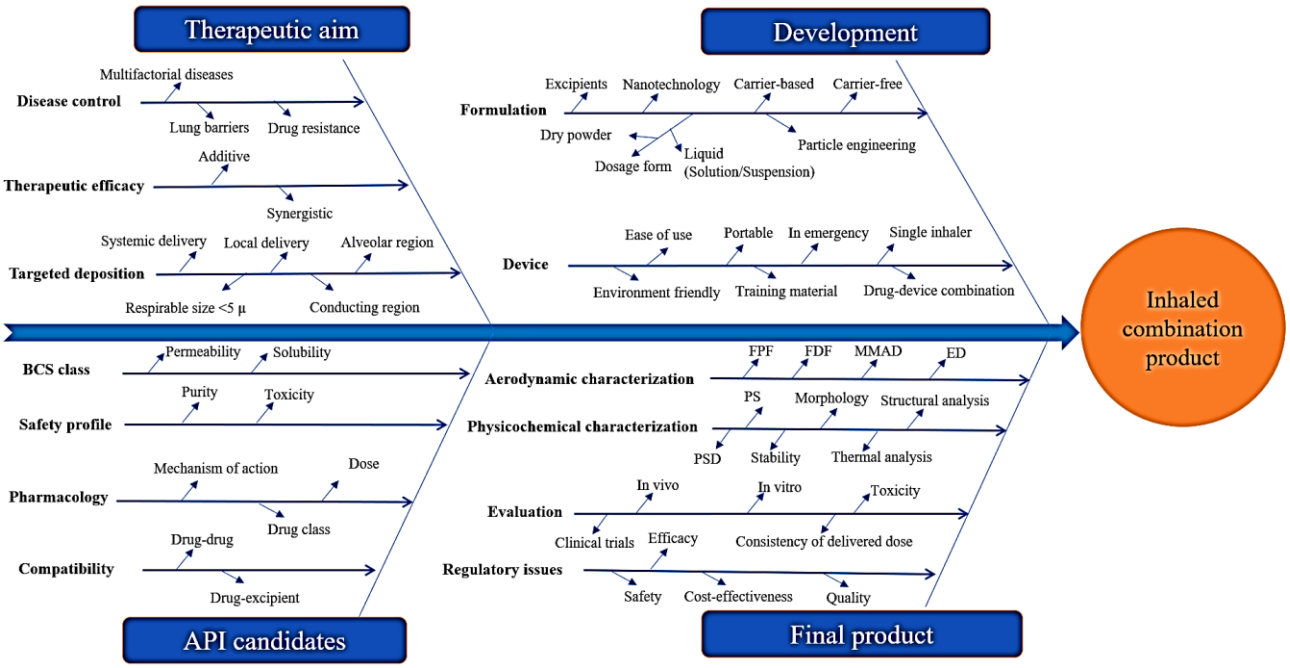

Figure 8: Fishbone diagram defining factors affecting the development of combined products for inhalation [1].

The Ishikawa diagram supported the definition of the QTPP for combination therapies, such as KTP–mannitol (Table 6). Based on the QTPP, key CQAs were identified, including formulation technique, deposition site, particle size, aerosol performance, drug compatibility, and stability. Accordingly, spray-dried KTP–mannitol combinations were prepared and characterized to align with the defined QTPP.

The proper application of a QbD approach from the early development phase offers clear advantages in inhaled combination therapy development, including: (i) enhanced production capability, (ii) more efficient use of development time and resources, (iii) reduced product variability and defects, and (iv) a smoother FDA submission and approval process.

Table 6: QTPP of KTP-mannitol combination for inhalation as dry powders [1].

QTPP	Target	Justification	Reference
Route of administration	Pulmonary	Enables direct lung targeting with rapid onset and reduced systemic side effects.	[165]
Dosage form	Inhalable powder	Offers high stability and allows higher drug loading.	[166]
Delivery target	Local/systemic	Inhalation enables both local targeting (e.g., for inflammation) and systemic absorption via alveolar transfer.	[29,167]
Formulation design	Carrier or carrier-free	Allows flexibility using traditional carriers or advanced particle engineering.	[168]
Device	Capsule or non-capsule based	Both formats are feasible for pulmonary delivery.	[169,170]
Deposition site	Conducting/alveolar zone	Site selection depends on drug action and disease localization.	[171]
Therapeutic effect	Synergistic/additive	Combining drugs may enhance efficacy through synergy or additive effects.	[172,173]
Particle size	<5 µm	Required for deep lung deposition.	[33]
Morphology	Spherical/corrugated	Corrugated particles improve lung deposition.	[17,18]
Compatibility	Drug-drug, drug-excipient, drug-device	Ensures stability and safety across formulation components.	[174]
Dissolution	Rapid	Minimizes mucociliary clearance and enhances bioavailability.	[175]
Stability	No agglomeration or size change	Maintains consistent delivery performance.	[176]
Density	ρb < 0.3 g/mL, ρt <0.4 g/mL	Improves lung deposition.	[15,16]

ρ_b: bulk density, ρ_t: tapped density.

6.2.2. Particle size and density

Table 7 shows that our particle engineering strategies were effective, as spray drying did not significantly increase KTP particle size, indicating good redispersibility and minimal aggregation. ZP values outperformed previous PVA-stabilized formulations for pulmonary delivery [177]. The highest PDI was observed in the mannitol-free sample (F0), suggesting that mannitol improved dispersity.

Furthermore, our formulations had low tapped densities (0.18–0.22 g/cm³) (Table 7), which are optimal for pulmonary delivery [178–180].

Table 7: Characteristics of spray-dried samples (F0-F2), including yield (%), drug loading (DL), particle size (DLS), density measurements, aerodynamic characteristics (ACI), and viscosity measurement [146].

Analysis	Parameter	F0	F0.5	F1	F2
Yield (%)	Yield (%)	52.95 ± 3.54	54.86 ± 6.12	57.29 ± 1.98	58.68 ± 9.73
Drug content	DL (%)	57.47 ± 1.44	84.12 ± 2.91	84.87 ± 7.13	84.72 ± 3.65
Particle size (DLS)	PS (nm)	204.9 ± 3.07	222.5 ± 4.11	240.7 ± 6.32	251.4 ± 2.84
	PDI	0.336 ± 0.003	0.127 ± 0.021	0.064 ± 0.008	0.156 ± 0.039
	ZP (mV)	−8.88 ± 0.27	−12.3 ± 0.43	−7.44 ± 0.18	−11.9 ± 0.33
Density	ρt (g/mL)	0.180 ± 0.002	0.192 ± 0.011	0.201 ± 0.009	0.228 ± 0.052
	ρb (g/mL)	0.124 ± 0.012	0.123 ± 0.003	0.120 ± 0.031	0.139 ± 0.024
Aerosol performance	MMAD (µm)	2.40 ± 0.17	2.80 ± 0.06	4.51 ± 0.41	4.90 ± 0.16
	FPF <5 (%)	56.16 ± 2.51	71.02 ± 1.19	64.32 ± 1.34	32.21 ± 3.67
	EF (%)	97.06 ± 3.22	96.60 ± 1.65	94.82 ± 2.79	95.70 ± 2.89
Rheology	Viscosity (Pa.s)	0.033 ± 1.98	0.031 ± 2.12	0.025 ± 1.37	0.030 ± 4.19

DLS: dynamic light scattering, PS: particle size, PDI: polydispersity index, ZP: zeta potential, ρt: tapped density, ρb: bulk density, MMAD: mass median aerodynamic size, FPF: fine particle fraction and EF: emitted fraction.

6.2.3. Drug loading and yield

Spray-dried samples showed yields of 53–59% (Table 7). Increasing mannitol concentration positively affected the yield by reducing cohesive forces between particles, as low spray-drying yields are often associated with particle cohesion [181]. These yields surpass those reported in similar spray-drying studies [182–184].

DL ranged from 57% to 85%, with no significant impact from mannitol concentration (F0.5–F2).

6.2.4. Morphology

Figure 9 shows SEM images of spray-dried samples (F0–F2), revealing nearly spherical particles with corrugated rough surfaces. Spherical shapes offer stability for pulmonary delivery [185], while rough surfaces improve lung deposition by increasing contact angles and enhancing cell attachment [17,18].

Particle sizes, measured by ImageJ, revealed that mannitol-free sample (F0) had the smallest size, but increasing mannitol content (F0.5–F2) had no significant effect on particle size.

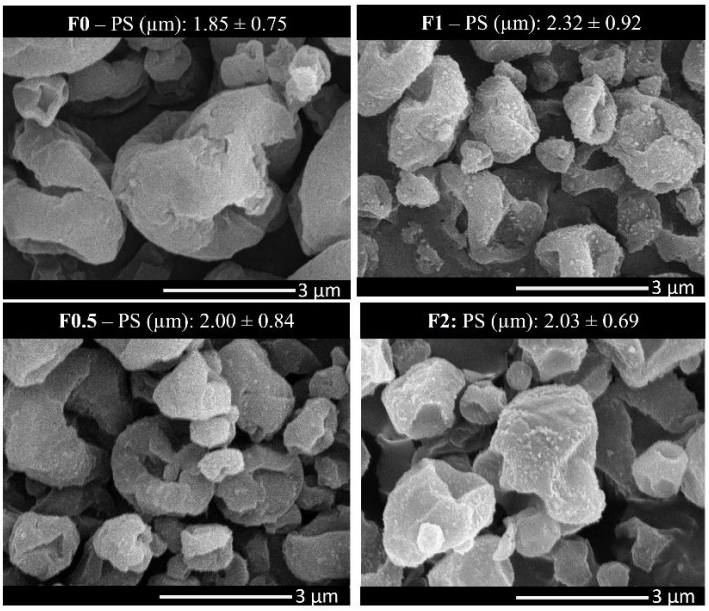

Figure 9: Morphology images using scanning electron microscope (SEM) of spray-dried samples with the diameter of final product measured by Image-J software. PS: particle size [146].

6.2.5. Solid-state analysis

DSC thermograms showed a sharp endothermic peak for raw KTP at 97.83 °C, indicating its crystalline nature (Figure 10A). In formulations, KTP's melting point shifted to ~90 °C, reflecting nanosizing effects and increased amorphous content. Mannitol exhibited a distinct peak at 171.33 °C, confirming its crystalline form. In samples F0.5, F1, and F2, mannitol retained crystallinity, with melting peaks observed at 152.17 °C, 154.50 °C, and 155.83 °C, respectively. The presence of crystalline mannitol is advantageous, since it contributed to improved *in vitro* dissolution and diffusion profiles in pulmonary delivery [186,187]. Increasing mannitol also reduced KTP peak intensity and broadened its thermal signal, suggesting reduced crystallinity—consistent with previous findings [188]. Overall, the results support the compatibility of KTP–mannitol combinations.

Furthermore, DPI formulations require low moisture for effective aerosolization. TGA analysis showed residual water content of 1.08–2.12% in our samples (results not shown), lower than values reported in previous studies [189,190].

XRPD was used to assess crystallinity (Figure 10B). Raw KTP showed sharp peaks at 5.79°, 12.9°, 14.20°, 17.12°, 18.30°, and 21.83° 2θ, confirming its crystalline nature. All formulations (F0–F2) showed lower-intensity KTP peaks, indicating partial amorphization. Crystallinity percentages of KTP were 60.30% (F0), 44.54% (F0.5), 41.96% (F1), and 28.36% (F2), confirming that increasing mannitol content reduced KTP crystallinity, consistent with DSC results.

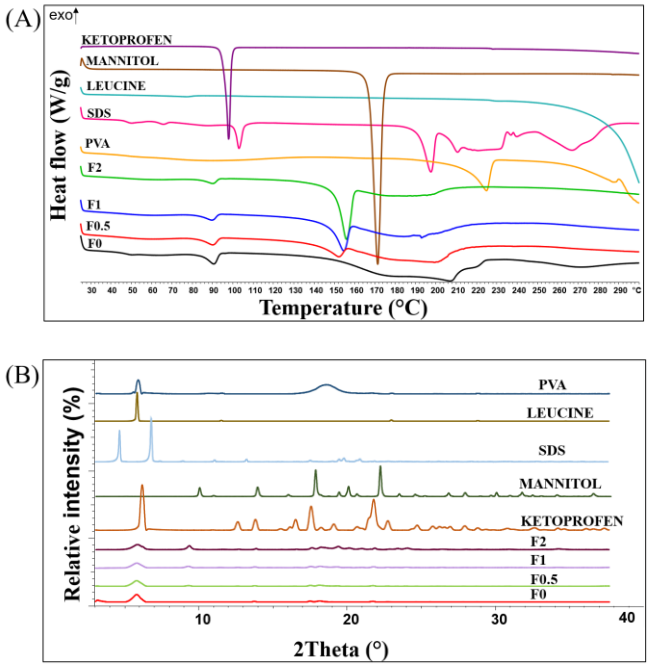

Figure 10: Thermal and structural analysis of raw materials and spray-dried samples analysed by (**A**) DSC (**B**) XRPD [146].

6.2.6. *In vitro* release study

In vitro dissolution in simulated lung fluid (pH 7.4) showed ~80% KTP release from spray-dried samples within 5 min, compared to 40% from the PM (Figure 11). This improvement is mainly due to nanosized KTP, while mannitol's wettability also enhanced disintegration and drug release [191]. F1 showed the fastest release (~100% in 10 min), whereas both lower (F0.5) and higher (F2) mannitol concentrations reduced this effect, highlighting the need for precise optimization of mannitol concentration, which is crucial for maximizing the therapeutic potential and performance of this combination.

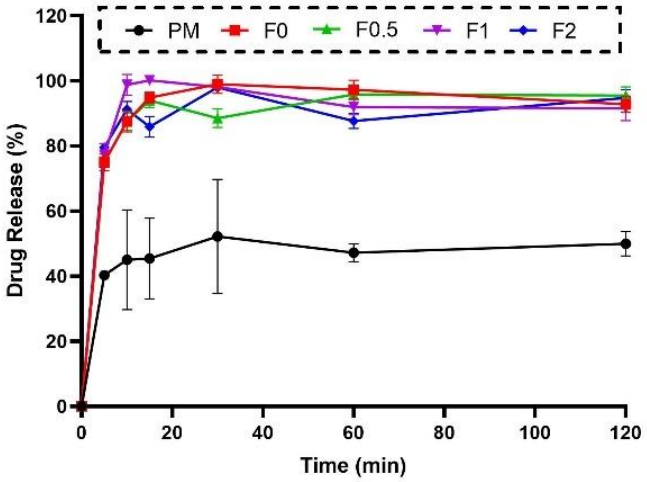

Figure 11: *In vitro* release study of physical mixture (PM) and samples F0, F0.5, F1 and F2 in simulated lung media (SLM). Results are expressed as mean ± SD (n=3) [146].

6.2.7. *In vitro* aerosol performance

Aerodynamic evaluation using ACI confirmed the suitability of all samples for pulmonary delivery (Table 7). Increasing mannitol content increased the MMAD, while maintaining high FPF of 71.02% for F0.5 and 64.32% for F1—values exceeding some marketed products [192]. All samples met the EF criteria (95–97%) [182]. Deposition data (Figure 12) showed that F0.5 and F1 favored deeper lung regions (stages 3 and 4), whereas the high mannitol formulation (F2) deposited mainly in the USP induction port and ACI inlet cone, indicating predominant extra-thoracic deposition. The mannitol-free sample (F0) also showed high deposition in the USP induction port and filter. These findings highlight that both the inclusion and concentration of mannitol significantly influence deposition behavior and optimal lung targeting.

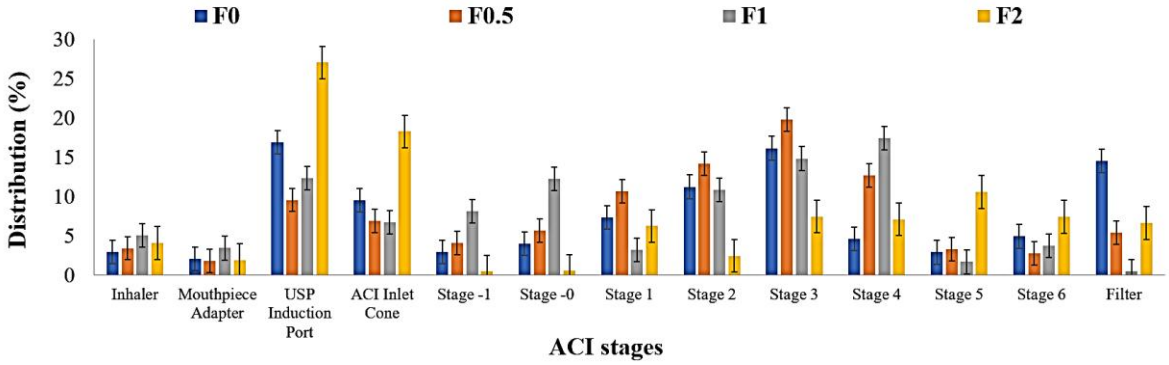

Figure 12: *In vitro* aerodynamic distribution of spray-dried samples at a flow rate of 60 L/min. Results are expressed as mean ± SD (n=3) [146].

6.2.8. Viscosity measurement

Viscosity abnormalities contribute to many respiratory diseases [193], so we assessed our formulations' effect on mucin viscosity (Table 7). Mucin solutions were prepared at 2%, 5%, and 10% based on previous studies [194–196]. The 2% solution was too dilute to measure, while 5% and 10% had viscosities of 0.019 and 0.035 Pa·s, respectively—within the range reported in CF and COPD patients [197,198]. Consequently, 10% mucin (0.035 ± 5.44 Pa·s) was selected for testing. Among all formulations, only F1 resulted in a notable viscosity reduction. This effect may be attributed to the optimal mannitol concentration in F1, which enhances mucin hydration.

These findings suggest a concentration-dependent mechanism, where mannitol at an appropriate level facilitates mucus thinning—a key therapeutic goal in conditions like CF. Thus, F1 represents a promising formulation, meriting deeper exploration for its mucolytic

potential in combination with KTP. Accordingly, F1 was selected for continued evaluation, with F0 serving as a reference.

6.2.9. Anti-inflammatory effect

We assessed IL-6 expression in LPS-stimulated A549 and U937 cells to evaluate the anti-inflammatory effects of our formulations. LPS, a proinflammatory trigger [199], induced IL-6—a key cytokine in pulmonary inflammation [200]. U937 cells, known for strong IL-6 response due to high COX-2 expression [201,202], showed significantly higher IL-6 levels than A549 cells (15.5 vs. 3.4, $p < 0.01$).

All samples significantly reduced IL-6 in U937 cells (Figure 13A), and mannitol did not impair this effect, confirming a promising KTP-mannitol combination. In contrast, no reduction was observed in A549 cells (Figure 13B), aligning with previous findings [203].

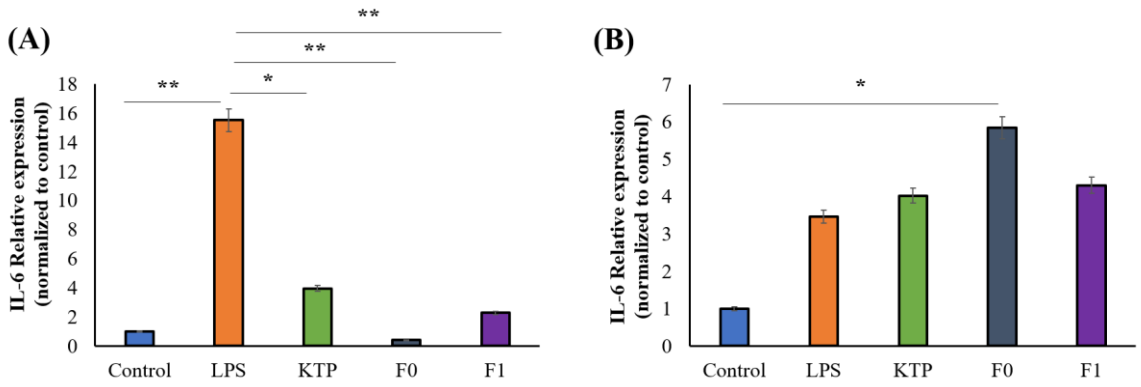

Figure 13: Relative expression of IL-6 on two cell lines; (**A**) U937 and (**B**) A549. Control is the untreated cell line, LPS is the treated cell line, raw KTP, F0, F0.5, F1 and F2 are treated with LPS. Results are expressed as mean ± SD (n=3). Level of significance: *$p < 0.05$, **$p < 0.01$ [146].

6.2.10. Cell line evaluation

6.2.10.1. Cell viability

To ensure pulmonary safety, cell viability was assessed using real-time impedance measurements. In A549 cells, only sample F1 slightly reduced impedance at high concentrations (Figure 14A), while both F0 and F1 had no effect on CFBE cells (Figure 14B), indicating good biocompatibility across formulations and nearly all concentrations which is consistent with previously published findings [204].

Accordingly, KTP concentration of 50 µg/mL was selected for permeability studies.

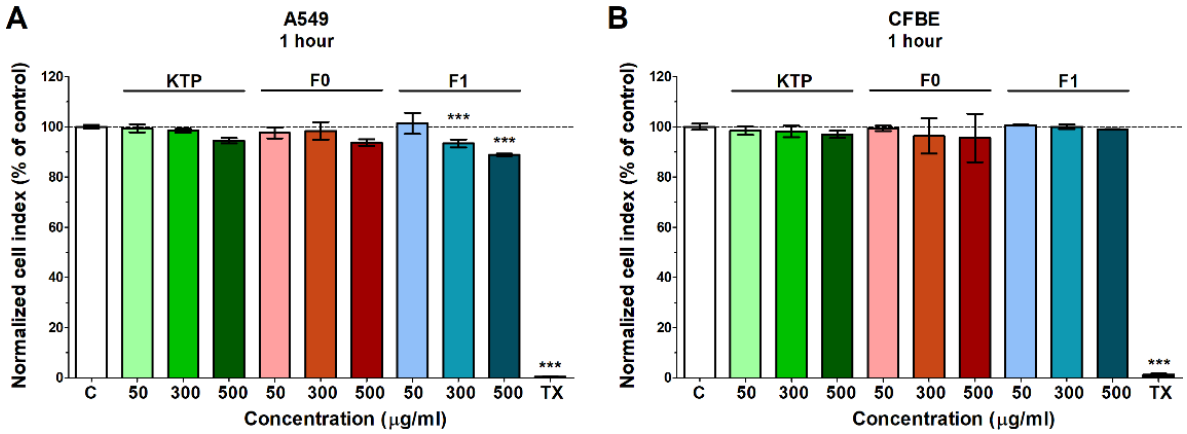

Figure 14: Cell viability of (**A**) A549 alveolar and (**B**) CFBE bronchial epithelial cells after 1-h treatments with raw KTP and spray-dried samples F0, F1 measured by impedance. Values are presented as means ± SD, n = 5–6. *** $p < 0.001$ compared to the C (control group) [90].

6.2.10.2. Cell permeability

Permeability was evaluated in A549 and CFBE cells at 30 and 60 min (Figure 15). KTP showed lower permeability across bronchial (CFBE) than alveolar (A549) barriers, likely due to cell line nature differences [205]. Both F0 and F1 improved KTP permeability in the alveolar model, with F1 enhancing it 1.4-fold at 30 min—possibly due to mannitol's effect on particle surface or epithelial interaction, facilitating better permeation [206].

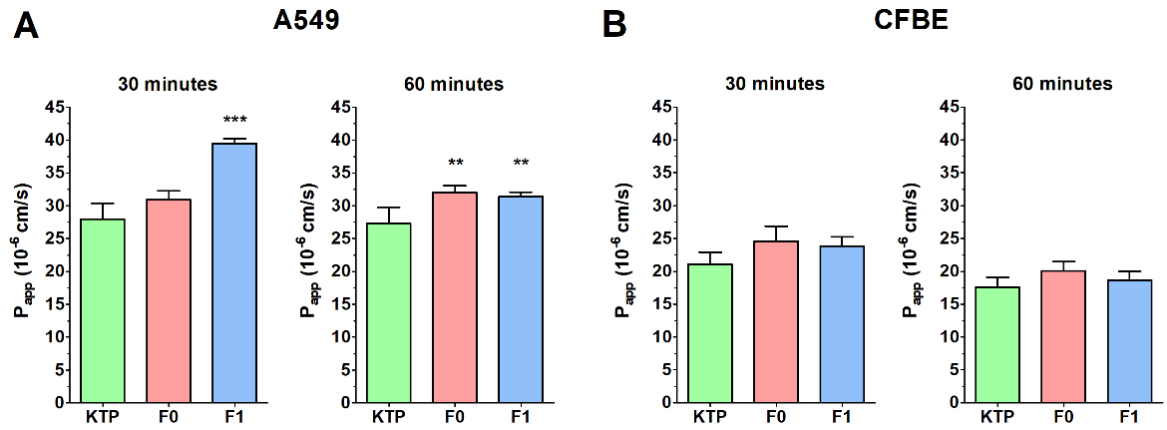

Figure 15: Permeability of raw KTP, F0, and F1 (50 µg/mL KTP concentration in the donor compartment) across the co-culture model of (**A**) alveolar epithelial cells and (**B**) bronchial epithelial cells after 30- and 60-min assay time. Values are presented as means ± SD, n = 4. ** $p < 0.01$, *** $p < 0.001$ [90].

Barrier integrity was confirmed by TEER measurements and permeability assays using sodium fluorescein and Evans Blue-labeled albumin, with no observed morphological changes in cell–cell junctions (results not shown) [90].

Hence, this study confirms that combining mannitol and KTP in 1:1 mass ratio as a single DPI is promising for targeting pulmonary inflammations and simultaneously improving cell diffusion and mucus clearance.

6.3. Nanocrystal-based dry powder for systemic delivery evaluations

6.3.1. Factorial design

A BBD was used to optimize the nano spray-drying process by varying pump rate, inlet temperature, and feed concentration across 15 runs. Key responses—median particle size (D[0.5]), span, and yield—were analyzed using Pareto charts and 3D surface plots (Figure 16) [147]. Since D[0.5] and span are critical for pulmonary delivery performance, they were prioritized. Increasing pump rate reduced D[0.5] and span due to finer atomization [207], while higher feed concentrations increased particle size [208]. Low feed concentrations led to broader spans, indicating poor droplet stability. Higher inlet temperatures (100–110 °C) caused particle aggregation and size growth [106], whereas 90 °C produced smaller, more uniform particles. Based on these findings, optimal conditions—50% pump rate, 90 °C inlet temperature, and 5% feed concentration—were selected to produce mannitol- and/or leucine-based NCA formulations.

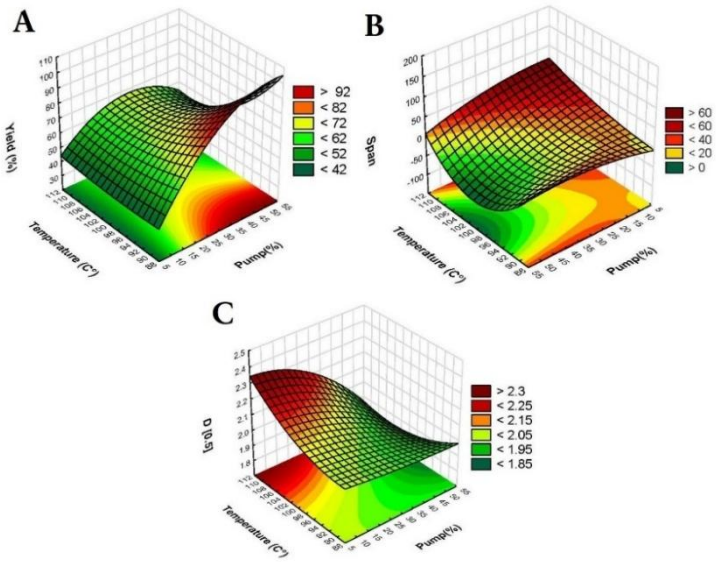

Figure 16: 3D surface plots of the effect of temperature (°C) and pump (%) on (**A**): yield (%), (**B**): span and (**C**): D[0.5] [147].

6.3.2. Particle size and density

Following process optimization, laser diffraction (Table 8) showed K1 had a D[0.5] of 1.708 ± 0.074 µm. Adding leucine (K1L) slightly increased size (1.893 ± 0.017 µm) due to droplet stabilization during drying [209], while mannitol (K1M) led to larger particles (3.337 ± 0.190 µm) from its high crystallinity [210]. The combination (K1ML) yielded an intermediate size (2.046 ± 0.064 µm). Compared to K1, Leucine and/or mannitol also reduced span values, suggesting more uniform particles and potentially better lung deposition.

Table 8: Characteristics of NCAs, including particle size (laser diffraction), drug loading (DL), encapsulation efficiency (EE), density measurements, and aerodynamic performance assessed by ACI [3,147].

Analysis	Parameter	K1	K1M	K1L	K1ML
Particle size	D[0.5]	1.708 ± 0.074	3.337 ± 0.190	1.893 ± 0.017	2.046 ± 0.064
	span	1.412 ± 0.071	1.390 ± 0.118	1.372 ± 0.070	1.387 ± 0.008
	SSA (m^2/g)	3.945 ± 0.247	2.09 ± 0.156	3.56 ± 0.001	3.290 ± 0.057
Drug content	DL (%)	41.38 ± 3.54	26.24 ± 6.12	30.08 ± 1.98	20.55 ± 9.73
	EE (%)	84.83 ± 1.44	80.04 ± 2.91	91.73 ± 7.13	83.24 ± 3.65
Density	ρt (g/mL)	0.225	0.097	0.225	0.34
	ρb (g/mL)	0.144	0.064	0.144	0.189
Aerosol performance	MMAD (µm)	2.016 ± 0.17	4.50 ± 0.06	0.927 ± 0.41	2.661 ± 0.16
	FPF <5 (%)	84.07 ± 1.51	25.05 ± 1.19	89.96 ± 1.34	69.30 ± 3.67
	FPF <3 (%)	74.73 ± 1.23	20.65 ± 1.91	79.88 ± 1.42	52.75 ± 1.57
	EF (%)	95.56 ± 3.22	97.05 ± 1.65	96.23 ± 2.79	92.67 ± 2.89
	GSD	1.658	2.95	N/A	1.986

ρ_t: tapped density, ρ_b: bulk density, SSA: specific surface area. Results are expressed as mean ± SD (n=3 independent measurements).

The samples showed different densities (Table 8), influencing aerosol performance. K1L's density was similar to K1, indicating minimal impact from leucine. K1M had a lower density, forming a lighter powder, while K1ML was denser, potentially favoring deep lung deposition. All formulations met inhalation criteria, with bulk densities below 0.3 g/mL and tapped densities under 0.4 g/mL [15,16], confirming suitability for pulmonary delivery.

6.3.3. Drug loading and encapsulation efficiency

High DL and EE values in K1 demonstrated efficient drug incorporation in NCA without excipients. K1M and K1L saw reduced DL but maintained high EE, with leucine improving encapsulation due to its surfactant properties (Table 8).

6.3.4. Morphology

Morphology results are shown in Figure 17. Compared to the nano spray-dried stabilizer (Figure 17B), SEM images confirmed that KTP in K1 (Figure 17C) existed as nanocrystals agglomerated on the stabilizer surface, indicating high crystallinity without surface modification. Incorporating leucine (K1L, Figure 17D) produced a corrugated shell structure due to leucine's surface activity. In K1M (Figure 17E), mannitol promoted the

formation of larger, rough-surfaced, spherical particles. K1ML (Figure 17F) combined features of both a crystalline surface and shell-like structure, reflecting the effects of both excipients. Despite morphological differences, all samples exhibited rough surfaces, beneficial for lung deposition by enhancing contact angles and cell adhesion [17,18].

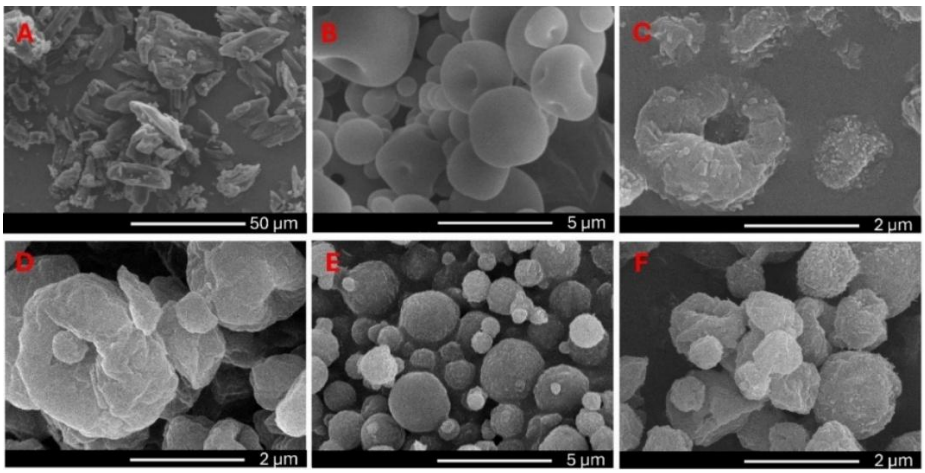

Figure 17: SEM images of (**A**) raw KTP, (**B**) nano spray dried-stabilizer system, (**C**) K1, (**D**) K1L, (**E**) K1M and (**F**) K1ML [3].

6.3.5. Solid-state analysis

Raw KTP showed a melting peak at 97.83 °C, which shifted to 91.5–93.17 °C in NCA samples due to particle size reduction. Mannitol-containing samples (K1M, K1ML) exhibited additional peaks at ~153 °C, corresponding to mannitol melting. Interestingly, K1ML showed an extra peak, suggesting distinct mannitol polymorphs, likely from spray drying at different ratios [211]. Further studies are needed to confirm this (Figure 18A). Also, TGA showed low water content across samples (0.16–1.8%; data not shown). K1 (without mannitol/leucine) had the highest (1.8%), while mannitol and leucine reduced moisture levels. Water content was within the acceptable range for DPI formulations [212,213].

XRPD analysis (Figure 18B) showed that all formulations (K1, K1M, K1L, K1ML) retained the characteristic crystalline peaks of raw KTP. Crystallinity, calculated relative to 100% for raw KTP, was 72.51% (K1), 30.18% (K1M), 75.20% (K1L), and 51.70% (K1ML). Mannitol reduced crystallinity, consistent with its known impact during co-spray drying [188], while leucine led to the highest crystallinity due to its surface coverage and solid-phase properties.

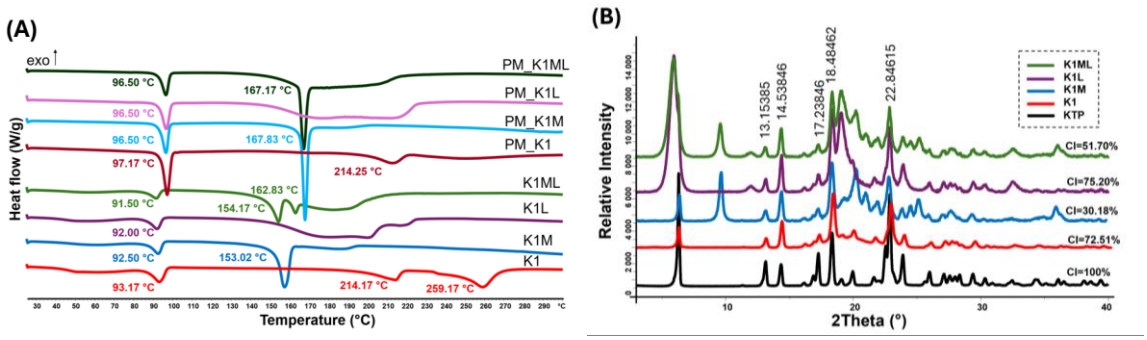

Figure 18: Results of solid-state analysis (**A**) Thermal analysis by DSC of NCAs samples and PMs, (**B**) Structural analysis by XRPD of raw KTP and NCAs samples with values of crystallinity index (%), PM: physical mixture, CI: crystallinity index [3].

FTIR analysis (Figure 19A) showed that all samples retained KTP's characteristic peaks (719, 971, 1286, 1658, and 1701 cm^{-1}), indicating no structural changes. Variations in peak intensity suggested differences in crystallinity. The C-H stretching peak (~2932 cm^{-1}) was preserved, while leucine reduced hydrogen bonding in PVA, seen by a narrower, weaker ~3367 cm^{-1} peak, likely due to its surface activity and interference with PVA's hydroxyl groups [214]. Mannitol caused a shift in the O-H stretching from 3367 to 3285 cm^{-1}, indicating new hydrogen bonding with PVA. FTIR spectra of PMs (Figure 19B) showed partial loss of PVA peaks, suggesting that nano spray drying prevents phase separation and aggregation.

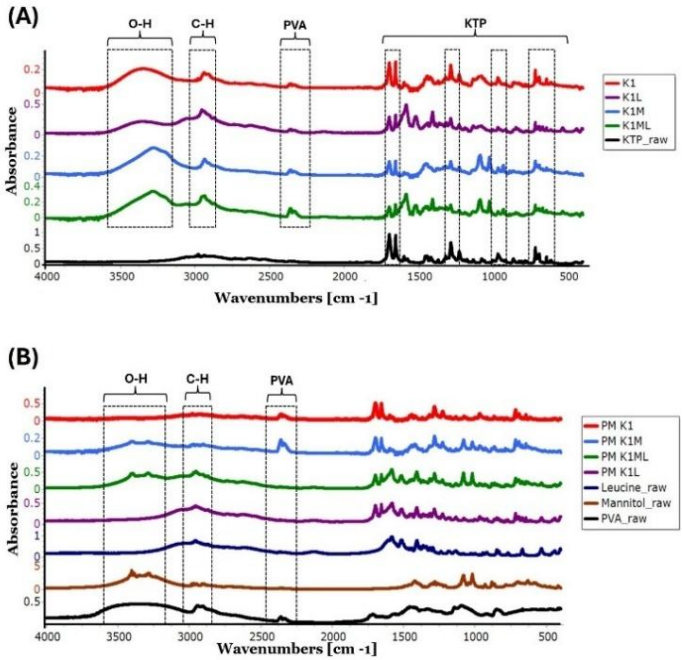

Figure 19: (**A**) FTIR results of raw KTP and NCAs samples with characteristic peak of KTP in fingerprint region, and (**B**) FTIR results of corresponding unprocessed physical mixture and raw materials. O-H: stands for O-H stretching vibration, and C-H: stands for C-H stretching vibration [3].

6.3.6. *In vitro* release study

For systemic effect in pulmonary delivery, it is essential for the drug to dissolve and release quickly upon deposition to minimize the risk of clearance mechanisms [175,177]. The data revealed that 93%, 94%, 98%, and 99% of the drug was released from K1, K1M, K1L, and K1ML, respectively, within the first 5 minutes, compared to 40% released from the PM (Figure 20). Although all NCAs samples exhibited an improved release profile, K1ML recorded the highest dissolution rate. A similar trend was observed in a previously published study [215]. Hence, the release profiles are affected by the size, surface area, crystallinity, and roles of mannitol and leucine in influencing dissolution rates through their effects on wettability and particle dispersion. The interplay of these factors resulted in slight variations in the release rates observed for NCAs samples.

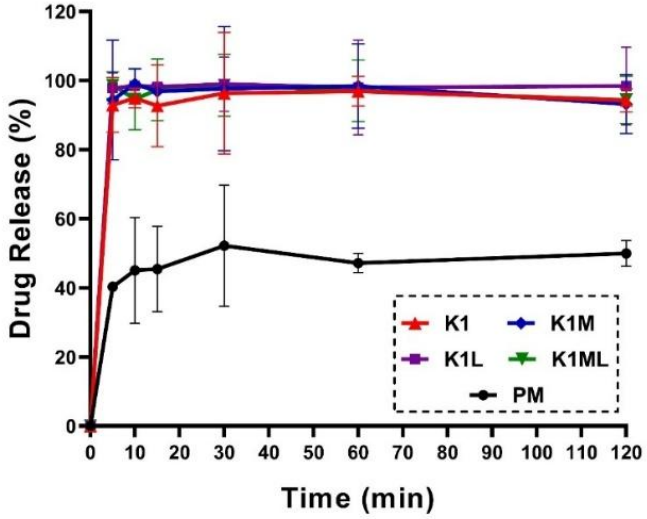

Figure 20: *In vitro* release study of physical mixture (PM) and developed NCAs (K1, K1M, K1L, and K1ML) in simulated lung media (SLM). Results are expressed as mean ± SD (n=3 independent measurements) [3].

6.3.7. Aerosol performance

6.3.7.1. Andersen cascade impactor

The ACI was used at 60 L/min to assess aerodynamic properties (Table 8). MMAD values ranged from 0.927 to 4.5 µm, indicating suitability for lung deposition. Mannitol in K1M increased MMAD and GSD, limiting deep lung delivery and suggesting broad size distributions. K1L showed the highest FPF due to leucine's dispersibility enhancement, but its low MMAD (<1 µm) raised exhalation risk. K1ML balanced MMAD and FPF, favoring deep lung deposition, consistent with a previous study [212]. EF values (92.67–97.05%) confirmed efficient delivery.

6.3.7.2. Aerosol particle sizer

In line with ACI analysis, APS results showed that K1L had the smallest median and geometric mean, while K1M had larger particle sizes, confirming that mannitol alone may not sufficiently optimize particle size for inhalation (results not shown) [147]. The combination of mannitol and leucine in K1ML resulted in intermediate particle sizes, offering a balance between the two excipients' properties. This was in line with a previous study by Pasero et al., (2025) where the aerosolization properties microparticle system (mannitol and salbutamol sulphate) was significantly improved up to maximum FPF (48 %) and MMAD (2 μm) when combined and spray freeze-dried with leucine at 10 % (w/w db) [216]. Another study found a highly significant and positive impact of leucine on enhancing the FPF of spray-dried mannitol particles [217].

6.3.7.3. In silico modelling

In silico predictions aligned with *in vivo* data for pulmonary delivery (Figure 21). The 5-second BH model assessed aerosol behavior, matching *in vitro* trends. K1M (mannitol) showed larger particles, lower lung deposition, and minimal exhalation due to size. K1L (leucine) had smaller particles but higher exhaled fraction. K1ML (mannitol + leucine) achieved optimal lung deposition, confirming prior findings [216]. Extended BH (10 s) improved deposition for all formulations. Based on aerosol performance, K1ML was selected for further study, with K1 as reference.

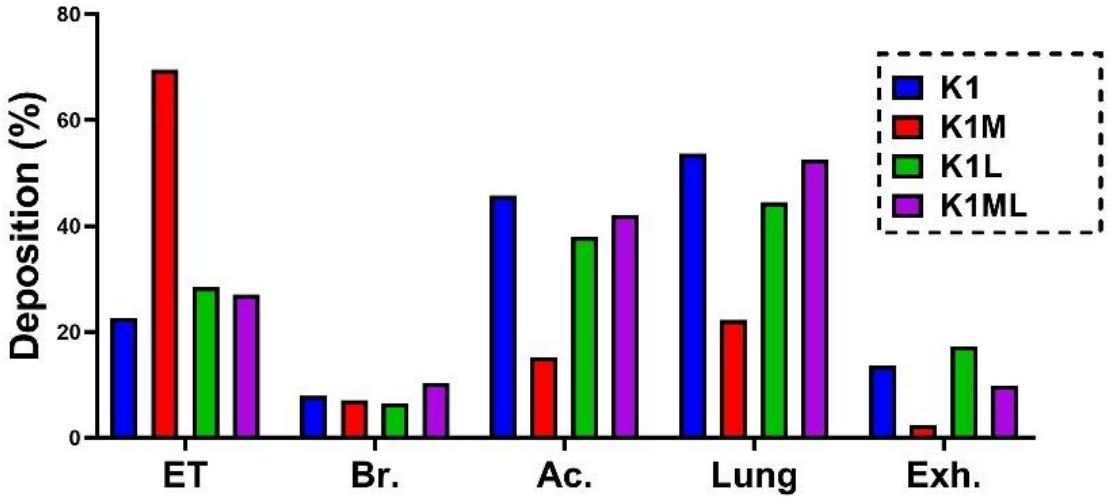

Figure 21: *In silico* results of deposited mass of NCA samples at a 5-second BH. ET: extra-thoracic, Br: bronchial, Ac: acinar, and EXH: exhaled [147].

6.3.8. Cell line measurements

6.3.8.1. Cell viability

While no significant changes were observed over a 1-hour period in CFBE (Figure 22A), a slight reduction in impedance was observed at high concentrations in A549 (treated with K1 and K1ML) (Figure 22B).

Hence, 50 µg/mL KTP concentration was selected for subsequent permeability experiments.

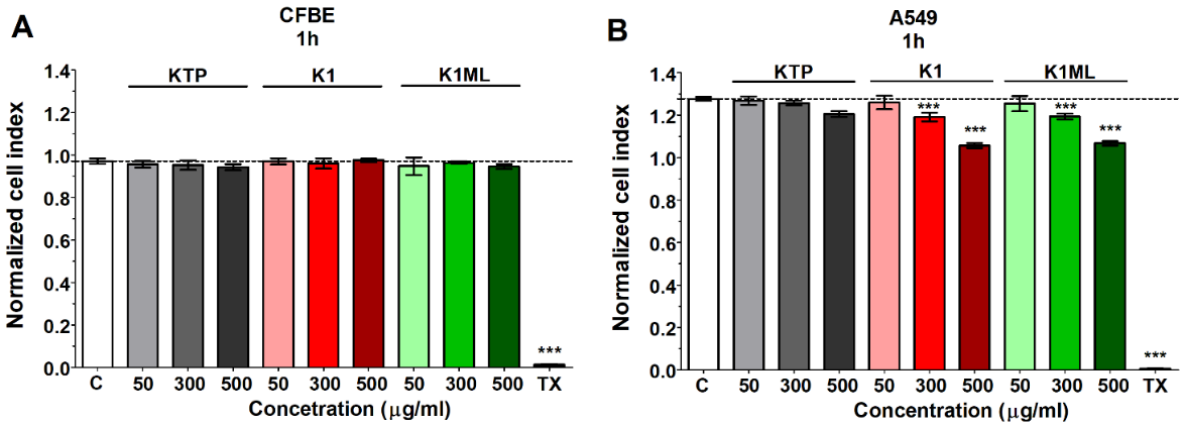

Figure 22: Cell viability of (**A**) CFBE bronchial epithelial and (**B**) A549 alveolar epithelial cells after 1-hour treatments with raw KTP, K1 and K1ML samples measured by impedance. Values are presented as means ± SD, n = 5-6. ***$p < 0.001$ compared to the C (control group) [3].

6.3.8.2. Cell permeability

The permeability of raw KTP and NCA formulations (K1, K1ML) was evaluated using bronchial and alveolar co-culture models over 1 hour (Figure 23). KTP showed efficient penetration, with higher P_{app} values in the A549 alveolar model, suggesting better absorption potential in the alveolar region [218,219].

K1ML slightly increased permeability in A549 cells, while K1 showed higher permeability in CFBE cells, indicating excipient effects vary by cell type [220]. However, neither formulation significantly altered KTP permeability compared to the raw drug, which is considered a favorable outcome. As KTP is a BCS Class II drug, the results suggest that the formulations may improve solubility without impairing epithelial permeability.

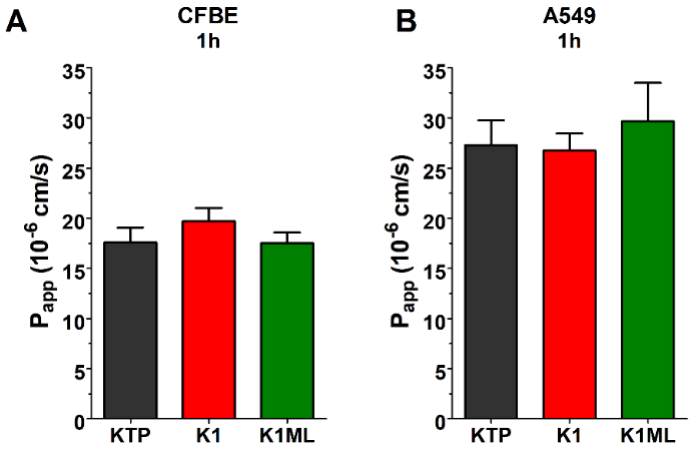

Figure 23: Permeability results of raw KTP, K1, and K1ML across co-culture models (**A**) CFBE cells and (**B**) A549 alveolar cells after a 1-hour assay. Data are expressed as mean ± SD, n = 4 [3].

6.3.8.3. Barrier integrity

Neither KTP nor NCA formulations (K1, K1ML) significantly affected barrier integrity, as confirmed by unchanged TEER values and low P_{app} for fluorescein and albumin (Figure 24). Fluorescein permeability was higher in A549 than CFBE models, consistent with permeability results. Interestingly, K1 reduced fluorescein permeability and lowered albumin permeability without affecting TEER (in A549), suggesting a barrier-tightening effect, similar to that seen with meloxicam in nasal epithelial models [221].

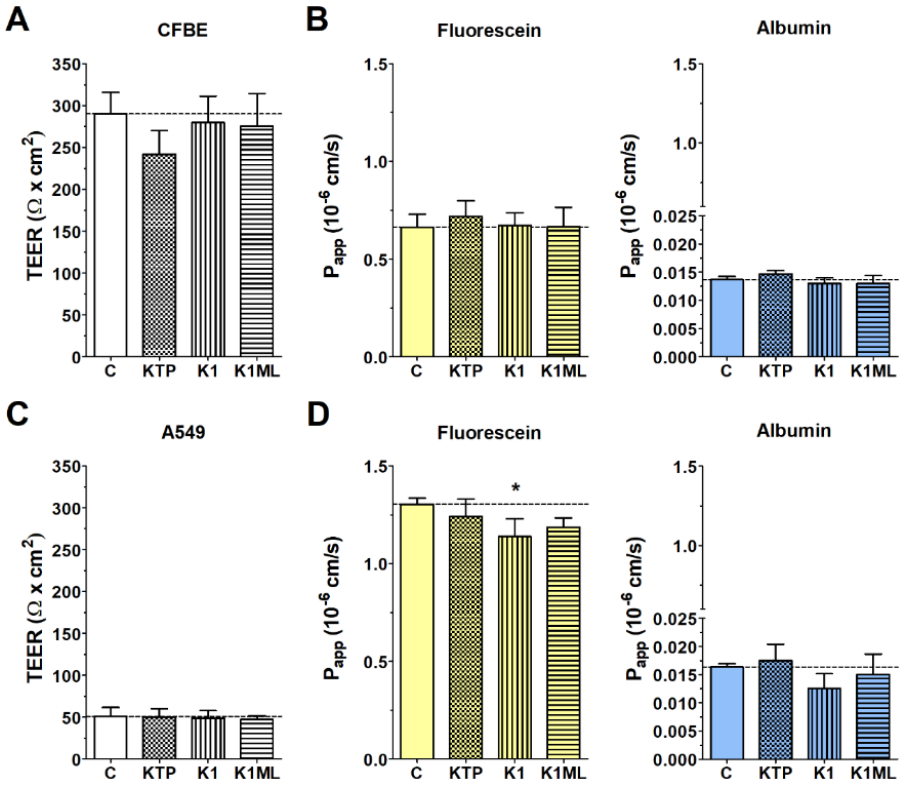

Figure 24: Assessment of barrier tightness in CFBE and A549 co-culture models following permeability assays: (**A**) and (**C**) TEER measurements, and (**B**) and (**D**) permeability of fluorescein and albumin marker molecules. Data are expressed as means ± SD, n = 4. *p < 0.05. C: control [3].

6.3.8.4. Immunocytochemistry

Immunostaining for ZO-1 (CFBE) and β-catenin (A549) was performed to assess cell morphology after exposure to raw KTP, K1, and K1ML (Figure 25). Strong, continuous staining was observed at cell junctions in both models, with no differences across groups. Morphological analysis confirmed that neither KTP nor NCA formulations compromised barrier integrity [3].

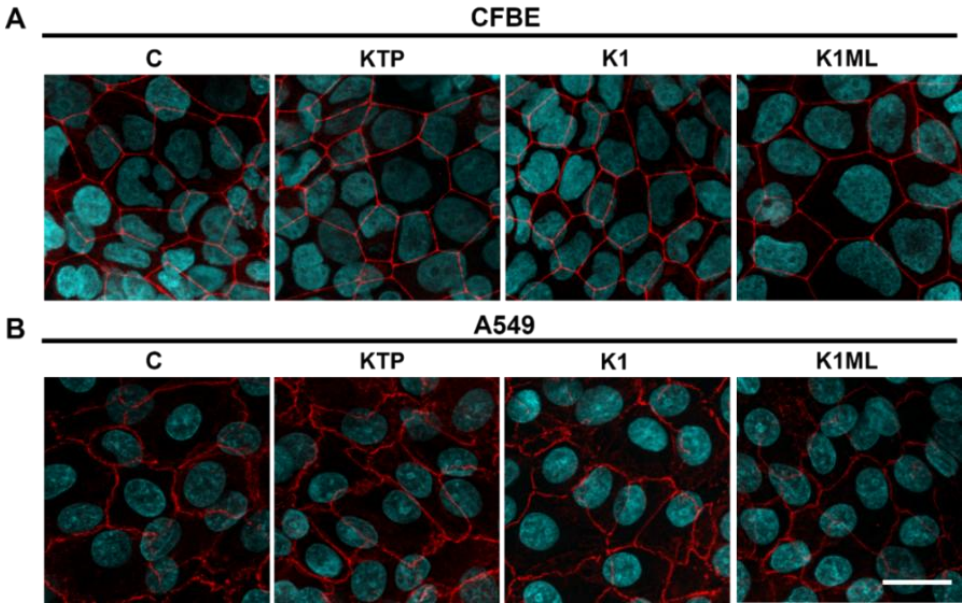

Figure 25: Barrier integrity assessed by immunostaining in (**A**) CFBE cells (ZO-1 staining) and (**B**) A549 cells (β-catenin staining) after permeability. Cyan: cell nuclei; red: junctional proteins. Bar = 20 µm [3].

6.3.9. Pharmacokinetic study in healthy rats

PK studies of KTP-RAW, KTP-NS, K1, and K1ML were conducted, and the concentration-time profiles in plasma and lungs are shown in Figure 26, with PK parameters in Table 9.

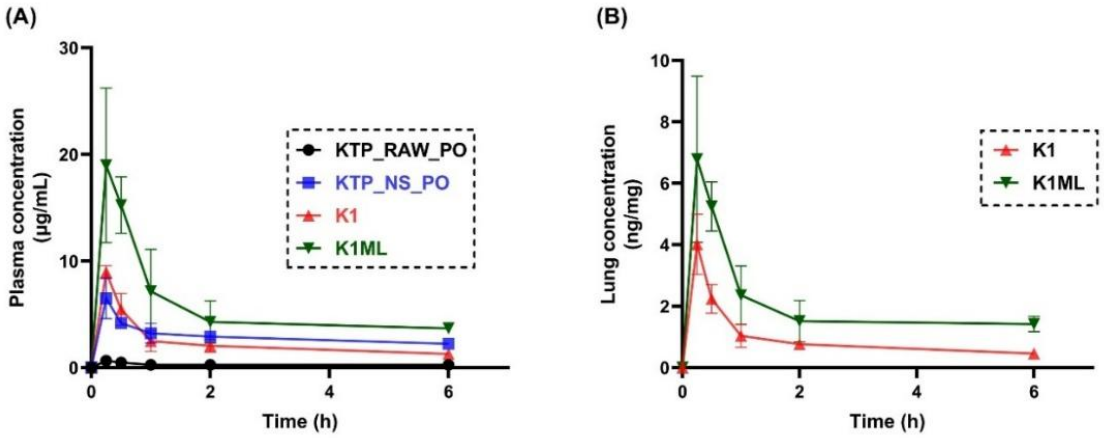

Figure 26: The concentration-time curve of KTP (**A**) in plasma after oral administration of KTP-raw and KTP-NS and intratracheal administration of K1 and K1ML, (**B**) in lungs after intratracheal administration of K1 and K1ML. Administered dose was 3 mg KTP/kg. Data are expressed as mean ± SD (n = 4) [3].

In plasma samples, K1ML showed 779.9% relative bioavailability vs. KTP-RAW, outperforming KTP-NS (451.9%) and K1 (258.6%). Inhalation delivery further increased the C_{max} values compared to orally delivered KTP-NS, by 1.4-fold for K1 and 3-fold higher than oral KTP-NS. Moreover, K1ML revealed superior $AUC_{0-\infty}$ compared to KTP-NS (72.76 vs 42.16 µg·h/mL). For comparison, K1ML's performance exceeded literature reports: its bioavailability (~73%) surpassed Huang et al.'s inhaled cyclosporine particles (44-48%) and Hou et al.'s IV KTP nanoparticles (52.04 %) [222,223].

The mannitol-leucine combination (K1ML) enabled 1.7-fold higher absorption than oral KTP-NS, demonstrating inhalation's advantages for systemic delivery with reduced gastric risks.

Table 9: The pharmacokinetic parameters of KTP obtained from both plasma and lung concentration-time curves by non-compartmental analysis after oral administration of KTP-RAW and KTP-NS, and intratracheal administration of NCA formulations (K1 and K1ML), (Mean ± SD, n = 4) [3].

	PK parameter	KTP-RAW	KTP-NS	K1	K1ML
Plasma	k_e (h−1)	0.0653 ± 0.0423	0.0919 ± 0.0164	0.1269[a]	0.1366[a]
	$t_{½}$ (h)	21.306 ± 4.509	7.720 ± 1.354[a]	5.460[a]	5.072[a]
	t_{max} (h)	0.25	0.25	0.25	0.25
	C_{max} (µg/mL)	0.646 ± 0.098	6.499 ± 1.9122	8.949 ± 0.611[a]	18.973 ± 7.246[a,b,c]
	$AUC_{0-\infty}$ (µg·h/mL)	9.329 ± 8.897	42.163 ± 3.150[a]	24.125[a,b]	72.763[a,b,c]
	F (to KTP_RAW)	-	4.519	2.586	7.799
	F (to KTP_NS)	0.221	-	0.572	1.726
Lung	k_e (h−1)	-	-	0.1535	0.1671
	$t_{½}$ (h)	-	-	4.515	4.147
	t_{max} (h)	-	-	0.25	0.25
	C_{max} (µg/mg)	-	-	0.00402 ± 0.00803	0.00678 ± 0.0136
	$AUC_{0-\infty}$ (µg·h/mg)	-	-	0.00843	0.02037
	f_t	-	-	0.0003912	0.0003241

k_e: elimination rate constant; $t_{½}$: elimination half-life; C_{max}: maximum KTP concentration; t_{max}: time to reach C_{max}; $AUC_{0-\infty}$: area under the zero to infinity concentration curve; F: relative bioavailability; f_t: tissue availability. [a]: indicates statistically significant difference from KTP-RAW ($P < 0.05$). [b]: indicates statistically significant difference from KTP-NS ($P < 0.05$). [c]: indicates statistically significant difference from K1 ($P < 0.05$).

In lung samples, inhalation delivery resulted in minimal lung retention (ng-range KTP), with no significant differences in elimination kinetics between K1 and K1ML (Figure 26B). Both formulations showed rapid systemic absorption (low f_t values). While K1ML had higher (but non-significant) C_{max} and AUC_{0-6} vs. K1, its significantly greater $AUC_{0-\infty}$ suggests potentially prolonged exposure and increased local effect risk.

6.3.10. Safety and tolerance in ovalbumin-sensitized rats

6.3.10.1. Lung function and respiratory mechanics measurement

The effect of increasing PEEP on four parameters (EELV, Raw, G, and H) was evaluated. As a result, increasing PEEP elevated EELV, while reduced Raw, G and H (all $p < 0.001$), validating experimental consistency. Notably, Group K1ML exhibited significantly higher EELV and Raw ($p < 0.001$) compared to other groups, suggesting airway narrowing and expiratory flow limitation. No differences were observed among other groups (Figure 27). The elevated Raw and EELV in K1ML may stem from:

(i) Enhanced KTP bioavailability, leading to heightened COX inhibition and a shift toward leukotriene production, which promotes bronchoconstriction [224–227]. Jin et al. (2013) reported lung injury in rats at high COX-2 inhibitor doses, suggesting that reducing the K1ML dose could prevent adverse effects [228].

(ii) Excipient-related effects: Mannitol, while aiding mucociliary clearance, may induce dose-dependent bronchoconstriction [229,230], potentially managed with bronchodilators like formoterol [231]. Leucine, at higher doses, might impair surfactant function or irritate airways [232]. These findings support exploring NSAID-bronchodilator combinations.

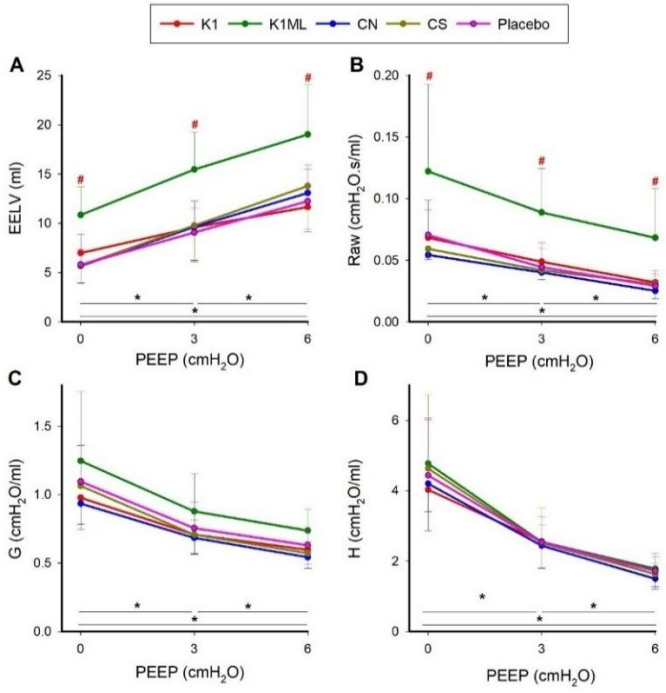

Figure 27: Lung function parameters in OVA-sensitized rats across varying PEEP levels: (**A**) End-expiratory lung volume (EELV), (**B**) airway resistance (Raw), (**C**) respiratory tissue damping (G) and (**D**) respiratory tissue elastance (H). Where *: $p<0.05$ for PEEP change in all groups and #: $p<0.05$ K1ML vs. other groups [3].

6.3.10.2. Airway responsiveness to pharmacological challenges

- **Methacholine (MCh) Challenge**

The non-specific muscarinic agonist MCh induced dose-dependent increases in airway resistance (Raw) and respiratory tissue mechanics (G and H) ($p<0.001$ for all parameters), confirming effective bronchoconstriction (Figure 28). No significant differences were observed between treatment groups, indicating none of the interventions affected lung responsiveness to this non-specific agonist.

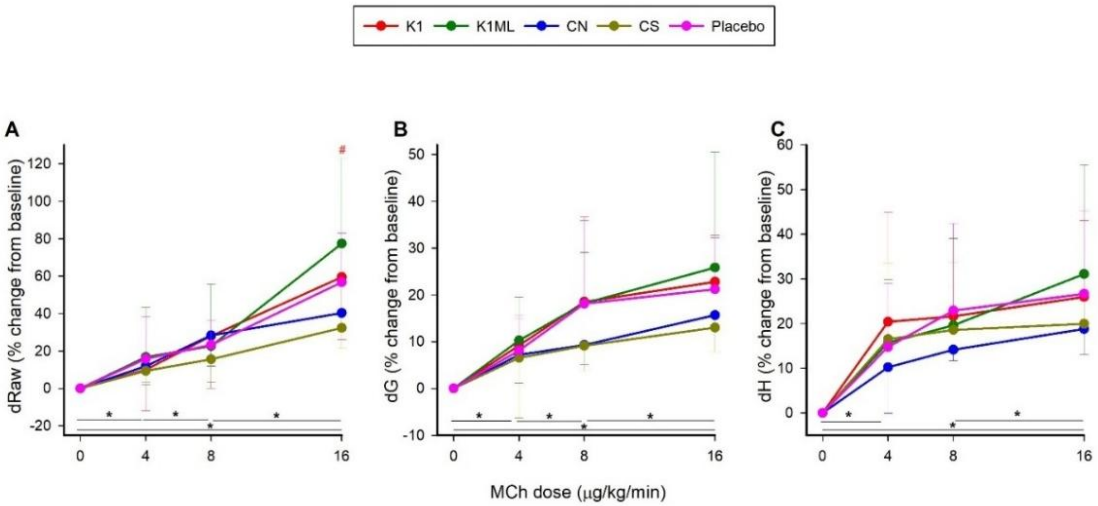

Figure 28: Changes during methacholine (MCh)-induced bronchoprovocation in (**A**) airway resistance (Raw), (**B**) respiratory tissue damping (G), and (**C**) respiratory tissue elastance (H) in naïve untreated animals (CN, n = 6), OVA-sensitized untreated animals (CS, n = 6), and OVA-sensitized animals receiving intratracheal administration of placebo (n = 12), K1 (n = 12), or K1ML (n = 12) formulations. Where *: $p<0.05$ for MCh dose change in all groups, #: $p<0.05$ K1ML vs. CN, CS [3].

- **Ovalbumin (OVA) Challenge:**

The specific allergen challenge confirmed successful sensitization, with sensitized animals showing pronounced bronchoconstriction responses (>25% peak Raw increase) compared to non-sensitized controls (<10% response).

Similar to MCh results, no differences were observed among sensitized treatment groups, demonstrating that neither K1 nor K1ML formulations altered the lung's response to specific allergen challenge (results not shown).

6.4. Stability assessment of selected samples

Table 10 presents the 3-month stability results of F1 and K1ML under stress conditions. F1 showed a significant increase in span, along with reduced FPF and a compromised release profile—likely due to solid-state changes or increased interparticle interactions reducing surface area [233], which is in line with previously published results [234].

In K1ML, D[0.5], span, and MMAD remained stable, but FPF declined, likely due to moisture-induced surface changes such as roughness or partial aggregation. This aligns with findings by Das et al. (2009), who observed a drop in FPF of salmeterol xinafoate from 11.3% to 4.9% with rising RH [235]. Despite FPF changes, release profile and DSC analyses remained consistent with partially preserved crystallinity, suggesting that the formulation maintains consistent performance throughout its intended shelf life under normal storage conditions.

Future studies should focus on investigating stability under different stress conditions to address moisture sensitivity observed on the particle surface.

Table 10: Stability of selected formulations (F1 and K1ML) after 3-month storage under accelerated conditions [90,147].

Analysis	F1	K1ML
D[0.5] (µm)	2.44	2.19
Span	121.28	1.42
FPF (%) <5 µm	26.6	33.10
MMAD	5.43	3.52
Crystallinity (%)	33.81	40.15
Melting point (°C)	90.39	91.07
Morphology	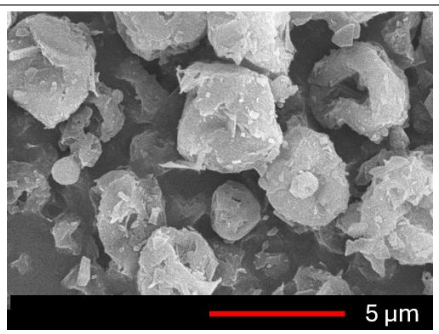 Nearly spherical Rougher corrugated surface	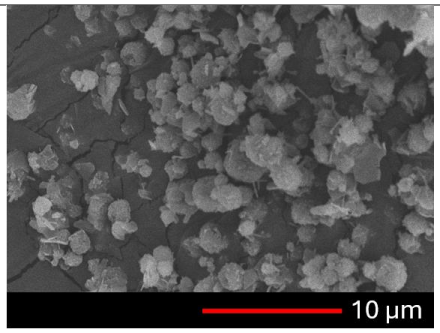 Spherical Fiber-like surface
Release	75% in 5 min	90% in 5 min

7. Conclusion

This dissertation employed a patient-centric strategy to address distinct therapeutic needs—local and systemic—through pulmonary delivery using KTP-based DPIs. Two formulations were developed from a unified nanocrystal platform: one designed to treat lung inflammation and mucus obstruction in CF, and the other optimized for systemic delivery with enhanced bioavailability. The main findings, organized according to the defined objectives, are summarized as follows:

A. Nanocrystal dispersion preparation

I. A stable nanocrystal suspension was successfully optimized using 1% PVA and 0.1% SDS. Over 45 days of refrigerated storage, only minimal particle size growth was observed, while size distribution remained consistent, qualifying the dispersion for downstream solidification and engineering.

B. Local pulmonary delivery (nanocrystal KTP-mannitol combination therapy)

II. A QbD framework supported the rationale for combining KTP with mannitol in a single inhaler to address both inflammation and mucus accumulation in CF, aiming to improve disease control and patient quality of life.

III. The optimized formulation (F1; containing KTP and mannitol in 1:1 mass ratio, with 84.9% DL) demonstrated efficient aerosol performance, with deposition primarily in ACI stages 3 and 4, confirming desired lung delivery. It achieved complete drug release (~100%) within 10 minutes in simulated lung fluid, notably reduced mucin viscosity without compromising KTP's anti-inflammatory effect, and showed good biocompatibility in alveolar and bronchial cells. A 1.4-fold increase in alveolar permeability was achieved. However, deviations from the 1:1 ratio (either higher or lower) negatively impacted performance.

IV. These findings highlight the formulation’s potential as a dual-function inhalable therapy for CF, though precise mannitol concentration remains critical to maintaining efficacy and performance. This novel inhaled combination supports patient-centric delivery by reducing doses burden, improving symptom control, and enhancing adherence.

C. Systemic pulmonary delivery (nanocrystal-engineered DPI)

V. A factorial design (BBD) optimized nano spray-drying parameters (50% pump rate, 5% (w/v) feed concentration and 90 °C inlet temperature), enabling the production of KTP engineered-nanocrystal agglomerates tailored for systemic absorption via the deep lung deposition.

VI. The inclusion of both mannitol and leucine demonstrated a synergistic effect on particle engineering, significantly enhancing aerosol behavior and dispersion compared to formulations with either excipient alone. The optimized mannitol-leucine formulation (K1ML; containing 2.5% KTP, 1.25% mannitol and 1.25% leucine (w/v)) achieved excellent *in vitro* aerosol performance (MMAD: 2.66 ± 0.16 μm; FPF: 69.3 ± 3.67%) and complete drug release (99% in 5 min). It also maintained biocompatibility across both CFBE and A549 cells, with greater permeability in alveolar cells.

VII. Pharmacokinetic evaluation of inhaled K1ML confirmed a 3-fold increase in C_{max} and 1.73-fold improvement in relative bioavailability (73% for K1ML vs. 42% for oral KTP-NS). Low lung tissue retention indicated efficient systemic absorption, supporting its suitability for extra-pulmonary indications and rapid systemic absorption. However, repeated dosing in an OVA-sensitized rat model revealed bronchial side effects (e.g., airway narrowing and reduced expiratory flow) for K1ML, indicating that dose adjustment is required to balance efficacy and pulmonary safety. The nanocrystal-engineered DPI system aligns with patient-centric goals by improving bioavailability, reducing gastrointestinal-related side effects, accelerating therapeutic onset, and potentially lowering dosing frequency.

D. Stability assessment

VIII. Over three months of ICH storage (40°C/75% RH), F1 exhibited a broadened particle size distribution (span), reduced FPF, and a compromised release profile, indicating the need for further optimization of mannitol concentration or incorporation of an additional stabilizing agent. In contrast, K1ML maintained its particle size, MMAD, and *in vitro* release characteristics, demonstrating robust stability and greater suitability for potential commercial development.

8. Novelty and practical relevance of the work

The main innovations and practical contributions of this study include:

- First application of a unified KTP nanocrystal suspension engineered to serve both local and systemic delivery via inhalable powders, developed using a patient-centric strategy.
- Novel QbD-driven Zero Phase formulation rationale proposed for a DPI combination therapy in CF, supporting dual functionality—anti-inflammatory action (via KTP) and mucus hydration (via mannitol).
- First demonstration of mannitol–leucine synergy in enhancing aerosolization, cellular permeability, and systemic bioavailability of a nanocrystal-engineered DPI.
- Development of the first NSAID-based DPI intended specifically for systemic absorption, offering a needle-free alternative to injectable and oral routes.
- First-time comprehensive assessment of potential respiratory risks associated with prolonged inhaled NSAID (KTP) use, using an OVA-sensitized rat model to evaluate lung function and airway mechanics in an asthmatic-like condition.
- Integration of KTP and mannitol in a single DPI formulation to address polytherapy needs in CF, by targeting inflammations and mucus overproduction simultaneously, aiming to improve adherence and simplify treatment.
- Implementation of a scalable and clinically relevant spray-drying process aligned with patient usability and regulatory trends in patient-focused drug design.
- Advancement of pulmonary drug delivery as a route for repurposing poorly soluble drugs, with potential for broad application to other therapeutic classes such as antivirals or immunomodulators.
- Supports regulatory interest in IVIVC and patient-centricity by demonstrating rational formulation design tied to improved therapeutic performance and usability.
- These innovations represent an important shift toward more effective and patient-aligned therapies.

References:

1. Banat H, Ambrus R, Csóka I. Drug combinations for inhalation: Current products and future addressing disease control and patient compliance. Int J Pharm [Internet]. 2023;123070. Available from: https://doi.org/10.1016/j.ijpharm.2023.123070
2. Banat HF, Ali DK, Jarrar Q, Alomary E, Dahmash EZ. Synthesis and preclinical evaluation of novel l-cystine-based polyamide nanocapsules loaded with a fixed-dose combination of thymoquinone and doxorubicin for targeted pulmonary anticancer drug delivery. Mater Adv [Internet]. 2025; Available from: http://dx.doi.org/10.1039/D4MA00972J
3. Banat H, Csoka I, Kun-szab F, Pet F, Party P, Sztojkov-ivanov A, et al. Mannitol-leucine synergy in nanocrystal agglomerates for enhanced systemic delivery of inhaled ketoprofen : Pharmacokinetics and safety in ovalbumin-sensitized rats. Int J Pharm. 2025;676.
4. Zurita-Lizza CC, Rodriguez-Sanchez I, Doreski PA. Repurposing Inhaled Ibuprofenate, a Non Steroidal Anti-Inflammatory Drug, as a Potential Adjuvant Treatment for Pneumonia, CARDS and its Aetiological Agent SARS-CoV-2. Clin Transl Discov. 2023;3.
5. Party P, Piszman ZI, Farkas Á, Ambrus R. Comprehensive In Vitro and In Silico Aerodynamic Analysis of High-Dose Ibuprofen- and Mannitol-Containing Dry Powder Inhalers for the Treatment of Cystic Fibrosis. Pharmaceutics. 2024;16.
6. Motzwickler-Németh A, Party P, Simon P, Sorrenti M, Ambrus R, Csóka I. Preparation of Ibuprofen-Loaded Inhalable γCD-MOFs by Freeze-Drying Using the QbD Approach. Pharmaceutics. 2024;16.
7. Emami S, Hemmati Z, Yaqoubi S, Hamishehkar H, Alvani A. Nanocrystal Agglomerates of Curcumin Prepared by Electrospray Drying as an Excipient-Free Dry Powder for Inhalation. Adv Pharmacol Pharm Sci Vol. 2024;2024.
8. Deng Q, Deng L, Miao Y, Guo X, Li Y. Particle deposition in the human lung: Health implications of particulate matter from different sources. Environ Res [Internet]. 2019;169:237–45. Available from: https://doi.org/10.1016/j.envres.2018.11.014
9. Darquenne C. Deposition Mechanisms. J Aerosol Med Pulm Drug Deliv. 2020;33:181–5.
10. Vu T V., Ondracek J, Zdímal V, Schwarz J, Delgado-Saborit JM, Harrison RM. Physical properties and lung deposition of particles emitted from five major indoor sources. Air Qual Atmos Heal [Internet]. 2017;10:1–14. Available from: http://dx.doi.org/10.1007/s11869-016-0424-1
11. Heyder J, Gebhart J, Rudolf G, Schiller CF, Stahlhofen W. Deposition of particles in the human respiratory tract in the size range 0.005-15 μm. J Aerosol Sci. 1986;17:811–25.
12. Dhoble S, Kapse A, Ghegade V, Chogale M, Ghodake V, Patravale V, et al. Design, development, and technical considerations for dry powder inhaler devices. Drug Discov Today [Internet]. 2024;29:103954. Available from: https://doi.org/10.1016/j.drudis.2024.103954
13. Darquenne C. Aerosol deposition in health and disease. J Aerosol Med Pulm Drug Deliv. 2012;25:140–7.
14. Miller DP, Tarara TE, Weers JG. Targeting of inhaled therapeutics to the small airways: Nanoleucine carrier formulations. Pharmaceutics. 2021;13.
15. Gradon L, Sosnowski TR. Formation of particles for dry powder inhalers. Adv Powder Technol [Internet]. 2014;25:43–55. Available from: http://dx.doi.org/10.1016/j.apt.2013.09.012
16. Simon A, Inês M, Mendes L, Marie A, Pereira V, Sousa D. Development of a novel dry powder inhalation formulation for the delivery of rivastigmine hydrogen tartrate. Int J Pharm [Internet]. 2016;501:124–38. Available from: http://dx.doi.org/10.1016/j.ijpharm.2016.01.066
17. Han C-S, Kang J-H, Park E hye, Lee H-J, Jeong S-J, Kim D-W, et al. Corrugated surface microparticles with chitosan and levofloxacin for improved aerodynamic performance. Asian J Pharm Sci [Internet]. 2023;100815. Available from: https://www.sciencedirect.com/science/article/pii/S1818087623000429
18. Focaroli S, Mah PT, Hastedt JE, Gitlin I, Oscarson S, Fahy J V, et al. A Design of Experiment (DoE) approach to optimise spray drying process conditions for the production of trehalose/leucine formulations with application in pulmonary delivery. Int J Pharm [Internet]. 2019;562:228–40. Available from: https://www.sciencedirect.com/science/article/pii/S0378517319301796
19. Hickey AJ. Back to the future: inhaled drug products. J Pharm Sci. 2013;102:1165–72.
20. Dallal Bashi YH, Mairs R, Murtadha R, Kett V. Pulmonary Delivery of Antibiotics to the Lungs: Current State and Future Prospects. Pharmaceutics. 2025;17:1–23.
21. Drugs.com. Tobi® Podhaler [Internet]. 2013. Available from: https://www.drugs.com/history/tobi-podhaler.html
22. AstraZeneca. Trixeo Aerosphere [Internet]. 2020. Available from: https://www.astrazeneca.com/
23. Anzueto A, Barjaktarevic IZ, Siler TM, Rheault T, Bengtsson T, Rickard K, et al. Ensifentrine, a Novel Phosphodiesterase 3 and 4 Inhibitor for the Treatment of Chronic Obstructive Pulmonary Disease: Randomized, Double-Blind, Placebo-controlled, Multicenter Phase III Trials (the ENHANCE Trials). Am J

Respir Crit Care Med. 2023;208:406–16.
24. Drugbank. Ensifentrine [Internet]. 2024. Available from: https://go.drugbank.com/drugs/DB16157
25. Respira. RT234 [Internet]. 2022. Available from: https://respiratherapeutics.com/pipeline-2/
26. West A, Chaudhuri N, Barczyk A, Wilsher ML, Hopkins P, Glaspole I, et al. Inhaled pirfenidone solution (AP01) for IPF: A randomised, open-label, dose-response trial. Thorax. 2023;78:882–9.
27. Avalyn Pharma. AP02 [Internet]. 2025. Available from: https://www.avalynpharma.com/
28. Santos Cavaiola T, Edelman S. Inhaled insulin: a breath of fresh air? A review of inhaled insulin. Clin Ther. 2014;36:1275–89.
29. Ye Y, Ma Y, Zhu J. The future of dry powder inhaled therapy: Promising or discouraging for systemic disorders ? Int J Pharm. 2020;
30. Rapoport AM. New acute treatments for headache. Neurol Sci. 2010;31:129–32.
31. Abdou EM. Could Inhaled Drug Formulations Be the Future of Acute Migraine treatment? Ther Deliv [Internet]. 2019;10:609–11. Available from: https://doi.org/10.4155/tde-2019-0068
32. Newman S. Improving inhaler technique, adherence to therapy and the precision of dosing: major challenges for pulmonary drug delivery. Expert Opin Drug Deliv. 2014;11:365–78.
33. He Y, Liang Y, Han R, Lu W-L, Mak JCW, Zheng Y. Rational particle design to overcome pulmonary barriers for obstructive lung diseases therapy. J Control Release [Internet]. 2019;314:48–61. Available from: https://www.sciencedirect.com/science/article/pii/S0168365919305991
34. Ciofu O, Smith S, Lykkesfeldt J. Antioxidant supplementation for lung disease in cystic fibrosis. Cochrane Database Syst Rev. 2019;10.
35. Ingbar DH. Fishman's pulmonary diseases and disorders, 5th edition. Ann. Am. Thorac. Soc. 2015.
36. Buzzetti R, Salvatore D, Baldo E, Forneris MP, Lucidi V, Manunza D, et al. An overview of international literature from cystic fibrosis registries : 1 . Mortality and survival studies in cystic fibrosis. J Cyst Fibros [Internet]. 2009;8:229–37. Available from: http://dx.doi.org/10.1016/j.jcf.2009.04.001
37. Kerem E, C M, Gold R. Pulmonary function and clinical course in patients with cystic fibrosis after pulmonary colonization with Pseudomonas aeruginosa. J Pediatr. 1990;116:714–9.
38. Chmiel JF, Konstan MW, Elborn JS. Antibiotic and Anti-Inflammatory Therapies for Cystic Fibrosis. Cold Spring Harb Perspect Med [Internet]. 2013;3:1–17. Available from: http://perspectivesinmedicine.cshlp.org/content/3/10/a009779
39. Phillips WJ, Currier BL. Analgesic pharmacology: II. Specific analgesics. J Am Acad Orthop Surg. 2004;12:221–33.
40. Diener H-C, Holle-Lee D, Nägel S, Dresler T, Gaul C, Göbel H, et al. Treatment of migraine attacks and prevention of migraine: Guidelines by the German Migraine and Headache Society and the German Society of Neurology. Clin Transl Neurosci. 2019;3:2514183X1882337.
41. Schoenfeld BJ. The use of nonsteroidal anti-inflammatory drugs for exercise-induced muscle damage: Implications for skeletal muscle development. Sport Med. 2012;42:1017–28.
42. Oladosu FA, Tu FF, Hellman KM. Nonsteroidal antiinflammatory drug resistance in dysmenorrhea: epidemiology, causes, and treatment. Am J Obstet Gynecol. 2018;218:390–400.
43. Crofford LJ. Use of NSAIDs in treating patients with arthritis. Arthritis Res Ther. 2013;15.
44. Oyler DR, Parli SE, Bernard AC, Chang PK, Procter LD, Harned ME. Nonopioid management of acute pain associated with trauma: Focus on pharmacologic options. J Trauma Acute Care Surg. 2015;79:475–83.
45. VANE JR. Inhibition of Prostaglandin Synthesis as a Mechanism of Action for Aspirin-like Drugs. Nat New Biol [Internet]. 1971;231:232–5. Available from: https://doi.org/10.1038/newbio231232a0
46. Sostres C, Gargallo CJ, Arroyo MT, Lanas A. Adverse effects of non-steroidal anti-inflammatory drugs (NSAIDs, aspirin and coxibs) on upper gastrointestinal tract. Best Pract Res Clin Gastroenterol. 2010;24:121–32.
47. Whelton A. Nephrotoxicity of nonsteroidal anti-inflammatory drugs: physiologic foundations and clinical implications. Am J Med. 1999;106:13S-24S.
48. Harirforoosh S, Asghar W, Jamali F. Adverse effects of nonsteroidal antiinflammatory drugs: an update of gastrointestinal, cardiovascular and renal complications. J Pharm Pharm Sci. 2013;16:821–47.
49. Altman R, Bosch B, Brune K, Patrignani P, Young C. Advances in NSAID development: Evolution of diclofenac products using pharmaceutical technology. Drugs. 2015;75:859–77.
50. Onischuk AA, Tolstikova TG, An'kov S V., Baklanov AM, Valiulin S V., Khvostov M V., et al. Ibuprofen, indomethacin and diclofenac sodium nanoaerosol: Generation, inhalation delivery and biological effects in mice and rats. J Aerosol Sci [Internet]. 2016;100:164–77. Available from: http://dx.doi.org/10.1016/j.jaerosci.2016.05.005
51. Yu Y, Yang Q, Wang Z, Ding Q, Li M, Fang Y, et al. The anti-inflammation and anti-nociception effect of ketoprofen in rats could be strengthened through co-delivery of a h2s donor, s-propargyl-cysteine. J Inflamm Res. 2021;14:5863–75.
52. Wang LM, Toyoshima A, Mineshita S, Wang XX, Yamamoto T, Nomura Y, et al. The anti-inflammatory

effects of ketoprofen in animal experiments. Drugs Exp Clin Res. 1997;23:1–6.
53. Sarzi-Puttini P, Atzeni F, Lanata L, Egan CG, Bagnasco M. Safety of ketoprofen compared with ibuprofen and diclofenac: A systematic review and meta-analysis. Trends Med. 2014;14:17–26.
54. Sarzi-Puttini P, Atzeni F, Lanata L, Bagnasco M. Efficacy of ketoprofen vs. ibuprofen and diclofenac: a systematic review of the literature and meta-analysis. Clin Exp Rheumatol. 2013;31:731–8.
55. Atzeni F, Masala IF, Bagnasco M, Lanata L, Mantelli F, Sarzi-Puttini P. Comparison of Efficacy of Ketoprofen and Ibuprofen in Treating Pain in Patients with Rheumatoid Arthritis: A Systematic Review and Meta-Analysis. Pain Ther [Internet]. 2021;10:577–88. Available from: https://doi.org/10.1007/s40122-021-00250-3
56. Yakushin S, Polyakova S, Shvarts Y, Kastanayan A, Krechikova D, Ershova O, et al. Comparison of the Efficacy and Safety of Ketoprofen Plaster and Diclofenac Plaster for Osteoarthritis-Related Knee Pain: A Multicenter, Randomized, Active-Controlled, Open-Label, Parallel-Group, Phase III Clinical Trial. Clin Ther [Internet]. 2021;43:1720–34. Available from: https://doi.org/10.1016/j.clinthera.2021.08.002
57. Stigliani M, Aquino RP, Del Gaudio P, Mencherini T, Sansone F, Russo P. Non-steroidal anti-inflammatory drug for pulmonary administration: Design and investigation of ketoprofen lysinate fine dry powders. Int J Pharm [Internet]. 2013;448:198–204. Available from: http://dx.doi.org/10.1016/j.ijpharm.2013.03.030
58. Lavorini F, Janson C, Braido F, Stratelis G, Løkke A. What to consider before prescribing inhaled medications : a pragmatic approach for evaluating the current inhaler landscape. Ther Adv Respir Dis. 2019;13:1–28.
59. Corradi M, Chrystyn H, Cosio BG, Pirozynski M, Loukides S, Louis R, et al. NEXThaler, an innovative dry powder inhaler delivering an extrafine fixed combination of beclometasone and formoterol to treat large and small airways in asthma. Expert Opin Drug Deliv. 2014;11:1497–506.
60. Hebbink GA, Jaspers M, Peters HJW, Dickhoff BHJ. Recent developments in lactose blend formulations for carrier-based dry powder inhalation. Adv Drug Deliv Rev [Internet]. 2022;189:114527. Available from: https://doi.org/10.1016/j.addr.2022.114527
61. Lechanteur A, Evrard B. Influence of Composition and Spray-Drying Process Parameters on Carrier-Free DPI Properties and Behaviors in the Lung : A review. Pharmaceutics. 2020;12:55.
62. Chvatal A, Benke E, Szabóné Révész P, Ambrus R. Új formulálási stratégiák a porinhalációs készítmények előállításában. Gyogyszereszet. 2016;1–10.
63. Healy AM, Amaro MI, Paluch KJ, Tajber L. Dry powders for oral inhalation free of lactose carrier particles. Adv Drug Deliv Rev. 2014;75:32–52.
64. Pilcer G, Amighi K. Formulation strategy and use of excipients in pulmonary drug delivery. Int J Pharm. 2010;392:1–19.
65. Shahin HI, Chablani L. A comprehensive overview of dry powder inhalers for pulmonary drug delivery: Challenges, advances, optimization techniques, and applications. J Drug Deliv Sci Technol. 2023;84:104553.
66. Liang Z, Ni R, Zhou J, Mao S. Recent advances in controlled pulmonary drug delivery. Drug Discov Today. 2015;20:380–9.
67. Zillen D, Beugeling M, Hinrichs WLJ, Frijlink HW, Grasmeijer F. Natural and bioinspired excipients for dry powder inhalation formulations. Curr Opin Colloid Interface Sci. 2021;56:101497.
68. Singh PA, Pandey RP, Awasthi R. Unveiling the role of nanoparticle-based therapeutic strategies for pulmonary drug delivery. J Drug Deliv Sci Technol [Internet]. 2025;104:106558. Available from: https://www.sciencedirect.com/science/article/pii/S1773224724012279
69. Andrade F, Rafael D, Videira M, Ferreira D, Sosnik A, Sarmento B. Nanotechnology and pulmonary delivery to overcome resistance in infectious diseases ☆. Adv Drug Deliv Rev journa. 2013;65.
70. Yan X, Sha X. Nanoparticle-Mediated Strategies for Enhanced Drug Penetration and Retention in the Airway Mucosa. Pharmaceutics. 2023;15.
71. Loira-Pastoriza C, Todoroff J, Vanbever R. Delivery strategies for sustained drug release in the lungs. Adv Drug Deliv Rev [Internet]. 2014;75:81–91. Available from: http://dx.doi.org/10.1016/j.addr.2014.05.017
72. Deng Z, Kalin GT, Shi D, Kalinichenko V V. Nanoparticle delivery systems with cell-specific targeting for pulmonary diseases. Am J Respir Cell Mol Biol. 2021;64:292–307.
73. K. K. SP, Narayansamy D. Advancements in nanotechnology for targeted drug delivery in idiopathic pulmonary fibrosis: a focus on solid lipid nanoparticles and nanostructured lipid carriers. Drug Dev Ind Pharm [Internet]. 2025;1–10. Available from: https://doi.org/10.1080/03639045.2025.2468811
74. Zuo X, Gu Y, Guo X, Zheng W, Zheng H, An Y, et al. Preparation of Budesonide-Loaded Liposomal Nanoparticles for Pulmonary Delivery and Their Therapeutic Effect in OVA-Induced Asthma in Mice. Int J Nanomedicine. 2024;19:673–88.
75. Grenha A, Al-Qadi S, Seijo B, Remuñán-López C. The potential of chitosan for pulmonary drug delivery. J Drug Deliv Sci Technol [Internet]. 2010;20:33–43. Available from:

https://www.sciencedirect.com/science/article/pii/S1773224710500042
76. Zacaron TM, Silva MLS e., Costa MP, Silva DM e., Silva AC, Apolônio ACM, et al. Advancements in Chitosan-Based Nanoparticles for Pulmonary Drug Delivery. Polymers (Basel). 2023;15.
77. Omidian H, Wilson RL. PLGA-Based Strategies for Intranasal and Pulmonary Applications. pharmacetics. 2025;8–10.
78. Menon JU, Ravikumar P, Pise A, Gyawali D, Hsia CCW, Nguyen KT. Polymeric nanoparticles for pulmonary protein and DNA delivery. Acta Biomater [Internet]. 2014;10:2643–52. Available from: https://www.sciencedirect.com/science/article/pii/S174270611400052X
79. García-Fernández A, Sancenón F, Martínez-Máñez R. Mesoporous silica nanoparticles for pulmonary drug delivery. Adv Drug Deliv Rev [Internet]. 2021;177:113953. Available from: https://www.sciencedirect.com/science/article/pii/S0169409X2100346X
80. Craparo EF, Cabibbo M, Scialabba C, Giammona G, Cavallaro G. Inhalable Formulation Based on Lipid-Polymer Hybrid Nanoparticles for the Macrophage Targeted Delivery of Roflumilast. Biomacromolecules. 2022;23:3439–51.
81. Peng S, Wang W, Zhang R, Wu C, Pan X, Huang Z. Nano-Formulations for Pulmonary Delivery: Past, Present, and Future Perspectives. Pharmaceutics. 2024;16.
82. Yue P, Zhou W, Huang G, Lei F, Chen Y, Ma Z, et al. Nanocrystals based pulmonary inhalation delivery system: advance and challenge. Drug Deliv [Internet]. 2022;29:637–51. Available from: https://doi.org/10.1080/10717544.2022.2039809
83. Sumaila M, Kumar P, Ubanako P, Adeyemi SA, Choonara YE. Dual Rifampicin and Isoniazid Mannose-Decorated Lipopolysaccharide Nanospheres for Macrophage-Targeted Lung Delivery. Curr Drug Deliv. 2022;
84. Alyami MH, Dahmash EZ, Ali DK, Alyami HS, Abdulkarim H, Alsudir SA. Novel Fluticasone Propionate and Salmeterol Fixed-Dose Combination Nano-Encapsulated Particles Using Polyamide Based on L-Lysine. Pharmaceutics. 2022;15.
85. Pan J, Mendes LP, Yao M, Filipczak N, Garai S, Thakur GA, et al. Polyamidoamine dendrimers-based nanomedicine for combination therapy with siRNA and chemotherapeutics to overcome multidrug resistance. Eur J Pharm Biopharm. 2019;136:18–28.
86. Xu X, Wang J, Wang Y, Zhao L, Li Y, Liu C. Formation of graphene oxide-hybridized nanogels for combinative anticancer therapy. Nanomedicine. 2018;14:2387–95.
87. Gupta P V, Nirwane AM, Belubbi T, Nagarsenker MS. Pulmonary delivery of synergistic combination of fluoroquinolone antibiotic complemented with proteolytic enzyme: A novel antimicrobial and antibiofilm strategy. Nanomedicine. 2017;13:2371–84.
88. Yang Y, Huang Z, Li J, Mo Z, Huang Y, Ma C, et al. PLGA Porous Microspheres Dry Powders for Codelivery of Afatinib-Loaded Solid Lipid Nanoparticles and Paclitaxel: Novel Therapy for EGFR Tyrosine Kinase Inhibitors Resistant Nonsmall Cell Lung Cancer. Adv Healthc Mater. 2019;8:e1900965.
89. Abd Elwakil MM, Mabrouk MT, Helmy MW, Abdelfattah E-ZA, Khiste SK, Elkhodairy KA, et al. Inhalable lactoferrin-chondroitin nanocomposites for combined delivery of doxorubicin and ellagic acid to lung carcinoma. Nanomedicine (Lond). 2018;13:2015–35.
90. Banat H, Gróf I, Deli MA, Ambrus R, Csóka I. Evaluation of Permeability, Safety, and Stability of Nanosized Ketoprofen Co-Spray-Dried with Mannitol for Carrier-Free Pulmonary Systems. Appl Sci. 2025;15.
91. Malamatari M, Taylor KMG, Malamataris S, Douroumis D, Kachrimanis K. Pharmaceutical nanocrystals: production by wet milling and applications. Drug Discov Today [Internet]. 2018;23:534–47. Available from: https://www.sciencedirect.com/science/article/pii/S1359644617304129
92. Siewert C, Moog R, Alex R, Kretzer P, Rothenhäusler B. Process and scaling parameters for wet media milling in early phase drug development: A knowledge based approach. Eur J Pharm Sci [Internet]. 2018;115:126–31. Available from: https://doi.org/10.1016/j.ejps.2017.12.022
93. Aldeeb MME, Wilar G, Suhandi C, Elamin KM, Wathoni N. Nanosuspension-Based Drug Delivery Systems for Topical Applications. Int J Nanomedicine. 2024;19:825–44.
94. Bartos C, Jójárt-Laczkovich O, Katona G, Budai-Szűcs M, Ambrus R, Bocsik A, et al. Optimization of a combined wet milling process in order to produce poly(vinyl alcohol) stabilized nanosuspension. Drug Des Devel Ther. 2018;12:1567–80.
95. Wang Y, Zheng Y, Zhang L, Wang Q, Zhang D. Stability of nanosuspensions in drug delivery. J Control Release [Internet]. 2013;172:1126–41. Available from: http://dx.doi.org/10.1016/j.jconrel.2013.08.006
96. Böck NC, Sundermann J, Koziolek M, Keller BL, Mäder K. Impact of stabilizers on particle size and dispersion behavior in biorelevant media in solid nanocrystal formulations. Eur J Pharm Biopharm. 2025;208.
97. Muralidharan P, Malapit M, Mallory E, Hayes D, Mansour HM. Inhalable nanoparticulate powders for respiratory delivery. Nanomedicine Nanotechnology, Biol Med [Internet]. 2015;11:1189–99. Available

from: http://dx.doi.org/10.1016/j.nano.2015.01.007
98. Scherlie R, Bock S, Bungert N, Neustock A, Valentin L. Particle engineering in dry powders for inhalation. Eur J Pharm Sci. 2022;172.
99. Chishti N, Dehghan MH. Nano-embedded microparticles based dry powder inhaler for lung cancer treatment. J Res Pharm. 2020;24:425–35.
100. Heyder J. Deposition of inhaled particles in the human respiratory tract and consequences for regional targeting in respiratory drug delivery. Proc Am Thorac Soc. 2004;1:315–20.
101. Thorley AJ, Tetley TD. New perspectives in nanomedicine. Pharmacol Ther. 2013;
102. Das SC, Khadka P, Shah R, McGill S, Smyth HDC. Nanomedicine in pulmonary delivery. Theory Appl. Nonparenteral Nanomedicines. Elsevier Inc.; 2021.
103. Tsapis N, Bennett D, Jackson B, Weitz DA, Edwards DA. Trojan particles: large porous carriers of nanoparticles for drug delivery. Proc Natl Acad Sci U S A. 2002;99:12001–5.
104. Vehring R. Pharmaceutical particle engineering via spray drying. Pharm Res. 2008;25:999–1022.
105. Alhajj N, O'Reilly NJ, Cathcart H. Designing enhanced spray dried particles for inhalation: A review of the impact of excipients and processing parameters on particle properties. Powder Technol [Internet]. 2021;384:313–31. Available from: https://www.sciencedirect.com/science/article/pii/S0032591021001340
106. Arpagaus C. Pharmaceutical Particle Engineering via Nano Spray Drying - Process Parameters and Application Examples on the Laboratory-Scale. Int J Med Nano Res. 2018;5.
107. Yang D, Liu R, Wei Y, Sun Q, Wang J. Micro-sized nanoaggregates : Spray-drying-assisted fabrication and applications. Particuology [Internet]. 2024;85:22–48. Available from: https://doi.org/10.1016/j.partic.2023.03.013
108. LeClair DA, Cranston ED, Xing Z, Thompson MR. Optimization of Spray Drying Conditions for Yield, Particle Size and Biological Activity of Thermally Stable Viral Vectors. Pharm Res [Internet]. 2016;33:2763–76. Available from: http://dx.doi.org/10.1007/s11095-016-2003-4
109. Arte KS, Tower CW, Mutukuri TT, Chen Y, Patel SM, Munson EJ, et al. Understanding the impact of mannitol on physical stability and aerosolization of spray-dried protein powders for inhalation. Int J Pharm [Internet]. 2024;650:123698. Available from: https://doi.org/10.1016/j.ijpharm.2023.123698
110. Chang RY, Wong J, Mathai A, Morales S, Kutter E, Britton W, et al. Production of highly stable spray dried phage formulations for treatment of Pseudomonas aeruginosa lung infection. Eur J Pharm Biopharm [Internet]. 2017;121:1–13. Available from: https://www.sciencedirect.com/science/article/pii/S093964111730807X
111. Branchu S, Forbes RT, York P, Petrén S, Nyqvist H, Camber O. Hydroxypropyl-β-cyclodextrin inhibits spray-drying-induced inactivation of β-galactosidase. J Pharm Sci [Internet]. 1999;88:905–11. Available from: https://www.sciencedirect.com/science/article/pii/S0022354915508629
112. Kumar Subramani P, P N R, Narayanasamy D. The Role of Pulmonary Drug Delivery in Modern Therapeutics: An Overview. Cureus. 2024;16.
113. European Medicines Agency. ICH Q1A (R2) Stability testing of new drug substances and drug products - Scientific guideline. 2003.
114. Pallagi E, Ambrus R, Szabó-Révész P, Csóka I. Adaptation of the quality by design concept in early pharmaceutical development of an intranasal nanosized formulation. Int J Pharm [Internet]. 2015;491:384–92. Available from: http://dx.doi.org/10.1016/j.ijpharm.2015.06.018
115. Csóka I, Pallagi E, Paál TL. Extension of quality-by-design concept to the early development phase of pharmaceutical R&D processes. Drug Discov Today [Internet]. 2018;23:1340–3. Available from: https://doi.org/10.1016/j.drudis.2018.03.012
116. Mardikasari SA, Sipos B, Csóka I, Katona G. Nasal route for antibiotics delivery: Advances, challenges and future opportunities applying the quality by design concepts. J Drug Deliv Sci Technol. 2022;77.
117. Akel H, Ismail R, Csóka I. Progress and perspectives of brain-targeting lipid-based nanosystems via the nasal route in Alzheimer's disease. Eur J Pharm Biopharm [Internet]. 2020;148:38–53. Available from: https://doi.org/10.1016/j.ejpb.2019.12.014
118. Barbalata CI, Porfire AS, Casian T, Muntean D, Rus I, Tertis M, et al. The Use of the QbD Approach to Optimize the Co-Loading of Simvastatin and Doxorubicin in Liposomes for a Synergistic Anticancer Effect. Pharmaceuticals. 2022;15.
119. Mistree RY, Chodhary UM, Shah CN, Upadhyay U, Professor A. Quality by Design Approach for Pharmaceutical Product Development: A Comprehensive Review. J Pharm Sci Med Technol. 2020;2:33–49.
120. Mire-sluis A, Dobbins J, Moore CM V, Pepper T, Rellahan B, Riker K, et al. Patient-Centric Quality Standards. J Pharm Sci. 2024;113.
121. Menditto E, Orlando V, Rosa G De, Minghetti P, Musazzi UM, Cahir C, et al. Patient Centric Pharmaceutical Drug Product Design — The Impact on Medication Adherence. 2020;1–23.
122. Clive P. Peter J. Barnes. Pharmacology and Therapeutics of Asthma and COPD. J.E. Barrett P, V. Flockerzi H, M.A. Frohman, Stony Brook N, P. Geppetti F, F.B. Hofmann M, M.C. Michel M, et al., editors.

London: Springer International Publishing AG; 2016.
123. Bäckman P, Adelmann H, Petersson G, Jones CB. Advances in inhaled technologies: Understanding the therapeutic challenge, predicting clinical performance, and designing the optimal inhaled product. Clin Pharmacol Ther. 2014;95:509–20.
124. Anderson S, Atkins P, Bäckman P, Cipolla D, Clark A, Daviskas E, et al. Inhaled Medicines: Past, Present, and Future. Page C, editor. Pharmacol Rev [Internet]. 2022;74:48–118. Available from: http://pharmrev.aspetjournals.org/lookup/doi/10.1124/pharmrev.120.000108
125. Nelson HS, Chapman KR, Pyke SD, Johnson M, Pritchard JN. Enhanced synergy between fluticasone propionate and salmeterol inhaled from a single inhaler versus separate inhalers. J Allergy Clin Immunol. 2003;112:29–36.
126. Taki M, Esmaeili F, Martin GP. The scientific basis and challenges of combination inhaled products. J Drug Deliv Sci Technol [Internet]. 2011;21:293–300. Available from: http://dx.doi.org/10.1016/S1773-2247(11)50046-2
127. Gina reports [Internet]. 2021 [cited 2022 Oct 4]. Available from: https://ginasthma.org/reports.
128. Gold reports [Internet]. 2020 [cited 2022 Oct 9]. Available from: https://goldcopd.org/gold-reports
129. Peters R, Shanley A, Haigney S, Siew A, Markarian J, Mirasol F, et al. APIs, EXCIPIENTS & MANUFACTURING. Iselin, USA: PharmTech.com; 2017.
130. Theophilus A, Moore A, Prime D, Rossomanno S, Whitcher B, Chrystyn H. Co-deposition of salmeterol and fluticasone propionate by a combination inhaler. Int J Pharm. 2006;313:14–22.
131. US FDA. Guidance for industry immediate release solid oral dosage forms scale-up and postapproval changes: chemistry, manufacturing, and controls, in vitro dissolution testing, and in vivo bioequivalence documentation. FDA. 1995.
132. FDA. Patient-Focused Drug Development: Methods to Identify What is Important to Patients [Internet]. FDA. 2022. Available from: https://www.fda.gov/media/131230/download
133. National Center for Biotechnology Information. PubChem Compound Summary for CID 3825, Ketoprofen [Internet]. 2025 [cited 2025 Apr 16]. Available from: https://pubchem.ncbi.nlm.nih.gov/compound/Ketoprofen.
134. Faizi HS, Vora LK, Nasiri MI, Wu Y, Mishra D, Anjani QK, et al. Deferasirox Nanosuspension Loaded Dissolving Microneedles for Intradermal Delivery. Pharmaceutics. 2022;
135. Chan SY, Chung YY, Cheah XZ, Tan EYL, Quah J. The characterization and dissolution performances of spray dried solid dispersion of ketoprofen in hydrophilic carriers. Asian J Pharm Sci [Internet]. 2015;10:372–85. Available from: http://dx.doi.org/10.1016/j.ajps.2015.04.003
136. Bilgili E, Rahman M, Palacios D, Arevalo F. Impact of polymers on the aggregation of wet-milled itraconazole particles and their dissolution from spray-dried nanocomposites. Adv Powder Technol [Internet]. 2018;29:2941–56. Available from: https://doi.org/10.1016/j.apt.2018.09.039
137. Canpınar H, Gülba S. A new nanosuspension prepared with wet milling method for oral delivery of highly variable drug Cyclosporine A: development, optimization and in vivo evaluation. Eur J Pharm Sci. 2022;171.
138. Peltonen L, Hirvonen J. Pharmaceutical nanocrystals by nanomilling: critical process parameters, particle fracturing and stabilization methods. J Pharm Pharmacol. 2010;56:1569–79.
139. Flume PA, Amelina E, Daines CL, Charlton B, Leadbetter J, Guasconi A, et al. Efficacy and safety of inhaled dry-powder mannitol in adults with cystic fibrosis: An international, randomized controlled study. J Cyst Fibros [Internet]. 2021;20:1003–9. Available from: https://www.sciencedirect.com/science/article/pii/S1569199321000461
140. Lu P, Li J, Liu C, Yang J, Peng H, Xue Z, et al. Salvianolic acid B dry powder inhaler for the treatment of idiopathic pulmonary fibrosis. Asian J Pharm Sci [Internet]. 2022;17:447–61. Available from: https://doi.org/10.1016/j.ajps.2022.04.004
141. Laaksonen T, Liu P, Rahikkala A, Peltonen L, Kauppinen EI, Hirvonen J, et al. Intact Nanoparticulate Indomethacin in Fast-Dissolving Carrier Particles by Combined Wet Milling and Aerosol Flow Reactor Methods. Pharm Res. 2011;2403–11.
142. National Center for Biotechnology Information. PubChem Compound Summary for CID 6251, Mannitol [Internet]. 2025 [cited 2025 Apr 17]. Available from: https://pubchem.ncbi.nlm.nih.gov/compound/Mannitol
143. National Center for Biotechnology Information. PubChem Compound Summary for CID 6106, Leucine [Internet]. 2025 [cited 2025 Apr 17]. Available from: https://pubchem.ncbi.nlm.nih.gov/compound/Leucine
144. National Center for Biotechnology Information. PubChem Compound Summary for Polyvinyl Alcohol [Internet]. 2025 [cited 2025 Apr 17]. Available from: https://pubchem.ncbi.nlm.nih.gov/compound/Polyvinyl-Alcohol.
145. National Center for Biotechnology Information. PubChem Compound Summary for CID 3423265, Sodium Lauryl Sulfate [Internet]. 2025 [cited 2025 Apr 17]. Available from:

https://pubchem.ncbi.nlm.nih.gov/compound/Sodium-Lauryl-Sulfate
146. Banat H, Csóka I, Paróczai D, Burian K, Farkas Á, Ambrus R. A Novel Combined Dry Powder Inhaler Comprising Nanosized Ketoprofen-Embedded Mannitol-Coated Microparticles for Pulmonary Inflammations : Development , In Vitro – In Silico Characterization , and Cell Line Evaluation. pharmaceuticals [Internet]. 2024;17. Available from: https://doi.org/10.3390/ ph17010075
147. Banat H, Nagy A, Farkas Á, Ambrus R. Comprehensive Aerodynamic and Physicochemical Stability Evaluations of Nanocrystal-Based Dry Powder Inhalers : The Role of Mannitol and Leucine in Enhancing Performance. pharmacetics. 2025;17:436.
148. Koblinger L, Hofmann W. Monte Carlo modeling of aerosol deposition in human lungs. Part I: Simulation of particle transport in a stochastic lung structure. J Aerosol Sci [Internet]. 1990;21:661–74. Available from: https://www.sciencedirect.com/science/article/pii/002185029090121D
149. García-Díaz M, Birch D, Wan F, Nielsen HM. The role of mucus as an invisible cloak to transepithelial drug delivery by nanoparticles. Adv Drug Deliv Rev [Internet]. 2018;124:107–24. Available from: https://doi.org/10.1016/j.addr.2017.11.002
150. Peták F, Bánfi A, Tóth-Szüki V, Baráti L, Bari F, Székely E, et al. Airway responsiveness and bronchoalveolar lavage fluid profiling in individual rats: Effects of different ovalbumin exposures. Respir Physiol Neurobiol. 2010;170:76–82.
151. Jánosi TZ, Adamicza Á, Zosky GR, Asztalos T, Sly PD, Hantos Z. Plethysmographic estimation of thoracic gas volume in apneic mice. J Appl Physiol. 2006;101:454–9.
152. Peták F, Hantos Z, Adamicza Á, Asztalos T, Sly PD. Methacholine-induced bronchoconstriction in rats: Effects of intravenous vs. aerosol delivery. J Appl Physiol. 1997;82:1479–87.
153. Hantos Z, Daróczy B, Suki B, Nagy S, Fredberg JJ. Input impedance and peripheral inhomogeneity of dog lungs. J Appl Physiol. 1992;72:168–78.
154. Franken H, Cement J, Cauberghs M, Woestijne KP Van de. Oscillating Flow of a Viscous Compressible Fluid Through a Rigid Tube: A Theoretical Model. IEEE Trans Biomed Eng. 1981;BME-28:416–20.
155. Abdollahi S, Raissi H, Farzad F. Examine stability polyvinyl alcohol-stabilized nanosuspensions to overcome the challenge of poor drug solubility utilizing molecular dynamic simulation. Sci Rep [Internet]. 2024;14:1–11. Available from: https://doi.org/10.1038/s41598-024-68362-2
156. Hou J, Ci H, Wang P, Wang C, Lv B, Miao L, et al. Nanoparticle tracking analysis versus dynamic light scattering: Case study on the effect of Ca2+ and alginate on the aggregation of cerium oxide nanoparticles. J Hazard Mater [Internet]. 2018;360:319–28. Available from: https://www.sciencedirect.com/science/article/pii/S0304389418306885
157. Maguire CM, Sillence K, Roesslein M, Hannell C, Suarez G, Sauvain JJ, et al. Benchmark of nanoparticle tracking analysis on measuring nanoparticle sizing and concentration. J Micro Nano-Manufacturing. 2017;5.
158. Lands LC, Stanojevic S. Oral non-steroidal anti-inflammatory drug therapy for lung disease in cystic fibrosis. Cochrane database Syst Rev. 2013;CD001505.
159. Adi H, Young PM, Chan H, Agus H, Traini D. Co-spray-dried mannitol – ciprofloxacin dry powder inhaler formulation for cystic fibrosis and chronic obstructive pulmonary disease. Eur J Pharm Sci [Internet]. 2010;40:239–47. Available from: http://dx.doi.org/10.1016/j.ejps.2010.03.020
160. Macleod DL, Barker LM, Sutherland JL, Moss SC, Gurgel JL, Kenney TF, et al. Antibacterial activities of a fosfomycin / tobramycin combination: a novel inhaled antibiotic for bronchiectasis. J Antimicrob Chemother. 2009;64:829–36.
161. Cayli YA, Sahin S, Buttini F, Balducci AG, Montanari S, Vural I, et al. Dry powders for the inhalation of ciprofloxacin or levofloxacin combined with a mucolytic agent for cystic fibrosis patients. Drug Dev Ind Pharm [Internet]. 2017;0:000. Available from: http://dx.doi.org/10.1080/03639045.2017.1318902
162. Buttini F, Rozou S, Rossi A, Zoumpliou V, Rekkas DM. The application of Quality by Design framework in the pharmaceutical development of dry powder inhalers. Eur J Pharm Sci [Internet]. 2018;113:64–76. Available from: https://doi.org/10.1016/j.ejps.2017.10.042
163. Pilcer G, De Bueger V, Traina K, Traore H, Sebti T, Vanderbist F, et al. Carrier-free combination for dry powder inhalation of antibiotics in the treatment of lung infections in cystic fibrosis. Int J Pharm [Internet]. 2013;451:112–20. Available from: http://dx.doi.org/10.1016/j.ijpharm.2013.04.069
164. Pallagi E, Jójárt-Laczkovich O, Németh Z, Szabó-Révész P, Csóka I. Application of the QbD-based approach in the early development of liposomes for nasal administration. Int J Pharm [Internet]. 2019;562:11–22. Available from: https://doi.org/10.1016/j.ijpharm.2019.03.021
165. Sun Y, Cui Z, Sun Y, Qin L, Zhang X, Liu Q, et al. Exploring the potential influence of drug charge on downstream deposition behaviour of DPI powders. Int J Pharm [Internet]. 2020;588:119798. Available from: https://www.sciencedirect.com/science/article/pii/S0378517320307833
166. Scherließ R, Etschmann C. DPI formulations for high dose applications – Challenges and opportunities. Int J Pharm [Internet]. 2018;548:49–53. Available from:

https://www.sciencedirect.com/science/article/pii/S0378517318304368
167. Taki M, Marriott C, Zeng X-M, Martin GP. Aerodynamic deposition of combination dry powder inhaler formulations in vitro: A comparison of three impactors. Int J Pharm [Internet]. 2010;388:40–51. Available from: https://www.sciencedirect.com/science/article/pii/S0378517309009053
168. Sun Y, Qin L, Liu C, Su J, Zhang X, Yu D, et al. Exploring the influence of drug content on DPI powder properties and potential prediction of pulmonary drug deposition. Int J Pharm [Internet]. 2020;575:119000. Available from: https://www.sciencedirect.com/science/article/pii/S0378517319310610
169. Wauthoz N, Hennia I, Ecenarro S, Amighi K. Impact of capsule type on aerodynamic performance of inhalation products: A case study using a formoterol-lactose binary or ternary blend. Int J Pharm [Internet]. 2018;553:47–56. Available from: https://www.sciencedirect.com/science/article/pii/S0378517318307695
170. Berkenfeld K, Lamprecht A, McConville JT. Devices for dry powder drug delivery to the lung. AAPS PharmSciTech. 2015;16:479–90.
171. de Pablo E, O'Connell P, Fernández-García R, Marchand S, Chauzy A, Tewes F, et al. Targeting lung macrophages for fungal and parasitic pulmonary infections with innovative amphotericin B dry powder inhalers. Int J Pharm [Internet]. 2023;635:122788. Available from: https://www.sciencedirect.com/science/article/pii/S0378517323002089
172. Yu S, Wang S, Zou P, Chai G, Lin Y-W, Velkov T, et al. Inhalable liposomal powder formulations for co-delivery of synergistic ciprofloxacin and colistin against multi-drug resistant gram-negative lung infections. Int J Pharm [Internet]. 2020;575:118915. Available from: https://www.sciencedirect.com/science/article/pii/S0378517319309603
173. Alhajj N, O'Reilly NJ, Cathcart H. Developing ciprofloxacin dry powder for inhalation: A story of challenges and rational design in the treatment of cystic fibrosis lung infection. Int J Pharm [Internet]. 2022;613:121388. Available from: https://www.sciencedirect.com/science/article/pii/S0378517321011947
174. Stegemann S, Faulhammer E, Pinto JT, Paudel A. Focusing on powder processing in dry powder inhalation product development, manufacturing and performance. Int J Pharm [Internet]. 2022;614:121445. Available from: https://www.sciencedirect.com/science/article/pii/S0378517321012515
175. Nokhodchi A, Chavan S, Ghafourian T. In Vitro Dissolution and Permeability Testing of Inhalation Products: Challenges and Advances. Pharmaceutics. 2023;983.
176. Benke E, Ambrus R. Stability and In Vitro Aerodynamic Studies of Inhalation Powders Containing Ciprofloxacin Hydrochloride Applying Different DPI Capsule Types. Pharmaceutics. 2021;
177. Liu Q, Guan J, Sun Z, Shen X, Li L, Jin L, et al. Influence of stabilizer type and concentration on the lung deposition and retention of resveratrol nanosuspension-in-microparticles. Int J Pharm [Internet]. 2019;569:118562. Available from: https://www.sciencedirect.com/science/article/pii/S0378517319306064
178. Zhou QT, Tang P, Leung SSY, Chan JGY, Chan H-K. Emerging inhalation aerosol devices and strategies: where are we headed? Adv Drug Deliv Rev. 2014;75:3–17.
179. Suzuki ÉY, Amaro MI, de Almeida GS, Cabral LM, Healy AM, de Sousa VP. Development of a new formulation of roflumilast for pulmonary drug delivery to treat inflammatory lung conditions. Int J Pharm [Internet]. 2018;550:89–99. Available from: https://www.sciencedirect.com/science/article/pii/S0378517318306136
180. Bosquillon C, Lombry C, Préat V, Vanbever R. Influence of formulation excipients and physical characteristics of inhalation dry powders on their aerosolization performance. J Control Release [Internet]. 2001;70:329–39. Available from: https://www.sciencedirect.com/science/article/pii/S016836590000362X
181. Seville PC, Learoyd TP, Li H, Williamson IJ, Birchall JC. Amino acid-modified spray-dried powders with enhanced aerosolisation properties for pulmonary drug delivery. 2007;178:40–50.
182. Lewis D, Rouse T, Singh D, Edge S. Defining the 'Dose' for Dry Powder Inhalers: The Challenge of Correlating In- Vitro Dose Delivery Results with Clinical Efficacy. Am Pharm Rev. 2017;
183. Xia D, Shrestha N, Streek J Van De, Mu H, Yang M. Spray drying of fenofibrate loaded nanostructured lipid carriers. Asian J Pharm Sci [Internet]. 2016;11:507–15. Available from: http://dx.doi.org/10.1016/j.ajps.2016.01.001
184. Myat HH, Ritthidej GC. Impact of formulation parameters on physical characteristics of spray dried nanoemulsions and their reconstitutions. Asian J Pharm Sci [Internet]. 2016;11:197–8. Available from: http://dx.doi.org/10.1016/j.ajps.2015.11.038
185. Nandiyanto ABD, Okuyama K. Progress in developing spray-drying methods for the production of controlled morphology particles: From the nanometer to submicrometer size ranges. Adv Powder Technol [Internet]. 2011;22:1–19. Available from: https://www.sciencedirect.com/science/article/pii/S0921883110001883
186. Leung SSY, Wong J, Guerra HV, Samnick K, Prud'homme RK, Chan H-K. Porous mannitol carrier for pulmonary delivery of cyclosporine A nanoparticles. AAPS J. 2017;19:578–86.
187. Kang J-H, Kim Y-J, Yang M-S, Shin DH, Kim D-W, Park IY, et al. Co-Spray Dried Nafamostat Mesylate with Lecithin and Mannitol as Respirable Microparticles for Targeted Pulmonary Delivery:

Pharmacokinetics and Lung Distribution in Rats. Pharmaceutics. 2021;13.
188. Pomázi A, Ambrus R, Sipos P, Szabó-révész P. Analysis of co-spray-dried meloxicam - mannitol systems containing crystalline microcomposites. J Pharm Biomed Anal. 2011;56:183–90.
189. Li X, Vogt FG, Hayes D, Mansour HM. Design, Characterization, and Aerosol Dispersion Performance Modeling of Advanced Co-Spray Dried Antibiotics with Mannitol as Respirable Microparticles/Nanoparticles for Targeted Pulmonary Delivery as Dry Powder Inhalers. J Pharm Sci [Internet]. 2014;103:2937–49. Available from: https://www.sciencedirect.com/science/article/pii/S0022354915304287
190. Belotti S, Rossi A, Colombo P, Bettini R, Rekkas D, Politis S, et al. Spray-dried amikacin sulphate powder for inhalation in cystic fibrosis patients: The role of ethanol in particle formation. Eur J Pharm Biopharm [Internet]. 2015;93:165–72. Available from: https://www.sciencedirect.com/science/article/pii/S0939641115001563
191. Saffari M, Ebrahimi A, Langrish T. A novel formulation for solubility and content uniformity enhancement of poorly water-soluble drugs using highly-porous mannitol. Eur J Pharm Sci [Internet]. 2016;83:52–61. Available from: https://www.sciencedirect.com/science/article/pii/S0928098715300907
192. Chapman KR, Fogarty CM, Peckitt C, Lassen C. Delivery characteristics and patients' handling of two single-dose dry-powder inhalers used in COPD. Int J COPD. 2011;353–63.
193. Requena S, Ponomarchuk O, Castillo M, Rebik J, Bo J, Gryczynski I, et al. Imaging viscosity of intragranular mucin matrix in cystic fibrosis cells. Sci Rep. 2017;1–6.
194. Hill DB, Button B, Rubinstein M, Boucher RC. Physiology and Pathophysiology of Human Airwaymucus. Physiol Rev. 2022;102:1757–836.
195. Anderson WH, Coakley RD, Button B, Henderson AG, Zeman KL, Alexis NE, et al. The relationship of mucus concentration (hydration) to mucus osmotic pressure and transport in chronic bronchitis. Am J Respir Crit Care Med. 2015;192:182–90.
196. Odziomek M, Sosnowski TR, Gradoń L. The Influence of Functional Carrier Particles (FCPs) on the Molecular Transport Rate Through the Reconstructed Bronchial Mucus: In Vitro Studies. Transp Porous Media. 2015;106:439–54.
197. Serisier DJ, Carroll MP, Shute JK, Young SA. Macrorheology of cystic fibrosis, chronic obstructive pulmonary disease & normal sputum. Respir Res. 2009;10:1–8.
198. Leal J, Smyth HDC, Ghosh D. Physicochemical properties of mucus and their impact on transmucosal drug delivery. Int J Pharm [Internet]. 2017;532:555–72. Available from: http://dx.doi.org/10.1016/j.ijpharm.2017.09.018
199. Tanaka T, Narazaki M, Kishimoto T. IL-6 in Inflammation, Immunity, and Disease. Cold Spring Harb Perspect Biol. 2014;6:1–16.
200. Yu M, Zheng X, Witschi H, Pinkerton KE. The role of interleukin-6 in pulmonary inflammation and injury induced by exposure to environment air pollutants. Toxicol Sci. 2002;68:488–97.
201. Mitchell JA, Belvisi MG, Akarasereenont P, Robbins RA, Kwon O -Jung, Croxtall JJ, et al. Induction of cyclo-oxygenase-2 by cytokines in human pulmonary epithelial cells: regulation by dexamethasone. Br J Pharmacol. 1994;113:1008–14.
202. Grkovich A, Johnson CA, Buczynski MW, Dennis EA. Lipopolysaccharide-induced cyclooxygenase-2 expression in human U937 macrophages is phosphatidic acid phosphohydrolase-1-dependent. J Biol Chem [Internet]. 2006;281:32978–87. Available from: http://dx.doi.org/10.1074/jbc.M605935200
203. Party P, Kókai D, Burián K, Nagy A, Hopp B, Ambrus R. Development of extra-fine particles containing nanosized meloxicam for deep pulmonary delivery: In vitro aerodynamic and cell line measurements. Eur J Pharm Sci [Internet]. 2022;176:106247. Available from: https://www.sciencedirect.com/science/article/pii/S0928098722001324
204. Rajamohan R, Kamaraj E, Muthuraja P, Murugavel K, Govindasamy C, Prabakaran DS, et al. Enhancing ketoprofen's solubility and anti-inflammatory efficacy with safe methyl-β-cyclodextrin complexation. Sci Rep [Internet]. 2024;14:1–15. Available from: https://doi.org/10.1038/s41598-024-71615-9
205. Hiemstra PS, Tetley TD, Janes SM. Airway and alveolar epithelial cells in culture. Eur Respir J [Internet]. 2019;54:1900742. Available from: https://publications.ersnet.org//content/erj/54/5/1900742.abstract
206. Ménard S, Cerf-Bensussan N, Heyman M. Multiple facets of intestinal permeability and epithelial handling of dietary antigens. Mucosal Immunol [Internet]. 2010;3:247–59. Available from: http://dx.doi.org/10.1038/mi.2010.5
207. Lee SH, Heng D, Ng WK, Chan HK, Tan RBH. Nano spray drying: A novel method for preparing protein nanoparticles for protein therapy. Int J Pharm [Internet]. 2011;403:192–200. Available from: http://dx.doi.org/10.1016/j.ijpharm.2010.10.012
208. Chopde S, Datir R, Deshmukh G, Dhotre A, Patil M. Nanoparticle formation by nanospray drying & its application in nanoencapsulation of food bioactive ingredients. J Agric Food Res [Internet]. 2020;2:100085.

Available from: https://doi.org/10.1016/j.jafr.2020.100085
209. Ordoubadi M, Gregson FKA, Wang H, Nicholas M, Gracin S, Lechuga-ballesteros D, et al. On the particle formation of leucine in spray drying of inhalable microparticles. Int J Pharm [Internet]. 2021;592:120102. Available from: https://doi.org/10.1016/j.ijpharm.2020.120102
210. Schweizer RT, Ordoubadi M, Prather CA, Vehring R, Shepard KB. The Processing Space of the Spray-Dried Mannitol-Leucine System for Pulmonary Drug Delivery. Pharmaceutics. 2024;16:398.
211. Valentin M, Coibion D, Vertruyen B, Malherbe C, Cloots R, Boschini F. Macroporous Mannitol Granules Produced by Spray Drying and Sacrificial Templating. Materials (Basel). 2023;16:1–16.
212. Malamatari M, Somavarapu S, Kachrimanis K, Buckton G, Taylor KMG. Preparation of respirable nanoparticle agglomerates of the low melting and ductile drug ibuprofen : Impact of formulation parameters. Powder Technol [Internet]. 2017;308:123–34. Available from: http://dx.doi.org/10.1016/j.powtec.2016.12.007
213. Benke E, Winter C, Szabó-révész P, Roblegg E, Ambrus R. The effect of ethanol on the habit and in vitro aerodynamic results of dry powder inhalation formulations containing ciprofloxacin hydrochloride. Asian J Pharm Sci [Internet]. 2021;16:471–82. Available from: https://doi.org/10.1016/j.ajps.2021.04.003
214. Molina C, Kaialy W, Nokhodchi A. The crucial role of leucine concentration on spray dried mannitol-leucine as a single carrier to enhance the aerosolization performance of Albuterol sulfate. J Drug Deliv Sci Technol [Internet]. 2019;49:97–106. Available from: https://doi.org/10.1016/j.jddst.2018.11.007
215. Malamatari M, Somavarapu S, Bloxham M, Buckton G. Nanoparticle agglomerates of indomethacin : The role of poloxamers and matrix former on their dissolution and aerosolisation efficiency. Int J Pharm [Internet]. 2015;495:516–26. Available from: http://dx.doi.org/10.1016/j.ijpharm.2015.09.013
216. Pasero L, Sulpizi A, Guidi T, Pisano R. Spray freeze-drying for inhalable L-leucine, mannitol-based microparticles: The impact of process variables, L-leucine, and crystallinity on Aerosolization properties. Powder Technol [Internet]. 2025;455:120788. Available from: https://doi.org/10.1016/j.powtec.2025.120788
217. Sou T, Orlando L, McIntosh MP, Kaminskas LM, Morton DAV. Investigating the interactions of amino acid components on a mannitol-based spray-dried powder formulation for pulmonary delivery: A design of experiment approach. Int J Pharm [Internet]. 2011;421:220–9. Available from: http://dx.doi.org/10.1016/j.ijpharm.2011.09.018
218. Enlo-Scott Z, Swedrowska M, Forbes B. Chapter 10 - Epithelial permeability and drug absorption in the lungs. In: Kassinos S, Bäckman P, Conway J, Hickey AJBT-IM, editors. Inhaled Med Optim Dev Through Integr Silico, Vitr Vivo Approaches [Internet]. Academic Press; 2021. p. 267–99. Available from: https://www.sciencedirect.com/science/article/pii/B9780128149744000043
219. Matthay MA, Robriquet L, Fang X. Alveolar epithelium: Role in lung fluid balance and acute lung injury. Proc Am Thorac Soc. 2005;2:206–13.
220. Brune K, Frank J, Schwingshackl A, Finigan J, Sidhaye VK. Pulmonary epithelial barrier function: Some new players and mechanisms. Am J Physiol - Lung Cell Mol Physiol. 2015;308:L731–45.
221. Katona G, Sipos B, Budai-Szűcs M, Balogh GT, Veszelka S, Gróf I, et al. Development of in situ gelling meloxicam-human serum albumin nanoparticle formulation for nose-to-brain application. Pharmaceutics. 2021;13.
222. Huang Y, Tang H, Liu D, Liu Y, Meng X, Chen B, et al. Cyclosporine A-loaded chitosan extra-fine particles for deep pulmonary drug delivery: In vitro and in vivo evaluation. J Control Release [Internet]. 2023;362:243–56. Available from: https://doi.org/10.1016/j.jconrel.2023.08.050
223. Hou X, Zhang W, He M, Lu Y, Lou K, Gao F. Preparation and characterization of β-cyclodextrin grafted N-maleoyl chitosan nanoparticles for drug delivery. Asian J Pharm Sci [Internet]. 2017;12:558–68. Available from: https://doi.org/10.1016/j.ajps.2017.07.007
224. Doña I, Blanca-López N, Cornejo-García JA, Torres MJ, Laguna JJ, Fernández J, et al. Characteristics of subjects experiencing hypersensitivity to non-steroidal anti-inflammatory drugs: Patterns of response. Clin Exp Allergy. 2011;41:86–95.
225. Andersén H, Ilmarinen P, Honkamäki J, Tuomisto LE, Hisinger-Mölkänen H, Backman H, et al. NSAID-exacerbated respiratory disease: a population study. ERJ open Res. 2022;8.
226. Busse WW. Leukotrienes and inflammation. Am J Respir Crit Care Med. 1998;157.
227. Hwa J, Martin K. The Eicosanoids: Prostaglandins, Thromboxanes, Leukotrienes, & Related Compounds. In: Katzung BG, editor. Basic & Clin Pharmacol 14e [Internet]. New York, NY: McGraw-Hill Education; 2017. Available from: http://accessmedicine.mhmedical.com/content.aspx?aid=1148435429
228. Jin L Da, Wang LR, Wu LQ, Shan YL, Zhao XY, Xiong XQ, et al. Effects of COX-2 inhibitor on ventilator-induced lung injury in rats. Int Immunopharmacol [Internet]. 2013;16:288–95. Available from: http://dx.doi.org/10.1016/j.intimp.2013.03.031
229. Brannan JD, Anderson SD, Perry CP, Freed-Martens R, Lassig AR, Charlton B. The safety and efficacy of inhaled dry powder mannitol as a bronchial provocation test for airway hyperresponsiveness: a phase 3

comparison study with hypertonic (4.5%) saline. Respir Res. 2005;6:144.
230. Jaques A, Daviskus E, Turton JA, Mckay K, Cooper P, Chb MB, et al. Inhaled Mannitol Improves Lung Function in Cystic Fibrosis. Chest. 2008;133.
231. Brannan JD, Gulliksson M, Anderson SD, Chew N, Seale JP, Kumlin M. Inhibition of mast cell PGD 2 release protects against mannitol-induced airway narrowing. Eur Respir J. 2006;944–50.
232. Liao Y, Li D, Zhou X, Peng Z, Meng Z, Liu R, et al. Pyruvate Might Bridge Gut Microbiota and Muscle Health in Aging Mice After Chronic High Dose of Leucine Supplementation. Front Med. 2021;8:1–13.
233. Chu KR, Lee E, Jeong SH, Park ES. Effect of particle size on the dissolution behaviors of poorly water-soluble drugs. Arch Pharm Res. 2012;35:1187–95.
234. Scrivens G. Prediction of the Long-Term Dissolution Performance of an Immediate-Release Tablet Using Accelerated Stability Studies. J Pharm Sci [Internet]. 2019;108:506–15. Available from: https://doi.org/10.1016/j.xphs.2018.10.025
235. Das S, Larson I, Young P, Stewart P. Influence of Storage Relative Humidity on the Dispersion of Salmeterol Xinafoate Powders for Inhalation. J Pharm Sci [Internet]. 2009;98:1015–27. Available from: https://www.sciencedirect.com/science/article/pii/S002235491632891X

Acknowledgement

I would like to express my sincere gratitude to the Head of the Institute and my supervisor, **Prof. Dr. Ildikó Csóka**, for fostering a supportive environment and for cultivating a diverse scientific culture at our Institute. My deepest appreciation goes to my co-supervisor, **Prof. Dr. Rita Ambrus**, for her constant encouragement, rigorous scientific mentorship, and unwavering support throughout my PhD journey. I consider myself deeply fortunate to have had her as a mentor.

I would like to acknowledge all my co-authors and collaborators: **Dr. Árpád Farkas** (Institute for Energy Security and Environmental Safety, HUN-REN Centre for Energy Research); **Dr. Dóra Paróczai** and **Prof. Dr. Katalin Burián** (Department of Medical Microbiology, University of Szeged); **Dr. Ilona Gróf** and **Prof. Dr. Mária A. Deli** (Institute of Biophysics, HUN-REN Biological Research Centre); **Fruzsina Kun-Szabó**, **Dr. Gergely H. Fodor**, **Petra Somogyi**, and **Prof. Dr. Ferenc Peták** (Department of Medical Physics and Informatics, University of Szeged); **Dr. Anita Sztojkov-Ivanov** and **Dr. Eszter Ducza** (Institute of Pharmacodynamics and Biopharmacy, University of Szeged); **Dr. Róbert Berkecz** (Institute of Pharmaceutical Analysis, University of Szeged); **Dr. Petra Party** (Institute of Pharmaceutical Technology and Regulatory Affairs, University of Szeged); and **Dr. Attila Nagy** (Wigner Research Centre for Physics, Hungarian Academy of Sciences). Also, special thanks are extended to **Erika Feczkóné Boda**, **Klára Kovács**, and **Balázs Béniám** for their technical assistance.

This work was financially supported by **Tempus Public Foundation** through the **Stipendium Hungaricum Program** (Registry no. **SHE-40702-004/2021**). Further support was provided by the **NKFIH OTKA K_146148 project** and **Project No. TKP2021-EGA-32**.

Finally, I am eternally grateful to my father, **Fayez**, whose steadfast emotional and financial support has been a cornerstone of this journey, and to my beloved mother, **Intisar**, whose endless love, care, and prayers have been a constant source of strength and comfort. My deepest thanks go also to my cherished siblings—**Dr. Mahmoud**, **Haneen**, **Dr. Hadeel**, **Hayat**, and **Lamar**—for their unconditional love and understanding throughout my studies. I am forever grateful to those **dear souls** who never leave us—their presence a constant strength, far beyond any distance.

Above all, I thank **Allah** for granting me the strength, patience, and resilience to complete this journey. Every success I have achieved is by His will and grace, "الحمدلله".